

**DEVELOPMENT AND MECHANICAL
CHARACTERIZATION OF HALLOYSITE
NANOTUBES REINFORCED POLYMER
SYNTACTIC NANOCOMPOSITE FOAMS FOR
WEIGHT-SENSITIVE STRUCTURAL
APPLICATIONS**

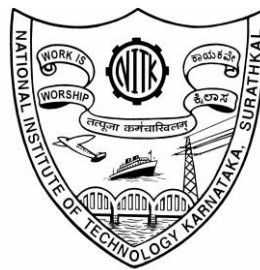
Thesis

Submitted in partial fulfillment of the requirement for the degree
of

DOCTOR OF PHILOSOPHY

by

MOHAMMED SOHAIL BAKSHI



**DEPARTMENT OF MECHANICAL ENGINEERING
NATIONAL INSTITUTE OF TECHNOLOGY
KARNATAKA, SURATHKAL, MANGALORE – 575025,
INDIA
AUGUST 2023**

*This dissertation is dedicated to my
Father and Mother, who instilled in
me the virtues of perseverance and
commitment and relentlessly
encouraged me to strive for
excellence.*

DECLARATION

I hereby *declare* that the Research Thesis entitled **DEVELOPMENT AND MECHANICAL CHARACTERIZATION OF HALLOYSITE NANOTUBES REINFORCED POLYMER SYNTACTIC NANOCOMPOSITE FOAMS FOR WEIGHT-SENSITIVE STRUCTURAL APPLICATIONS**, which is being submitted to the *National Institute of Technology Karnataka, Surathkal* in partial fulfillment of the requirements for the award of the Degree of *Doctor of Philosophy* is a *bonafide report of the research work carried out by me*. The material contained in this thesis has not been submitted to any University or Institution for the award of any degree.

Register Number: **177125ME008**

Name of the Research Scholar: **MOHAMMED SOHAIL BAKSHI**

Signature of the Research Scholar: 

Department of Mechanical Engineering

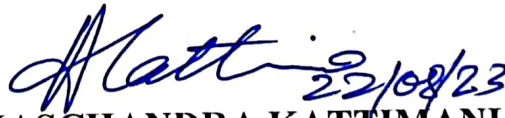
Place: NITK, Surathkal

Date: **22-08-2023**

CERTIFICATE

This is to *certify* that the Research Thesis entitled **DEVELOPMENT AND MECHANICAL CHARACTERIZATION OF HALLOYSITE NANOTUBES REINFORCED POLYMER SYNTACTIC NANOCOMPOSITE FOAMS FOR WEIGHT-SENSITIVE STRUCTURAL APPLICATIONS**, submitted by **MOHAMMED SOHAIL BAKSHI**, (Register Number: 177125ME008) as the record of the research work carried out by him, is *accepted* as the *Research Thesis submission* in partial fulfilment of the requirements for the award of the degree of **Doctor of Philosophy**.

Research Guide



Dr. SUBHASCHANDRA KATTIMANI

Associate Professor

Department of Mechanical Engineering




Chairman-DRPC

Department of Mechanical Engineering

National Institute of Technology Karnataka

Surathkal, Mangalore - 575025

ACKNOWLEDGEMENTS

First and foremost, I would like to express my sincere gratitude and profound thanks to my research guide **Dr. Subhaschandra Kattimani**, Associate Professor, Department of Mechanical Engineering, National Institute of Technology Karnataka, Surathkal, for his exemplary guidance and encouragement throughout my research work. His eternal supervision helped me understand the subject better and completion of this thesis. The time I have spent with him will be remembered and cherished all my life.

I would like to express my sincere gratitude and profound thanks to **Dr. Ravikiran Kadoli**, Professor and Head, Department of Mechanical Engineering, National Institute of Technology Karnataka, Surathkal, for guiding me throughout my research journey.

I sincerely thank the RPAC members, Dr. M R Rahman, Department of Metallurgical and Materials Engineering, and Dr. Sharnappa Joladarashi, Department of Mechanical Engineering, for providing valuable suggestions and support extended to me on all occasions.

I am thankful for the unending help and support received from my fellow research scholars, Mr. Chetan H C, Dr. Vinayak Kallannavar, Dr. Naveen Kumar H S, Dr. Esayas, Mr. Madhu Mohan, Mr. Shada Sai Kumar in the course of my research work. Further, I am enormously indebted to Mr. Asif Gulfarosh, Dr. Mohammed Khalifa, Dr. Kiran Shahapurkar, and Dr. S Sharmas Vali for their massive support during my research journey.

I am grateful to my friends Dr. Rakesh Patil, Prof. Purna Chandra Tanti, Mr. Arunkumar D. S, Dr. Antonio Dylan Carvalho, Dr. Gangadhar Kanaginahal, Dr. Vijay G, Dr. Satish Kanakanavar, Mr. Sachin Hirannaiah for their encouragement and moral support during my research work. The days I spent with them in NITK were unforgettable.

I take this opportunity to thank, Mr. Md Rafeeq M, Mr. Preetam C, Mr. Md Mohiuddin S, Mr. Maneesh K, Mr. Bhimaraya B, Mr. Yadram M, for their huge kindness in supporting me in the challenging times during this course of journey. I am indbted to the love and unending support given by Mr. Roshan Zameer H, Mr. Muneer P, Mr. Asif M during the course of time.

I would like to thank the Almighty for giving me the strength, knowledge, ability, and opportunity to understand this research study and to persevere and complete it satisfactorily.

I would like to thank my father, **Mohammad Ayyub Bakshi**, mother, **Zareena Begaum Inamdar**, and brothers **Mohammad Muzammil Bakshi** and **Khwaja Bandenawaz Bakshi** for their immense love and support throughout my life. Without them, achieving this goal would not have been possible.

(Mohammed Sohail Bakshi)

ABSTRACT

Lightweight syntactic foam composites exhibit high specific strength and modulus. Thus, these are popularly used, from electric vehicle construction to space applications. In the present work, syntactic foam composites are fabricated using cenospheres. Cenosphere, a waste by-product of thermal power plants, is chosen as hollow filler in composites for eco-friendly redressal curbing its environmental impact. Also, a halloysite nanotube (HNT) is an abundantly available natural nanofiller that is utilized to uphold the load-bearing and thermal characteristics of reinforced syntactic foam (RSF) composites.

The RSF composite fabrication involves the probe sonication of HNTs and homogenizing them with an epoxy matrix. Later the cenospheres are gently mixed in the HNTs/epoxy blend to obtain a uniformly dispersed mixture and is thus solution casted in the aluminum molds. A constant content of 1 vol.% addition of HNTs is maintained to fabricate all the RSF composites with cenospheres content being varied from 20 - 50 vol.%. Furthermore, the cenosphere epoxy syntactic foam (CESF) composites are fabricated without HNTs addition for comparison study. In this work, the influence of HNTs reinforcement in syntactic foam on mechanical, water absorption, viscoelastic, and thermal properties are studied. Furthermore, the impact of post-curing on the mechanical and thermal characteristics is also investigated.

The tensile and flexural tests are carried out to evaluate the mechanical performance of CESF and HNTs RSF composites. The enhancement in tensile modulus and flexural modulus was witnessed by up to 42% and 66%, respectively, for the HNTs RSF as compared to CESF composites. The morphology studies prove the existence of hydrogen bonding among the HNTs, cenosphere, and neat epoxy matrix in RSF composite. Field emission-scanning-electron-microscopy (FESEM) affirms the unique crack deflection phenomenon by HNTs, thus elucidating the structure-property correlation. Furthermore, the effect of post-curing on flexural and compressive properties is discussed. The post-cured HNTs RSF containing 40 vol.% cenospheres (NSF40_H) exhibited a compressive modulus of 33.2% higher than room temperature cured neat epoxy due to improved crosslinking. The addition of HNTs in NSF40_H augments the flexural modulus up to 26.9% compared to post-cured neat epoxy.

Moreover, the glass transition temperature (T_g) of CESF composites with 40 vol.% cenospheres was increased by 24.3 °C compared to the room temperature cured sample. The positive shift in T_g can be attributed to the beneficial impact of post-curing, as indicated by differential scanning calorimetry study. A water absorption study is carried out to characterize the efficiency of the HNTs RSF composites exposed to the marine environment. The HNTs addition considerably reduces the diffusion coefficient, sorption coefficient, and permeability of the syntactic foam composites. The compressive modulus of wet HNTs RSF composite registered a higher value than the corresponding sample without HNTs.

Dynamic mechanical analysis with temperature sweep (30 – 140 °C) reveal that the storage and loss modulus of RSFs is 1 - 36% and 59 - 113% higher than the neat epoxy. Storage modulus increases with an increase in cenospheres content in the epoxy matrix. However, with the incorporation of HNTs, the storage modulus obtained is higher than that of neat epoxy but still lower as compared to CESFs. With the increase in cenospheres content, loss modulus reduces due to increased frictional energy dissipation compared to matrix viscoelasticity. The thermal studies depict that the T_g value ameliorates with HNTs reinforcement. Also, better thermal stability with appreciable char content is reported from gravimetric analysis with HNTs addition. Further, to understand the underlying mechanism of filler interaction with the matrix, structure-property correlations of evaluated properties are presented using exhaustive SEM, FESEM, and TEM images.

Keywords: Halloysite nanotubes; Syntactic foam; Epoxy; Cenosphere; Post-curing; Mechanical properties; Thermal properties; Dynamic mechanical analysis.

TABLE OF CONTENTS

ACKNOWLEDGEMENTS	i
ABSTRACT.....	iii
LIST OF TABLES	ix
LIST OF FIGURES	xi
LIST OF ABBREVIATIONS	xv
1. INTRODUCTION	1
1.1 COMPOSITE MATERIALS.....	1
1.2 PARTICULATE COMPOSITES	2
1.3 FILLER MATERIALS	3
1.4 SYNTACTIC FOAM COMPOSITES	4
1.5 STRUCTURE OF SYNTACTIC FOAM COMPOSITES	6
1.6 REINFORCED SYNTACTIC FOAM COMPOSITES	7
1.7 STRUCTURE OF HALLOYSITE NANOTUBE (HNT)	8
1.8 PROCESSING OF REINFORCED SYNTACTIC FOAM COMPOSITES	10
1.9 POLYMER MATRIX AND ROLE OF CURING/AGING CONDITIONS	12
1.10 LITERATURE REVIEW	15
1.10.1 LITERATURE STUDY ON THE MECHANICAL RESPONSE OF COMPOSITES TO THE CURING CONDITIONS	16
1.10.2 LITERATURE REVIEW ON MECHANICAL BEHAVIOR OF COMPOSITES UNDER DIFFERENT LOADING CONDITIONS	19
1.10.3 LITERATURE STUDY ON DYNAMIC MECHANICAL ANALYSIS OF COMPOSITES	25
1.11 MOTIVATION OF WORK	28
1.12 OBJECTIVES AND SCOPE OF WORK	29
1.13 OUTLINE OF THESIS	30
2. MATERIALS, FABRICATION, AND CHARACTERIZATION TECHNIQUES.....	31
2.1 CONSTITUENTS.....	31
2.1.1 MATRIX	31
2.1.2 REINFORCEMENT.....	32

2.2	PARTICLE SIZE ANALYSIS, FTIR SPECTROSCOPY, AND X-RAY DIFFRACTION	35
2.3	DSC AND TG ANALYSIS	36
2.4	SAMPLE PREPARATION	37
2.5	DENSITY MEASUREMENT	41
2.6	POST-CURING OF SYNTACTIC FOAMS	41
2.7	TENSILE TESTING	41
2.8	FLEXURAL TESTING	42
2.9	COMPRESSION TESTING	44
2.10	DYNAMIC MECHANICAL ANALYSIS	45
2.11	MICROSCOPY	46
2.12	STANDARD DEVIATION AND ERROR MARGIN	47
3.	MECHANICAL BEHAVIOR OF REINFORCED SYNTACTIC FOAM COMPOSITES	49
3.1	FTIR STUDY	49
3.1.1	ANALYSIS OF FTIR SPECTRA OF ROOM TEMPERATURE CURED COMPOSITES	49
3.1.2	ANALYSIS OF FTIR SPECTRA OF POST-CURED COMPOSITES	50
3.2	XRD ANALYSIS	52
3.3	TENSILE RESPONSE	55
3.4	FLEXURAL RESPONSE OF ROOM TEMPERATURE CURED COMPOSITES	57
3.4.1	SPECTROSCOPY OF FRACTURE FEATURES OF POST-FLEXURAL TEST SPECIMENS	59
3.5	FLEXURAL RESPONSE OF POST-CURED COMPOSITES	63
3.6	COMPRESSIVE RESPONSE OF ROOM TEMPERATURE CURED AND POST-CURED COMPOSITES	68
3.6.1	MICROGRAPHIC IMAGE ANALYSIS OF POST-COMPRESSION TEST SPECIMENS	72
3.7	WATER ABSORPTION STUDIES	76
3.7.1	TRANSPORTATION COEFFICIENTS	78
3.7.2	ANALYSIS OF FTIR SPECTRA FOR WATER ABSORPTION	79
3.7.3	COMPRESSION BEHAVIOR OF WATER-IMMERSED RSF COMPOSITES	80
3.7.4	SPECTROSCOPY	82
3.8	SUMMARY	83

4.	VISCOELASTIC AND THERMAL STUDIES ON REINFORCED SYNTACTIC FOAMS COMPOSITES.....	85
4.1	DYNAMIC MECHANICAL ANALYSIS (DMA).....	85
4.1.1	STORAGE MODULUS	85
4.1.2	LOSS MODULUS.....	88
4.1.3	FRACTURE FEATURES OF DMA-TESTED SAMPLES	90
4.2	THERMOGRAVIMETRIC ANALYSIS (TGA).....	91
4.3	DIFFERENTIAL SCANNING CALORIMETRY (DSC) ANALYSIS	93
4.4	SUMMARY.....	94
5.	SUMMARY AND CONCLUSIONS	97
5.1	SUMMARY.....	97
5.2	CONCLUSIONS	97
	SCOPE OF FUTURE WORK	101
	REFERENCES.....	103
	CURRICULUM VITAE.....	123
	LIST OF PUBLICATIONS BASED ON THESIS.....	125

LIST OF TABLES

Table 2.1. Properties of epoxy resin and hardener.....	31
Table 2.2 Property details of cenospheres and halloysite nanotubes*.....	32
Table 3.1 Density and void content of room temperature cured RSF composites.	57
Table 3.2 Tensile modulus and strength properties of RSF composites.....	55
Table 3.3 Flexural modulus and strength properties of RSF composites.	58
Table 3.4 Flexural modulus and strength of room temperature cured and post-cure heated RSF composites.	67
Table 3.5 Compressive modulus and strength of room temperature cured and post-cure heated RSF composites.	70
Table 3.6 The maximum moisture absorption, diffusion coefficient, and permeability of neat epoxy and reinforced composites.....	79
Table 3.7 Compressive modulus and strength of dry and wet RSF composites.....	81
Table 4.1 Comparison of storage modulus at four representative temperatures.....	88
Table 4.2 Maximum loss modulus, room temperature loss modulus, and glass transition temperature (T_g) of all samples.....	90
Table 4.3 Degradation temperature values for 10, 30, and 50% mass loss in RSF composites.....	92
Table 4.4 Glass transition temperature values obtained from DSC analysis signifying the advantage of post-cure heating effect in RSF composites.	94

LIST OF FIGURES

Figure 1.1 Particulate composites reinforced with (a) hollow filler, (b) nanotubes, and (c) short fibers.	3
Figure 1.2 SEM image of as-received cenospheres depicting its shape and size.	5
Figure 1.3 Graphite-Epoxy Inboard Aileron on L-1011 Aircraft (Tenney et al. 2011). 6	
Figure 1.4 Depiction of schematic structure and (b) SEM micrograph of syntactic foam composite.	6
Figure 1.5 Depiction of SEM micrograph of syntactic foam composite.	7
Figure 1.6 Schematic representation of reinforced syntactic foam composite.	8
Figure 1.7 HNT structure in an epoxy nanocomposite.	10
Figure 1.8 Illustration of probe sonication process.	11
Figure 1.9 Illustration of syntactic foam composite fabrication steps.	12
Figure 1.10 Origin of physical aging as explained from a thermodynamic point of view (Kong 1986).	14
Figure 2.1 Chemical structure of (a) epoxy resin (LY556) and (b) hardener (HY951).	32
Figure 2.2 (a) Cenospheres, (b) Halloysite nanotubes, and (c) Epoxy resin and hardener.	34
Figure 2.3 FESEM image of as-received (a) cenospheres and (b) HNTs.	34
Figure 2.4 FTIR spectroscopy test setup.	35
Figure 2.5 XRD test setup.	36
Figure 2.6 DSC test setup.	37
Figure 2.7 TG analysis setup.	37
Figure 2.8 Casting mold for the sample fabrication.	40
Figure 2.9 Tensile setup.	43
Figure 2.10 Three-point bending test setup.	44
Figure 2.11 Compression test setup.	45
Figure 2.12 (a) DMA setup (b) test configuration.	46
Figure 3.1 FTIR spectra of neat epoxy, CESF, and RSF composites.	50
Figure 3.2 (a) FTIR spectra of neat epoxy and RSF composites, with an enlarged view reporting synergism between fillers and the epoxy as depicted in (b), and comparison	

of relative absorbance between the foams signifying advantage of post-cure treatment shown in (c).....	52
Figure 3.3 (a) XRD spectra of neat epoxy, pristine cenosphere, HNTs, and HNTs RSF composite, (b) TEM image depicting the occupancy of the epoxy network in the HNT lumen.....	53
Figure 3.4 TEM images showing (a) HNTs hollow structure, (b) planar dispersion of HNTs, and (c) loosely held HNTs.	54
Figure 3.5 Experimentally measured (a) tensile modulus (b) specific tensile modulus (c) tensile strength and (d) specific tensile strength of RSF composites.	57
Figure 3.6 Experimentally measured (a) flexural modulus (b) specific flexural modulus (c) flexural strength and (d) specific flexural strength of RSF composites.	59
Figure 3.7 Morphology of post flexural test specimens (a) Neat Epoxy (b) SF20, showing rough matrix failure (c) NSF20, displaying intactness of cenospheres within the matrix.	60
Figure 3.8 Morphology of post flexural test specimens (a) SF50, showing poor bondage and breakage of cenospheres in the matrix (b) NSF50, showing cenospheres intact with the matrix.	60
Figure 3.9 Schematic micrographs of SF40 post-flexural test specimen.....	61
Figure 3.10 Schematic micrographs of NSF40 post-flexural test specimen.....	62
Figure 3.11 Morphology of NSF40 post-flexural test specimens depicting (a) Crushing of fly ash cenosphere, (b) Presence of porosity within thin cenosphere walls, (c) Representative void introduced by entrapped volatiles, (d) Crack deflection in the matrix due to HNTs, and (e) deformation consolidation by HNTs.	63
Figure 3.12 The density of the RSF composites.	64
Figure 3.13 Flexural stress-strain curve of post-cure heated RSF composites.	65
Figure 3.14 Shows (a) flexural modulus (b) flexural strength (c) specific flexural modulus (d) specific flexural strength, for room temperature cured and post-cure heated RSF composites.	66
Figure 3.15 Compression stress-strain curves of (a) room temperature cured and (b) post-cure heated RSF composites.	68

Figure 3.16 Shows (a) compressive modulus (b) compressive strength (c) specific compressive modulus (d) specific compressive strength, for room temperature cured and post-cure heated RSF composites.	72
Figure 3.17 Morphology of (a) SF0, (b) SF20, (c) NSF20, (d) SF40, and (e) NSF40 post-compression test samples show the modification of matrix properties by HNTs inclusion.....	73
Figure 3.18 (a) SEM image of NSF40 post-compression test sample showing pull-out mechanism and (b) showing crack pinning mechanism of the HNT in the reinforced composites.....	75
Figure 3.19 Fracture features of post-compression test depicting possible fabrication challenges of the HNTs RSF composites.....	76
Figure 3.20 Water absorption of neat epoxy and reinforced composites.	77
Figure 3.21 Swelling thickness of neat epoxy and reinforced composites.	77
Figure 3.22 FTIR spectra of (a) neat epoxy, (b) SF40, and (c) NSF40 dry and wet samples.....	80
Figure 3.23 Compressive stress-strain curve of wet RSF composites.	81
Figure 3.24 Experimentally measured (a) Compressive modulus and (b) compressive strength of wet RSF composites.	82
Figure 3.25 Fracture features of (a) SF0_W, (b) SF40_W, and (c) NSF40_W RSF composites.....	83
Figure 4.1 Schematic representation of the variation of storage modulus against temperature.	86
Figure 4.2 Experimentally measured storage modulus values of (a) CESF and (b) HNTs RSF composites.	87
Figure 4.3 Experimentally measured loss modulus values of (a) CESF and (b) HNTs RSF composites.	89
Figure 4.4 Micrographs display fracture features of (a) Neat epoxy (b) SF20 (c) NSF20 (d) SF50 and (e) NSF50 post-DMA tests.	91
Figure 4.5 TGA curves of room temperature cured RSF composites.....	92
Figure 4.6 DSC curves of room temperature cured and post-cure heated RSF composites.....	94

LIST OF ABBREVIATIONS

Halloysite nanotubes	HNTs
Syntactic foam	SF
Cenosphere epoxy syntactic foam	CESF
Reinforced syntactic foam	RSF
Halloysite nanotubes reinforced syntactic foam	HNTs RSF
Carbon nanotubes	CNTs
Fourier transform infrared spectroscopy	FTIR
X-ray Diffraction	XRD
Differential scanning calorimetry	DSC
Scanning electron microscopy	SEM
Field emission scanning electron microscopy	FESEM
Transmission electron microscopy	TEM
Thermogravimetric analysis	TGA

CHAPTER 1

1. INTRODUCTION

1.1 COMPOSITE MATERIALS

In the course of human civilization, man has always attempted to meet ever-evolving needs of increasing levels of complexity. The geographical location of the ancient Mesopotamians made it possible for them to make heat-resistant, thermally stable, and aesthetically superior goods. Utilizing existing raw materials and transforming them into valuable goods has long been a fundamental principle. Materials are entities that go into making tools that improve human life. The use of two different phase materials combined to produce a value-added product with desirable properties that are superior to the separate components is what is often meant by the term "composite material." Composite material is defined as "the macroscopic combination of two or more distinct materials with a discernible interface"(Gauthier 1995). The term 'light weighting gained its significance when the composites came into existence and performed at par with traditional monolithic materials. The lightweight embedment of any engineering structure is crucial to decide its performance during design process (Pervaiz et al. 2016; Yang and Zhao 2015). The principal motive of emerging technologies is to obtain optimum performance in structures with energy-saving potential besides generating a circular economy. Right from current electric vehicle technology to space transportation, weight is the sensitive parameter in the design scenario (Czerwinski 2021; Pervaiz et al. 2016; Zhang et al. 2014). Composite materials are commonly used to improve mechanical properties of materials so they can withstand greater service loads. Composite materials can augment properties like strength, stiffness, corrosion and wear resistance, weight reduction, fatigue life, temperature-dependent behavior, and thermal properties. Due to their lightweight and high strength, composite materials are used extensively in aerospace, marine, and automobile industries (Fiore et al. 2011; Liu et al. 2014; Nunes and Silva 2016). A significant number of composites are used in almost all modes of transportation and sports equipment (Chauhan et al. 2022; González et al. 2017; Ullah et al. 2015; Wang et al. 2017).

Composites are categorized by their matrix and reinforcing phases. Matrix phase is continuous, while the reinforcement phase is dispersed or discontinuous. The composite's third phase is the interface between matrix phase and reinforcement. Composites can be categorized based on the matrix material as Metal matrix composite (MMC), Ceramic matrix composite (CMC), and Polymer matrix composite (PMC). PMCs are becoming attractive materials for various structural and automotive applications due to their advantageous mechanical property combinations (Barbero 2018). Due to their relative ease of production, low density, good electrical/thermal properties, and superior chemical/corrosion resistance, PMCs are widely employed in most industrial applications. Consequently, their applications range from specialist functions in aerospace and electronics engineering to consumer industries such as building and transportation (Dhanasekar et al. 2022; Liang et al. 2021; Sharma et al. 2019; Wang et al. 2017).

PMCs are composed of thermoplastic or thermosetting resin that is reinforced with filler (fiber, particle, etc.). These materials are capable of being molded into a range of forms and sizes. As a result of decreased density of its constituents, polymer composites frequently exhibit superior specific characteristics. Specifically, a polymer matrix has low strength and stiffness when compared to metal and ceramic. This means that there is a significant advantage achieved by reinforcing polymers with reinforcements such that they possess specific features. There is no need for high pressures and temperatures during the production of PMCs. Compared to composites with other matrices, PMCs are less susceptible to problems connected with the deterioration of reinforcement during production. Additionally, the equipment required for PMCs is less complex. As a result, PMCs evolved swiftly and were quickly adopted for structural applications.

1.2 PARTICULATE COMPOSITES

Sandwich composites use particulate composites as a core material. The incorporation of particle fillers into epoxies results in several advantageous features, including reduced density, greater impact strength, appropriate magnetic and electrical properties, excellent damage tolerance, and a lower price (Forintos and Czigany, 2019;

Li et al., 2013; Shakil et al. 2020; Wang et al. 2017b). Because of these properties, particle composites can be beneficial in applications that are sensitive to weight, such as construction of airplanes, as well as applications that are prone to damage, such as packaging (Agrawal and Satapathy 2019; Lee et al. 2022). High specific compressive strength and bending stiffness are particular benefits of sandwich structures with a core made of composite materials, including particle fillers (Dogan 2021; Omar et al. 2015; Pareta et al. 2020). Figure 1.1 schematically represents the three kinds of particulate composites with fillers as hollow particles, nanotubes, and short fibers.

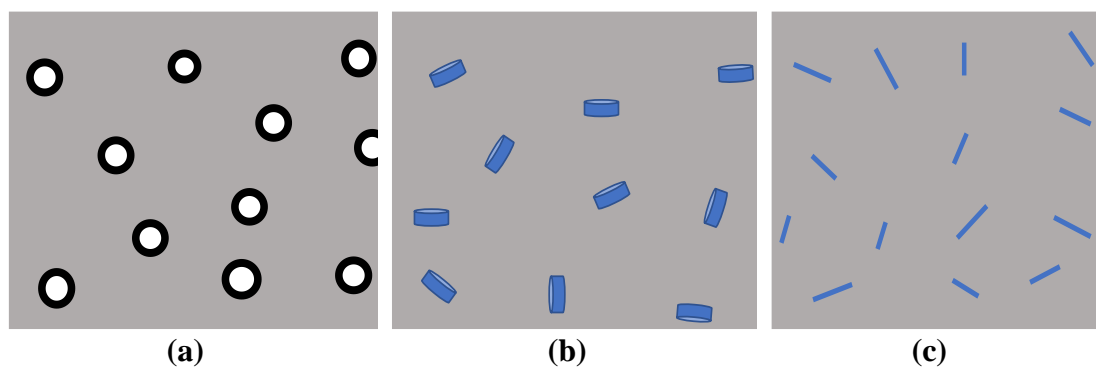


Figure 1.1 Particulate composites reinforced with (a) hollow filler, (b) nanotubes, and (c) short fibers.

1.3 FILLER MATERIALS

Numerous types of particles are utilized as fillers in composites (Platzer 1988). Fillers are used for a variety of reasons, ranging from reducing cost of pricey polymeric components to modifying their strength, magnetic, electrical, or fire-retardant qualities, as required by their intended uses. As fillers for polymers, a vast range of substances can be chosen, including mineral, metal, ceramic, polymer, and industrial waste particles (Gupta et al. 2001). Examples of common filler materials include alumina, silica, hollow and solid glass particles, wood chips, fly ash, and carbon black. The selection of materials is primarily determined by composite's intended qualities. The shape of the filler particles plays a significant impact in influencing qualities of the composite; hence, particles are often categorized according to their shapes. Common shapes include spherical, cubical, blocklike, flaky, and fibrous. These forms have varying surface areas for same volume, which influences the size of interfacial zone between the particle and matrix resin. Due to the various corner radius of curvature and

aspect ratios of each of these forms, stress concentration factor would vary for each. Popularity favors spherical particle fillers over other varieties. In recent years, use of cenospheres, which are hollow spherical particles, has expanded significantly in the creation of core materials with low density and excellent damage tolerance (Danish and Mosaberpanah 2020; Kumar and Ahmed 2016; Pareta et al. 2020; Waddar et al. 2018). These low-density substances are categorized as close-cell foams and are known as "Syntactic Foams." By regulating the constituent or density of cenospheres, density of syntactic foams can be modified over a broad range suiting it for weight-sensitive applications.

1.4 SYNTACTIC FOAM COMPOSITES

Since the 1960s, progress in hollow particle inclusion has fostered an excellent strength-to-weight ratio and better thermal properties (Samsudin et al. 2011). Hollow fillers comprise a cavity within their structure when dispersed in polymers, making them porous, eventually enhancing buoyancy and maritime industrial applications. According to recent data published by the Central Electricity Authority (CEA) of India, consumption of coal in India for the year 2021 by thermal power plants from April to September stood at 313 million tons (MT), which generated 106.37 MT of fly ash. ("Govt notifies norms for fly ash utilization by coal-fired power plants - The Hindu BusinessLine" 2022.) The cenosphere is a constituent of fly ash byproduct when used as a functional hollow filler, as shown in Figure 1.2, improves mechanical (Gupta et al. 2004; Kaur and Jayakumari 2016, 2019; Shahapurkar et al. 2019) and thermal (Gangwar and Pathak 2021; Labella et al. 2014; Ren et al. 2018) properties of polymer syntactic foams.

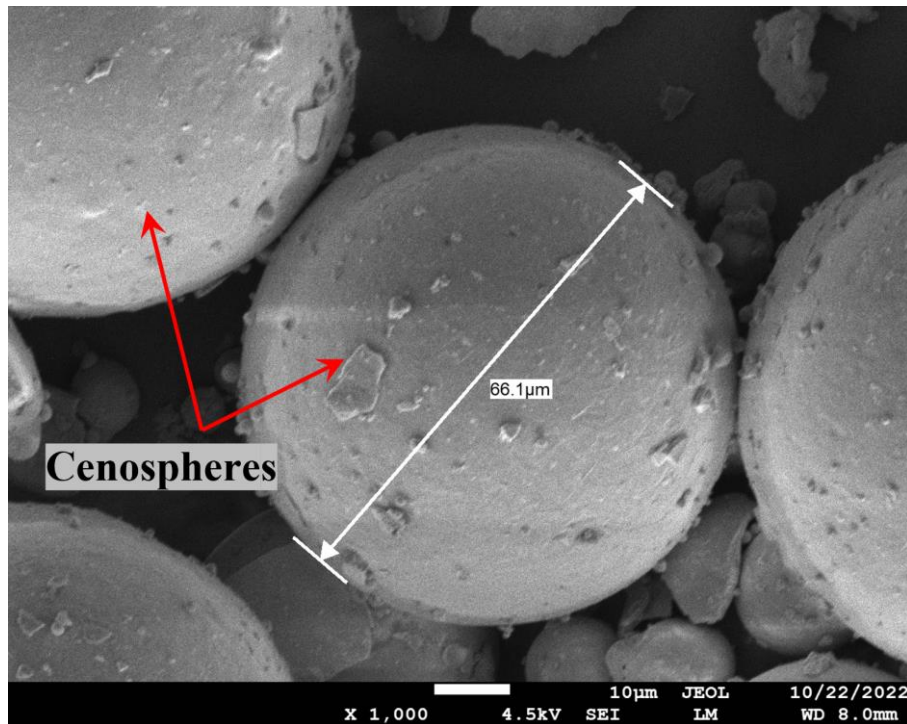


Figure 1.2 SEM image of as-received cenospheres depicting its shape and size.

Syntactic foams are distinguished by their high specific compressive strength, minimal moisture absorption, and superior damping characteristics. They are used as core member in sandwich composites for weight-sensitive engineering structures. Due to their wide-ranging mechanical properties, vibration damping properties, fire resistance, and flexibility to be produced in functionally graded forms, these foams are composite materials with multiple functions (Waddar et al. 2018). In the 1960s, these buoyancy aid materials were developed for deep water applications (Wright 1991). Currently, they are applied to aircraft, spacecraft, and marine structures (Bardella & Genna, 2001; Tenney et al., 2011), as schematically shown in Figure 1.3. One of their primary advantages is capacity to design and produce syntactic foams according to the application's physical and mechanical property requirements. Depending on service conditions, the matrix resin can be selected from a wide variety of thermosetting and thermoplastic resins. Similarly, cenospheres can be selected from polymer, ceramic, or metal (Feldman 1993; Nielsen 1966). The volume fractions of matrix and cenospheres within the structure are additional parameters that can be modified.

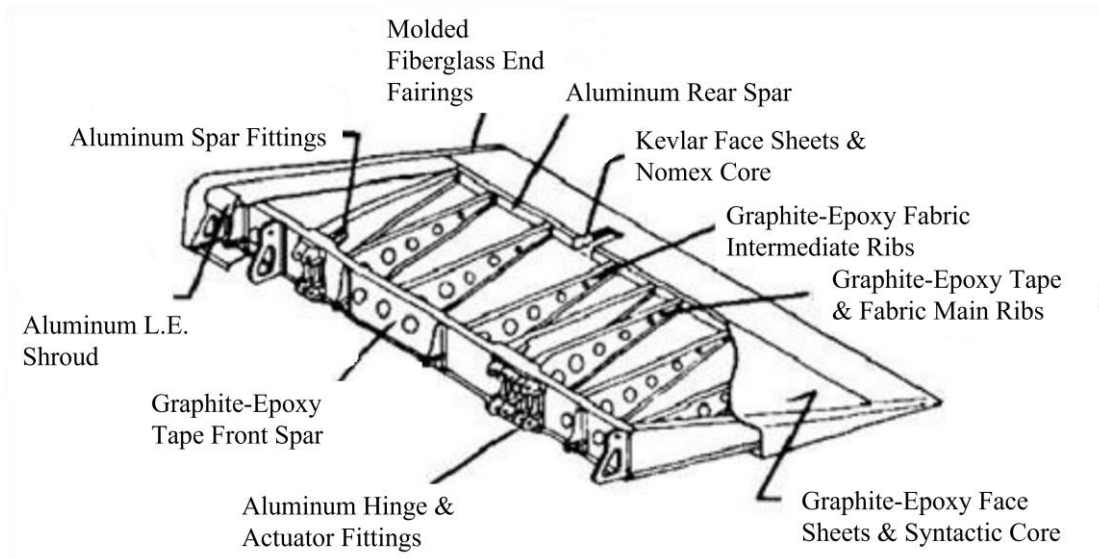


Figure 1.3 Graphite-Epoxy Inboard Aileron on L-1011 Aircraft (Tenney et al. 2011).

1.5 STRUCTURE OF SYNTACTIC FOAM COMPOSITES

Syntactic foams are composed of two distinct phases: matrix resin and fly ash cenospheres, as shown schematically in Figure 1.4. Micrograph portraying the structure of the syntactic foam is shown in Figure 1.5. Micrography is conducted on the cut surface of a sample of syntactic foam. The images reveals the cenospheres embedded within the matrix resin.

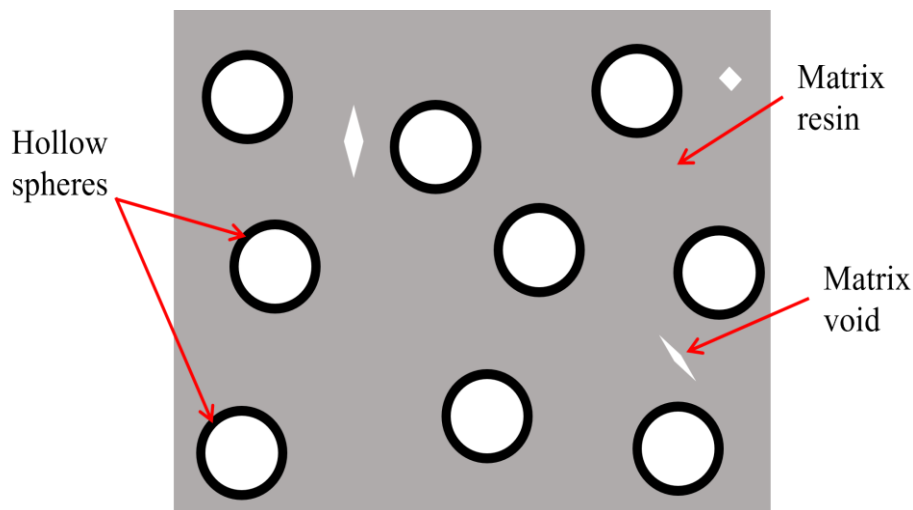


Figure 1.4 Depiction of schematic structure of a syntactic foam composite.

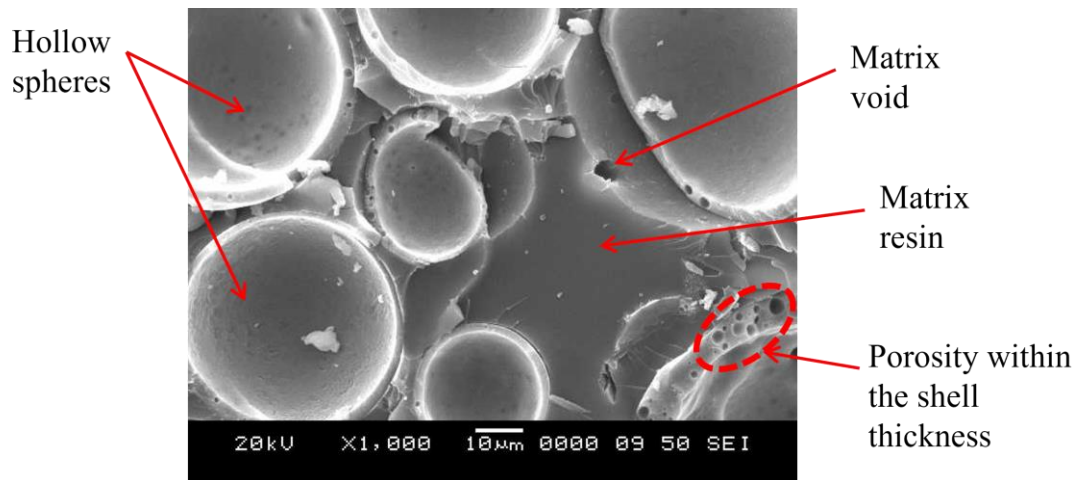


Figure 1.5 Depiction of SEM micrograph of syntactic foam composite.

Figure 1.5 depicts a three-phase structure, including voids in a matrix resin. During fabrication process, the air is invariably trapped in the microstructure of syntactic foams and appears as open-cell structured porosity. This trapped air is known as voids, and this makes syntactic foams three-phase materials. Also, the cenosphere (hollow sphere) has a porosity within its wall, as shown in Figure 1.5. This, in turn, makes the reinforcement applicable to weight-sensitive structural application.

1.6 REINFORCED SYNTACTIC FOAM COMPOSITES

Properties beyond those of plain syntactic foams, which include only hollow particles in a matrix resin, can be produced by adding micro- and nano-scale reinforcements (Gupta et al. 2013), as shown in Figure 1.6. For making reinforced syntactic foams, phenolic, vinyl-ester, and epoxy resins are frequently employed. The domain of multiscale reinforced composites has benefited significantly from recent developments in nanomaterials science and technology.

Syntactic foams are a helpful tooling material in the composites sector due to their low coefficients of thermal expansion and lightweight (Gupta et al. 2014). Syntactic foam tooling materials that can be utilized for laminate fabrication can be quickly and affordably machined due to the material's ease of usage. The US used syntactic foams' thermal insulation capabilities in space shuttle applications for the first time (Hodge et al. 2000). Solid rocket boosters and the exterior fuel tank were insulated using syntactic foams (Gupta et al. 2014). Carbon nanofibers and other nanomaterial

reinforced syntactic foams have been used, according to Air Force Research Laboratory for space reflectors. These materials can reach a zero or negative thermal expansion coefficient, which helps prevent geometrical distortion. In order to improve thermal conductivity of syntactic foams and maintain a constant temperature, carbon nanofibers were also utilized (Poveda et al. 2013).

Many studies have worked with incorporating secondary fillers to produce high-performance reinforced syntactic foam (RSF) (Ghamsari et al. 2015; Bao et al. 2020; Liu et al. 2019; Saha and Nilufar 2009; Suresha et al. 2006; Ullas et al. 2016; Wang et al. 2012; Wouterson et al. 2007; Yu et al. 2019). In order to improve value-added properties of syntactic foams, reinforcement was incorporated that ranged from fiber (Huang et al. 2006) to nano-level additions (Maharsia et al. 2006). Saha and Nilufar (2009) investigated the flexural and thermal properties of montmorillonite nanoclay reinforced syntactic foam. Glass microballoons were the hollow filler added to base epoxy matrix. Meanwhile, nanoclay reinforced syntactic foam has just recently been studied, despite being a proven effective reinforcement for polymers (Maharsia et al. 2006; Peter and Woldeesenbet 2008). Analyzing potential synergistic activity in hybrid syntactic foams made of a matrix, hollow microspheres, and nanoclay particles might be intriguing.

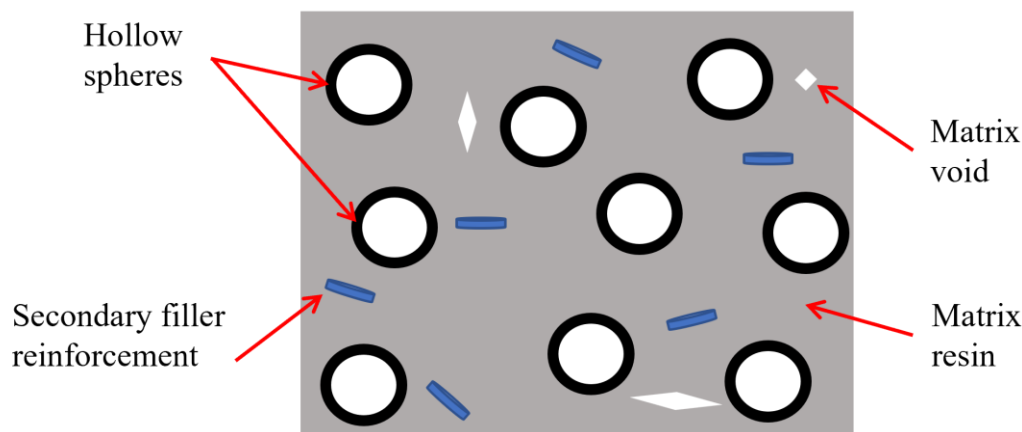


Figure 1.6 Schematic representation of reinforced syntactic foam composite.

1.7 STRUCTURE OF HALLOYSITE NANOTUBE (HNT)

Halloysite nanotubes (HNTs), a member of nanoclay family, analogous crystal structure to carbon nanotubes (CNTs) are useful in developing high-performance epoxy

composites that are of low cost and abundantly available (Woldesenbet 2008; Peter and Woldesenbet 2008). The HNTs possess positively charged aluminols at inner surface and negatively charged silicon oxides at outer surface. This difference in the chemistry of the surface allows them to easily functionalize their lumen, which is difficult for CNTs (Lvov et al. 2016). It was also reported that the issue of exfoliation or intercalation can be avoided in HNTs, as compared to other types of clays like montmorillonite, bentonite, and graphene sheets (Dando and Salem 2017). HNTs may be added to nanocomposites to improve their mechanical and thermal characteristics, as it is elucidated in various research studies. (Bai et al. 2020; Deng et al. 2009; Du et al. 2010; Prashantha et al. 2011a; Srivastava and Pandey 2019; Tang et al. 2011). Also, studies have shown that HNTs outperform in tensile property and thermal stability compared to modified silica reinforced in natural rubber (Rooj et al. 2010).

As shown in Figure 1.7, the HNTs are 1:1 phyllosilicates with one outer tetrahedral sheet with Si-O-Si and an inner octahedral sheet with Al-OH. These inorganic nanotubes are 1D tubular in shape, have good biocompatibility, rich functionality, high aspect ratio, and possess high mechanical strength. Eventually, it enhances properties of resultant nanocomposites, such as modulus and the coefficient of thermal expansion (Woldesenbet 2008; Ye et al. 2007). In most sandwich composites, the core is comprised of syntactic foam; hence, the rupture in the matrix causes the failure of core, thereby calling a need for matrix toughening. In such cases, HNTs may stand as a promising toughening agent in the epoxy nanocomposites without sacrificing other properties. Studies reported the improvement of impact strength with 4 vol. % TiO_2 nanoparticles in TiO_2 /epoxy nanocomposites by ~35% and 3 wt.% of montmorillonite (MMT) in MMT/epoxy nanocomposites by ~60%, whereas the impact strength improved by ~400% with only 2.3 wt. % of HNTs (Ye et al. 2007). This remains as one of the factors in choosing HNTs in anticipation of improvement in properties of syntactic foams for weight-sensitive applications. Additionally, in comparison with other nanoparticles such as fumed silica, carbon nanotubes, and MMT reinforcement in nanocomposites, the HNTs possess rod-like geometry, which disperses easily owing to its confined inter-tubular contact area (Du et al. 2010). The vital role of the nanoscale

fillers lies in improving properties of the matrix resin without considerably increasing the density of the composite.

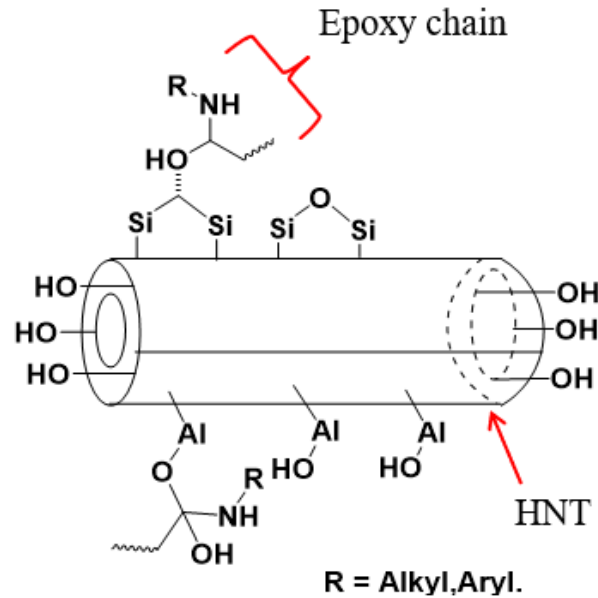


Figure 1.7 HNT structure in an epoxy nanocomposite.

1.8 PROCESSING OF REINFORCED SYNTACTIC FOAM COMPOSITES

Every material system possesses distinct physical, mechanical, and processing properties. To turn the material into its final form, an appropriate manufacturing technique must be selected. In latter half of the 20th century, the processes employed for manufacturing of composite materials-based products shifted from skilled labor operations to sophisticated microprocessor systems with automatically controlled equipment. Early pioneers employed hand lay-up techniques or spray-up in open molds to construct final system by combining raw components and curing them at room temperature. The advantages of polymer matrix composites have propelled these synthetic materials into practically every other business in the globe, from consumer products and automobiles to aircraft and bridges in weight-saving potentials. Such an expansion in product applications necessitated an expansion in materials technology, design methodologies, and production techniques (Arza Seidel 2012).

Efficient nanofiller dispersion in a matrix resin system is vital in achieving the intended property augmentation by the secondary filler reinforcement in syntactic foam

composites (Bittmann et al. 2009; Mahrholz et al. 2009). There are numerous methods for dispersing particle agglomerates in a liquid, with dissolver and bead mill being the most often used machinery (Bittmann et al. 2009). Dispersion by ultrasonic waves is a further possibility. As illustrated in Figure 1.8, high-intensity ultrasonic waves are discharged into a liquid particle-matrix mixture, where cavitation bubbles can form and increase over multiple cycles until they reach a critical diameter, which causes their implosion. This collapse generates locally extreme conditions, such as extremely high pressure and temperatures, a so-called hotspot (Xu et al. 2004). Due to these hotspots, particle agglomerates might get dispersed. The combination of shock waves from an implosive bubble collapse and micro-streaming caused by cavitation oscillations results in dispersion effects (Bittmann et al. 2009).

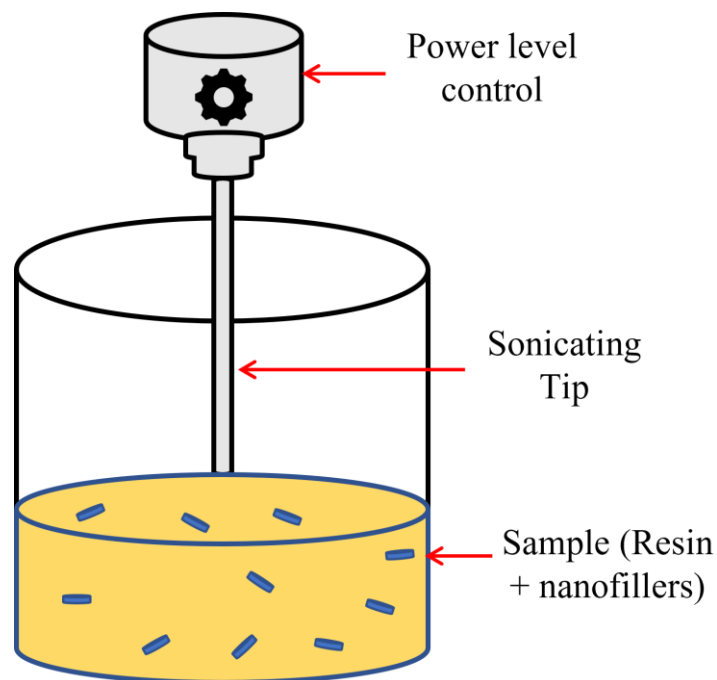


Figure 1.8 Illustration of probe sonication process.

When producing syntactic foam composites, the processing approach must be meticulously developed to reinforce hollow particles to prevent particle breakage. Also, undesired impact of a more porous matrix can be avoided by stabilizing gas bubbles in a polymer matrix. The processing procedures must be effective enough to facilitate reinforcement wetting by matrix resin, break clusters without harming reinforcement, and provide uniform reinforcement dispersion in a resin matrix.

Figure 1.9 depicts a typical process for fabricating thermoset-based syntactic foams. This approach employs a two-step mixing procedure. In the first phase, reinforcement (hollow microballoons) is added to resin and carefully mixed until a slurry of constant viscosity is achieved. In the second phase, the resin is progressively mixed with hardener or catalyst. The slurry is poured into the molds and cured per the resin's specifications.

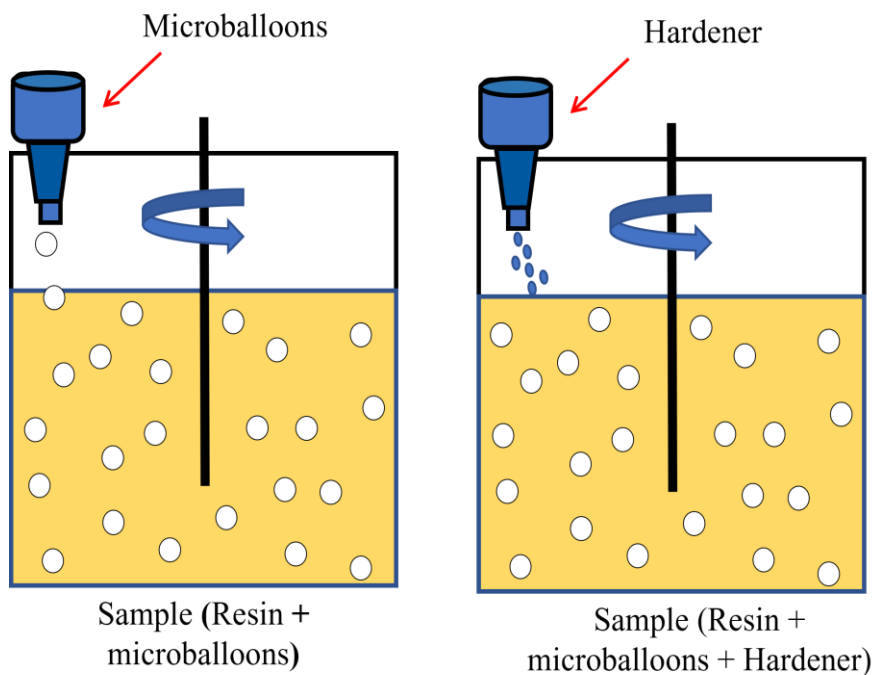


Figure 1.9 Illustration of syntactic foam composite fabrication steps.

1.9 POLYMER MATRIX AND ROLE OF CURING/AGING CONDITIONS

The long-chain organic macromolecules or polymers have numerous desirable characteristics, including high ductility, ease of formation, and non-corrosiveness. A designer has access to a large array of these materials. Thermosetting and thermoplastic polymers are examples of two such classes. Its first intended use was in aircraft industries, but it later became an effective replacement material in the sporting goods, automotive, and construction-related sectors (Gokhale et al. 2011; Mallik et al. 2011). In addition to Van der Waals forces, thermosetting polymers also contain covalent cross bonds (cross links) between molecules. These cross-bonds cause a thermosetting polymer to stay stiff after heating. The characteristics of thermoplastic polymers can be

altered repeatedly by heating and cooling them. They become softer when heated and hard when cooled. Thermosets, however, maintain their rigidity after warming until they are transformed into char. The relatively modest Van der Waals forces that operate between the molecules of thermoplastic polymers cause changes in their behavior upon heating. The molecular bonds significantly weaken with heat, making the substance pliable and soft.

Epoxy thermosetting resin is one of the most common polymeric matrix materials. It is available in a broad spectrum of formulations, ranging from low-viscosity liquids to high-melting solids, and can be adapted to various changes and processes. It provides high strength, minimal shrinkage, ease of curing by a range of chemical agents, great electrical insulation, excellent adhesion, and surface wetting (Bilyeu et al. 1999; Xiang and Xiao 2020). These attributes make epoxies appropriate for many usages in composites. Epoxy resins use the crosslinking of epoxide groups (one oxygen and two carbon atoms). The epoxy resins can be cured for usage at elevated temperatures by introducing chemical agents that produce an inflexible molecular structure. For composite applications, epoxies from phenolic glycidyl ether, aromatic glycidyl amine, and cycloaliphatic classes are most commonly used. Diglycidyl ether of bisphenol A (DGEBA), a kind of phenolic glycidyl ether, is the most commonly used epoxy. As hardeners for epoxy resins, most common curing agents are amines, amine derivatives, or anhydrides. Modifiers are compounds that can be used to alter mechanical and physical properties of cured or uncured resins. Rubbers, thermoplastics, fillers, flame retardants, and pigments are included as modifiers. Even though PMCs have higher initial material costs, low-cost versions could be created by combining plastic fillers with inexpensive environmental pollutants, such as cenospheres. Since 1991, when the Indian economy was liberalized, plastic consumption has increased dramatically. From 0.85 million tonnes in 1990 - 1991 to 1.79 million tonnes in 1995 - 1996, India's plastic consumption has increased by more than twofold. Demand for commodity plastics is growing annually at a rate of 15% (Shekhar 2012). With such a dramatic increase in the consumption of plastic, thermosetting syntactic foam composites with abundantly available fillers, such as fly ash cenospheres, may be

necessary to alleviate concerns regarding plastic management and environmental concerns associated with the disposal of fly ash from thermal power plants.

Simon (1931) published his findings that tiny molecules in their amorphous solid state do not maintain thermodynamic equilibrium at temperatures lower than their glass transition. In reality, these substances are supercooled liquids, and their volume, enthalpy, and entropy are all higher than they would be if they were contained in equilibrium, as shown in Figure 1.10. The free-volume idea provides a simple starting point for an explanation of a process of physical aging (Yoshida et al. 1982). This is a fundamental and self-evident principle that the chain mobility of macromolecules in a system that is densely packed is essentially governed by the degree of packing in a system. Consequently, the chain mobility quantification is inversely proportional to the degree of packing. In a similar vein, one could think of mobility as being exactly proportional to free volume. The idea of free volume can also be utilized in a qualitative meaning (Kong 1986).

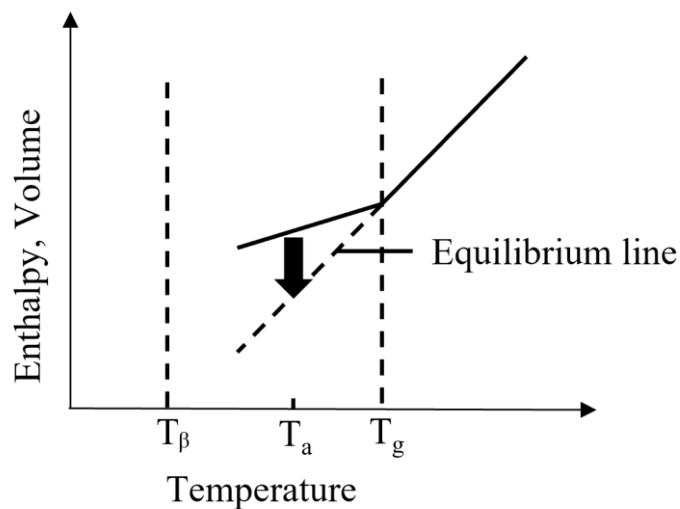


Figure 1.10 Origin of physical aging as explained from a thermodynamic point of view (Kong 1986)

The thermosetting epoxies consist of four phases, i.e., liquid, gelled rubbery, gelled glassy, and ungelled glassy states, based upon the gelation and vitrification of polymers (Chan et al. 1984). A sufficient amount of curing enhances crosslinking of such compounds. Meanwhile, one has to be careful about monomer degradation when thermally treated for a long time at elevated temperatures. Notable research has been

carried out in studying the influence of post-curing treatment on the morphological, mechanical, and thermal properties of polymer composites (Pattanaik et al. 2019; Sharma et al. 2019). Vidil et al. (2016) emphasized controlled polymerization of epoxy thermosets while taking the gel-point into account to produce well-defined chemistry of the polymer network. Also, it was reported that post-baking systems enable complete epoxy conversion that enhances thermo-mechanical properties. Khan et al. (2013) investigated sandwich structures with styrofoam and honeycomb as core members. They described that the compressive and flexural properties were enhanced by post-curing at 70 °C for 2 hours because of relief in thermal stresses that improved its crosslinking density. (Yuan et al. 2020) successfully fabricated hollow microspheres in the epoxy matrix. These syntactic foams were surface modified and exposed to heat treatments. It was concluded that, designed formulations of syntactic foam enhanced fracture toughness and compressive properties. (Wang and Gillham 1993) studied the effect of physical aging on thermosets by considering the variation in physical properties. They concluded that an anomaly exists in the isothermal modulus with the extent of cure. Also, it was pointed out that the T_g value is prominent in correlating properties rather than epoxies conversion in the system.

1.10 LITERATURE REVIEW

Reinforced syntactic foams are lightweight composites widely employed in various applications to reduce the weight of engineering structures. The degree to which they can be modified to provide a desired mechanical performance depends profoundly on the effective characteristics produced and more significantly, the relationship between these qualities and the microstructure. Therefore, analyzing the mechanical, thermal, and other pertinent properties of a certain microstructure and their spatial distribution is crucial for creating these lightweight syntactic foam composites. Recent reviews on a variety of syntactic foam topics under various curing/aging and loading situations have been published and are discussed in the following section.

1.10.1 LITERATURE STUDY ON THE MECHANICAL RESPONSE OF COMPOSITES TO THE CURING CONDITIONS

There is continual concern about how operational conditions may affect long-term durability of structural components made of polymer composites. In the early 1980s, Chan et al. (1984) threw light on cure kinetics and degradation of epoxy resin with triglycidyl ether of tris (hydroxyphenyl) methane diamino diphenyl sulfone using melt mixing the formulations. Their study revealed that fully cured di- and trifunctional epoxy materials' highest glass transition temperatures (T_g) were 229 °C and > 324 °C, respectively. Also, the isothermal time-temperature-transformation (TTT) diagrams were generalized to display gelation, vitrification, reduction in T_g , and char formation. The first event, which is witnessed by a reduction in rigidity, is devitrification of glass into rubber and is represented by a reduction in T_g from a higher to lower value of the isothermal temperature of cure. Later tensile and fracture properties of Epon-828 with a varied formulation of meta phenylene diamine: 7.5, 10, 14.5, 20, and 25 phr were experimented with by Gupta et al. (1985). They observed that in the glassy state, stiffness and yield point influence the molecular architecture. Also, crosslink density has a predominant effect on stiffness in the rubbery state. Further, in a glassy state, properties such as toughness, elongation-to-break, and strength are governed by intermolecular packing. Moreover, the toughness of sample increases with post-curing procedure, and low extension-to-break and low toughness characterize samples rich in epoxy. Cañavate et al. (2000) emphasized the curing kinetics of epoxy with isophorondiamine hardener. They noticed that linkages that are not involved in the reaction were indicated by the FTIR bands' continued invariance during curing. Thus, in contrast to invariable ones that serve as a quantitative reference, the relationships between the indicative bands of the reaction process (863 and 917 cm^{-1}) have been used as markers of resin curing. Also, they stated that as the amount of the curing agent was increased, the gelation time of the epoxies rapidly reduced.

Further, the study was carried out to analyze the effect of post-cure in epoxy carbon fiber composites by Khan et al. (2013). They employed a wet lay-up technique to impregnate woven carbon (0 and 90°) fiber with poly-epoxy to quantify compressive, flexural, and thermal properties. They presented that for average crashed energy

absorption, the effect of post-cure was noticed to be statistically insignificant, irrespective of the core material in the composites. Alongside this, the compressive strength in styrofoam and honeycomb core sandwich composites was ameliorated with post-curing process. Additionally, due to improved adhesion between the skin-core interface by post-curing, the bending stress exhibited an appreciable magnitude improvement. Also, T_g value augmentation was noticed for post-cure specimens compared to room-temperature cured panels. Bhanushali et al. (2017) fabricated carbon fiber composite prepreg (Hexply) with a manual lay-up method to study the bond strength by incorporating contaminants and defects. They affirmed that the contaminant introduced in the central bond area of lap joints reduced the bonding strength. And the kissing bond defect reported the lowest reduction in strength of the composite specimen. They stated that curing influenced the bond strength further the rapid cure resulted in a 50% reduction in the failure load. Similarly, the study on epoxy resin (DER 332) and iso-phorone diamine (IPDA) hardener was carried out by reinforcing natural fiber, i.e., flax fabric by Campana et al. (2018). These researchers processed unidirectional flax fabric with epoxy to characterize the tensile and glass transition temperature. In their study, the composites were post-cured for temperature values 100, 120, and 150 °C. Among these, samples post-cured at 150 °C reported 100% crosslinking with 167 °C T_g . It was recorded that, higher post-cure temperature decreased tensile strength and also elongation to break.

Particulate composites, like syntactic foams, are also subjected to property modulation because of the effect that environmental variability has on polymer matrix's behavior. In this concern, Shahapurkar et al. (2018) estimated the effect of arctic conditioning on syntactic foams' flexural properties, emphasizing density reductions in formulations considering lapox (L-12) syntactic foam. In their study, the cenospheres content varied as 20 vol.%, 40 vol.%, and 60 vol.% in the foam samples. Further, it was shown that, compared to neat resin samples, a maximum of 14% reduction in density was obtained by addition of cenospheres. Alongside, the arctic-conditioned samples observed an increase in flexural modulus by a maximum of 15% compared to room-temperature tested samples. Perhaps, arctic conditioning of syntactic foam composites rendered lower strains to failure. Seretis et al. (2018) fabricated E-glass fabric

reinforced epoxy (ES35A) composite with graphene nanoplatelets (GNPs) using a hand lay-up method and characterized composites with tensile, thermal degradation, and flexural properties. They concluded that greater values of post-curing parameters, such as temperature and time for nanocomposite laminae, resulted in a degradation of the mechanical performance. They revealed that the thermal properties of nanocomposite laminae were boosted due to greater values of post-curing parameters. This may be due to GNPs acting as a cooling-points within the matrix that delays the degradation. Further, the voids in the increased interface area of the nanocomposite laminae allowed undergoing a drop in mechanical performance way earlier compared to the nanocomposite laminate with lesser epoxy/fiber interfaces.

Efforts were attempted by Pattanaik et al. (2019b) to fabricate syntactic foams using a waste by-product of thermal power plants called fly ash cenospheres. They investigated tensile, and flexural properties of fly-ash reinforced epoxy composites by solution casting method. It was shown that the density of syntactic foams decreases with an increase in fly ash addition. Also, microwave curing required less heat energy to attain 99% crosslinking compared to an isothermal and oven-cured samples. In comparison to other curing techniques, microwave curing yields maximum tensile and flexural strengths of 117 MPa and 144 MPa, respectively, with a 10% fly ash addition. Further, in comparison to other curing techniques, microwave curing yields maximum tensile and flexural strengths of 117 MPa and 144 MPa, respectively, with a 10% fly ash addition. Moller et al. (2020) examined glass transition and tensile properties of the epoxy resin through molecular dynamics simulation. Their study concluded that the best agreement was observed between simulation and experimental results when etherification and dehydration were introduced. Furthermore, post-curing process of dehydrating water molecules affects the molecular structure and aids in augmenting mechanical properties. The study carried out by (Bakshi and Kattimani 2022) explored the post-curing effect of HNTs reinforced syntactic foam. Their results claimed enhancement in the T_g values by the thermal post-curing owing to the improved crosslinking in the composite.

1.10.2 LITERATURE REVIEW ON MECHANICAL BEHAVIOR OF COMPOSITES UNDER DIFFERENT LOADING CONDITIONS

The polymer composites may be subjected to different types of mechanical loads depending upon assembly of engineering structure and the desired structural application. The compressive behavior of syntactic foams with varied densities of cenospheres in formulations was carried out by N. Gupta and Woldesenbet (2003). Their study concluded that at room temperature, the moisture absorption of S22 and K46 synthetic foams was less than 1%. Also, in DI and salt water, S22-type syntactic foam absorbed 6.7% and 2.5% moisture, respectively, at 70 °C. At 70 °C, K46 syntactic foam absorbed 3.9 and 1.9% of the water. Further, in high-temperature specimens, the compression strength decreased by 34%, 31%, 36%, and 33% for K46 type DI water, K46 type salt water, S22 type DI water, and S22 type salt water, respectively. They also revealed that for S22 type samples, the modulus decreased by 51%, 9%, 65%, and 68% for low-temperature salt water, low-temperature DI water, high-temperature DI water, and high-temperature salt water, respectively. Later, the flexural properties of syntactic foamed sandwiched composites with a constant 35 vol.% of microballoons addition were examined by Gupta and Woldesenbet (2005). In their work glass fabric was used as a face sheet with four layers. Outcomes have shown that the microballoon radius ratio in three and four-point bending tests did not affect the core shear stress or skin bending stress. Also, core shear stress and bending stress in the short beam shear stress (SBS) tests were observed to diminish with decreasing values. Gupta and Nagorny (2006) employed a solution casting method to fabricate syntactic foams with microballoons content varied from 30, 40, 50, and 60 vol.% to study the tensile property. Their testing results revealed that strength of various types of foams diminished by 25 – 60% when the microballoons vol.% increased from 30 – 60%. Also, for all varieties of syntactic foams, strength was reduced by 60 – 80% as compared to neat resin. And, with an increase in microballoons density from 220 – 460 kg/m³ for a 30 vol.% of filler, modulus increased by 48.59%. In addition, an increase in the microballoon density was exhibited for an increased modulus between 30% and 90%. Microballoons with a lower radius ratio had improved strength and modulus results. Li and Jones (2007) fabricated hybrid syntactic foam by coating glass microballoons with

styrene-butadiene rubber and nanoclay and using milled glass fiber in reinforcing epoxies to constitute a core material. The E-glass plain woven fabric was used as a face sheet to produce a sandwich structure. Their test results pointed out that rubberized foam enhanced the energy-absorbing characteristics in composites with appreciable reinforcing mechanisms of nanoclay and milled glass fibers in the matrix.

Wouterson et al. (2007) developed syntactic foams with phenolic microspheres (BJO-093) with 30 vol.% and short carbon fiber at 1, 2, and 3 wt.% to account for tensile, fracture, and thermal properties. The fiber reinforcement at 3 wt.% enhanced plane strain-fracture toughness, tensile modulus, and tensile strength by 40, 115, and 95%, respectively. They found that tensile and fracture properties did not get affected by variations in the fiber length. Also, thermal stability of the syntactic foams depends on matrix and not on the length and fiber content. Further, with similar composition Wouterson et al. (2007) processed reinforced syntactic foam with phenolic microspheres, short carbon fiber, and nanoclay at 0.5, 1, 1.5, 2 wt.%. They studied tensile and fracture properties of composites under the influence of nanoclay addition. It was revealed from their tensile test results that, with addition of 2 wt.% of nanoclay a 13% decrease in tensile strength of nanoclay-reinforced syntactic foam and a rise in Young's modulus of 19.5% were obtained. Further, they explicated the presence of both nanoclay and short fiber increased the toughening effect in samples resulting in high values of fracture toughness and critical energy release rate. The compression and low-velocity tests of a hybrid grid stiffened core containing syntactic foam composites were explored by Li and Muthyala (2008). From their study, it was observed that orthogrid stiffened core augmented initiation energy and lowered the propagation energy, which is favorable in designing resilient engineering structural applications. The syntactic foams are damage tolerant and their design suit energy absorption applications. With this concern, Woldesenbet (2008) characterized the energy absorption response of syntactic foams with microballoons (60 vol.% and density: 220, 460 kg/m³) and I.30 nanoclay (1, 2, and 5 vol.%). Their outcomes have shown that the inclusion of nanoclay augmented the maximum load-taking capacity and initiation energy in all the syntactic foams. Also, with 1 vol.% of nanoclay content, optimum values of maximum load and initiation energy in the syntactic foams were reported. They proved that thicker-walled

microballoons absorb more energy. Peter and Woldesenbet (2008) investigated compressive property of montmorillonite nanoclay-reinforced syntactic foam. The nanoclay and microballoons content varied as 1, 2, and 5 vol.% and 10, 30, and 60 vol.%, respectively. They reported that syntactic foam containing 10 vol.% microballoons with and without nanoclay reinforcement displayed higher values of peak stress at higher strain rates compared to medium and lower strain rates. Alongside, an increase in peak stress was reported with an addition of nanoclay up to 5 vol.% at high and medium strain rates. Also, the syntactic foams containing 1 vol.% reported optimum augmentation in the modulus and, thus, peak stress values.

Finite element modeling in the estimation of tensile properties of vinyl-ester syntactic foam composites was carried out by Tagliavia et al. (2010b). In their work, the density values of the hollow glass particles added to the composites were 220, 320, 370, and 460 kg/m³. Their outcomes reported that the high-density syntactic foams exhibit a higher tensile modulus than neat resin. Further, the tensile modulus was 15 – 30% greater than the compressive modulus for the same syntactic foam formulations. Furthermore, the syntactic foams have a 50 – 75% greater specific modulus than clean vinyl-ester resin. Swetha & Kumar (2011) tested epoxy resins with hollow glass microspheres (HGM) with 10, 20, 30, 40, 50, and 60 vol.% additions to study the compressive response of the syntactic foam. They found that as the wall thickness of microspheres rises, the modulus and strength data indicate a declining trend with volume fraction of microspheres increasing. Alongside, the failure behavior of foams was determined by shape of stress-strain curves, which, in turn, depends on microspheres' wall thickness. Also, with an increase in addition of microspheres, the capacity to absorb energy improved by up to 50%. For the first time, the cenospheres were clubbed with titanium employing a powder metallurgy route to fabricate titanium (Ti)-cenosphere syntactic foam for energy absorption by Mondal et al. (2012). From their study, it was noticed that the cold compaction pressure along cenosphere introduction manifested a range of porosity of 51 – 70% in the specimens. Further, a numerical model was constituted, claiming that crushing of cenospheres, porosity function, and density remain reliant on applied pressure. Also, the cost-effective

titanium-cenosphere material was shown to exhibit appreciable compressive properties, suiting it to shock-absorbing applications.

Apart from epoxy polymer matrix reinforced by nanofiller, several other studies were also carried out to reinforce polymers and study mechanical, water absorption, and thermal properties of nanocomposites (Curtis et al. 2008; De'n~ve and Shanahan 1993; Popescu et al. 2020; Prolongo et al. 2012; Tham et al. 2016b). The HNTs' phase interactions with the polymer matrix are distinctive because, as nanoparticles, they have a higher surface area per unit volume. Consequently, water absorption characteristics of the nanotubes, nano platelets in the polymers remain inquisitive. To this end, the flexural and fracture properties of HNTs, nanoclay platelets, and nano-silicon carbide was experimented with by Alamri and Low (2012). It was found from their work that the flexural modulus values dropped but with an increase in strength values. Also, fracture strength was improved owing to the plasticization effect of the epoxy matrix subject to water exposures. Further, HNTs inclusion in vinyl-ester nanocomposites and their water absorption, thermal and mechanical behavior was explored by Alhuthali and Low (2013). Furthermore, water absorption was shown to reduce with 5 wt.% of HNTs addition to vinyl-esters. Also, reinforcing mechanism of HNTs aided in augmentation of the thermal and barrier properties of the nanocomposites.

In the fabrication of syntactic foams, the microballoons comprised of variable wall thicknesses affect the density and water absorption properties (Gupta and Woldesenbet 2003). Similarly, the effect of wall-thickness of microballoons added to vinyl-ester composites on water absorption was explored by Tagliavia et al. 2012. They concluded that the flexural modulus and strength, and water ingress increase with the increase in volume fraction of microballoons in the vinyl-ester syntactic foam composites. Jena et al. (2013) fabricated a hybrid composite using bamboo fiber (3, 5, 7, and 9 layered) and cenospheres (1.5, 3, 4.5, and 6 wt.%,) using hand lay-up technique to study tensile, flexural and impact properties of the composite. They concluded that in a 3, 5, and 7-layered bamboo-epoxy composite, the strength improves by 32, 9, and 11.2%, respectively. Also, a comparison of 3, 5, 7, and 9-layered bamboo-epoxy composites to neat samples showed improvements in the strength of 20 and 9% for 1.5 and 3 cenospheres wt.% and declines in the strength of 17.5 and 42.8% for 4.5 and 6

cenospheres wt.%, respectively. Further, with 3 wt.% cenospheres content and 7 layered bamboo fiber a maximum of 90.6% of an increase in interlaminar shear strength was noticed compared to neat sample. Zhang and Ma (2013) studied compressive, flexural, and fracture toughness of phenolic syntactic foam with carbon nanofibers added at 0.5, 1.0, 1.5, and 2.0 vol.% in the composites. They found that compressive strength of all samples remains almost constant. Additionally, the flexural strength and fracture strength was seen to be maximum at 1.5 vol.% CNF and thereafter reduces due to agglomeration of CNFs.

Poveda et al. (2013) used carbon nanofibers in the reinforcing epoxy foams containing glass hollow particles content 30 and 50 vol.% and density: 220 kg/m³, 460 kg/m³. Their study observed that quasi-static compressive modulus of samples was unaffected by exposure to moisture, although a strength reduction of ~30% was reported. Similarly, except for the syntactic foam with the lowest density and maximum glass particle content, all samples exhibit moisture absorption between 0.75 and 2%. Labella et al. (2014) fabricated fly ash/epoxy syntactic foams with 30, 40, 50, and 60 vol.% additions to ascertain flexural, compressive, and coefficient of thermal expansion (CTE) of the composites. They concluded that energy absorption increased with test strain rate and was higher at high strain rate compression compared to quasi-static compression. Furthermore, in comparison to matrix resin, the flexural strengths and modulus both demonstrated maximum decreases of 73 and 47%, respectively. Also, CTE values for syntactic foam containing 60 vol% showed a decrease of up to 67%. Thakur and Chauhan (2014) examined the size of cenospheres in the vinyl-ester syntactic foam to study the tensile, flexural, and wear response. It was concluded from their study that for 400 nm cenospheres reinforced composites, a little increase in tensile strength of 2.56% was observed. Similarly, the 400 nm cenosphere-filled vinyl-ester composite was 27.11% stronger than the 900 nm (15.25%) and 2 μm (10.16%) cenosphere-filled vinyl-ester composites. For 2 μm, 900 nm, and 400 nm, the volume fraction of void perceived was 9.4529, 8.0904, and 10.434, respectively. The study also inferred that to reduce specific wear rate, composites containing 6% submicron-sized particles were optimal.

Zeltmann et al. (2015) investigated flexural properties of syntactic foams with glass microballoons and carbon nanofiber reinforcement. They observed that all of the nanocomposites exhibited an increase in moisture uptake when compared to neat resin. Also, all of syntactic foams have a moisture absorption rate that was 18% higher than neat resin samples. Further, the strength of dry, conditioned, and unmodified resin was superior to all other samples. Due to weathering, the sample's strength decreases significantly to 53 MPa. Likewise, the composite containing 1% CNF had the maximum fracture strength, measuring 96.9 MPa. Thus, after weathering, composites containing 2 and 5 wt.% of CNF exhibit greater strength. Therefore, in comparison to a dry composite, higher CNF content was reported to have a 27% improvement in strength following immersion. Bharath Kumar et al. (2016) used brabending process in fabricating the filament containing the high density polyethylene (HDPE) with cenospheres 20, 40, and 60 wt.%. They pointed out that composites with a treated constituent, modulus, and strength were found to rise as cenospheres content does. Likewise, formulations containing 40 and 60 wt.% untreated brabender mixed cenospheres/HDPE exhibited the greatest modulus and strength of 37% and 17%, respectively. X. Zhang et al. (2017) investigated compressive behavior of multiwalled carbon nanotubes (MWCNT) reinforced with glass microballoons in epoxy resin by the solution casting method. From their study, it was noticed that, an addition of 0.3 wt.% MWCNTs increase the compression strength of HGMs/epoxy by 17–25%. Similarly, the water absorption in syntactic foams reduces owing to the reinforcement effect by MWCNTs. Also, fracture feature revealed a reinforcing mechanism of MWCNTs comprising a bridging effect in the matrix. Shahapurkar et al. (2018) examined compressive response of cenospheres reinforced in lapox (L12) resin. It was concluded from their research that compressive modulus of both treated and untreated cenospheres increases with cenospheres addition. Likewise, the compressive strength of all samples reduces with an increase in cenospheres content. Also, they stated that the arctic-conditioned samples reported lower modulus compared to room-temperature samples.

Jayavardhan and Doddamani, (2018) studied compressive property of HDPE syntactic foam with glass microballoons (GMB) at 20, 40, and 60 vol.% of additions. They claimed that values of modulus and yield strength are strain rate sensitive, and

rise with higher strain rates. Further, the high density foams with 60 vol.% glass microballoon content exhibit higher modulus and yield strength. In their comparison study, it was observed that neat HDPE has a lower specific modulus related to other syntactic foams. High velocity impact analysis was carried out by Ahmadi et al. (2020) on nano-reinforced cored sandwich panels. It was pointed out from their study that, with an increase in microballoons content the ballistic resistance was reduced. Further, a 10% in ballistic limit velocity was achieved with an addition of nano-reinforcement. Using 3D printing technology Bharatkumar et al. (2020) fabricated HDPE/glass microballoon syntactic foams and studied tensile, flexural, and melt flow index (MFI) of composites. They observed that MFI value decreases with an increase in microballoon content in the syntactic foam. Further, HDPE with 60 vol.% GMB content exhibited the highest increase in modulus, which was 48% greater than the neat HDPE printed sample. Their developed 3D-printed syntactic foam recorded 28% weight-saving potential and eventually superior specific mechanical properties. Kumar and Jena, (2022) used a hand lay-up method to fabricate glass fabric/epoxy composites by cenospheres with 10 and 20 wt.%, clamshells at 10 and 20 wt.%, and E-glass fiber mat at 38 wt.% to study the tensile properties. It was observed from their study that water absorption resistance of composites with cenospheres filler was higher than composites with clamshell filler. Similarly, an increase in filler content results in a decrease in equilibrium moisture content (EMC) values. When compared to neat sample, which has the highest EMC, the maximum EMC reduction of 20 wt.% cenospheres were 57.37% for distilled water and 52.06% for salt water, respectively.

1.10.3 LITERATURE STUDY ON DYNAMIC MECHANICAL ANALYSIS OF COMPOSITES

Sankaran et al. (2006) processed epoxy syntactic foams with microballoons additions at 62.12, 68.33, and 71.70 vol.%. They concluded that syntactic foam and plain resin both experience a drop in storage modulus as the temperature rises. Also, it was reported that mobility of polymeric chains in the interphase zone between matrix and filler was affected by presence of reinforcing hollow microballoons in syntactic foams, leading to a greater T_g compared to plain resin. The changes in T_g were primarily attributable to the volume percentage of components, showing that interfacial effects

have a significant impact on the T_g of composites. Likewise, damping of polymer composites is mostly determined by their composition. However, filler-matrix interactions also impacted damping behavior. The vinyl-ester syntactic foam with glass microballoons additions at 30, 40, 50, and 60 vol.%, and densities 220, 320, 380, and 460 kg/m³ were experimented with by Tagliavia et al. (2009). They observed that the storage modulus was reported to increase as microballoon wall thickness increases. However, the relationship between storage modulus and microballoon wall thickness was not monotonic. Also, increased volume fraction was advantageous to foams with thick-walled particles. Perhaps, due to brittle behavior of glass microballoons and the pronounced viscoelastic behavior of the resin, loss tangent of syntactic foams is reduced as the volume of resin diminishes.

Gu et al. (2009) experimented with epoxy consisting of glass microballoons additions at 30, 40, 50, and 60 vol.%, and densities: 220, 320, 380, and 460 kg/m³. They pointed out that the thermal stability was enhanced by increasing microballoon wall thickness, but its response to microballoon volume fraction was considerably lowered. Further, interfacial effects have a significant impact on the T_g of the composite, which may be inferred from the fact that changes in T_g were primarily attributable to the volume fraction of constituents. Additionally, the volume fraction of microballoons exhibited a more noticeable impact on glass transition temperature than the influence of wall thickness. The injection molding process was used by Das and Satapathy (2011) in fabrication of cenosphere/polypropylene syntactic foams. It was observed from their research that an appreciable damping and storage modulus improvement was achieved with cenospheres content of 10 wt.% and 30 wt.% in syntactic foams, respectively. Similarly, at lower/sub-zero temperatures in region of -25 to 0 °C, the storage modulus rises more rapidly with increasing cenosphere content. However, this rise was diminished at higher temperatures. Hu and Yu (2011) manufactured epoxy syntactic foams with hollow particles at 5, 10, 15, 20, and 25 vol.% to study the viscoelastic response of composites. They concluded that increasing amount of polymer particles raises the loss factor. Further, in temperature range of -20 to 90 °C, the loss factors of plain epoxy and syntactic foams containing 10% hollow particles show two relaxation peaks, with α - peak corresponding to the samples' T_g . Furthermore, lowest of the peaks were β -relaxation peaks associated with the local motion of molecular chains.

The short sisal fibers were used to process syntactic foams with glass microballoons additions at 30 vol.% by Ghamsari et al. (2015). They observed storage modulus improvement in both glass and rubbery regions, and the rubbery region registered a three-fold magnitude improvement compared to plain syntactic foams. Also, the loss modulus of plain syntactic foams was seen to be 300% lower than the sisal reinforced syntactic foamed composites. Poveda et al. (2014) studied the viscoelastic response of cenospheres reinforced epoxy syntactic foam composites. It was witnessed from their work that storage modulus augments with an increase in the cenosphere content. Similarly, the storage modulus of treated foam was 258 - 370% higher than the neat resin sample. Further, the treated foam with 60 vol.% cenospheres was reported to have the highest peak damping value of 0.914 at 87 °C among all foam samples. Doddamani (2020) employed 3D-printing in fabrication of HDPE/cenosphere foamed composites. He concluded that with an increase in temperature, the storage modulus of the printed samples reduces. Alongside, Maximum storage modulus, loss modulus, and damping values were attained in HDPE prints with a cenosphere content of 60 vol.%. The study carried out by Bakshi and Kattimani (2021) elucidated successful reinforcement of HNTs in syntactic foams containing cenospheres. It was revealed from their work that, HNTs reinforced syntactic foams exhibited better thermal stability, and enhanced storage and loss modulus values compared to the neat epoxy.

It is evident from the comprehensive literature review that the potential for developing thermosetting-based syntactic foams employing mechanical mixing technique while using secondary nano-reinforcement has not been adequately explored with environmental pollutants such as fly ash cenospheres. In addition,

- Work on halloysite nanotubes (HNTs) reinforced epoxy syntactic foams with cenospheres is not reported in the literature.
- Most of the studies carried out composite testing with room temperature curing conditions, while studies based on post-curing of syntactic foams are not explored well.
- Concerning HNTs reinforcement along with cenospheres, the water absorption

behavior of syntactic foams is not investigated.

Hence, the present work deals with development and characterization of lightweight, eco-friendly reinforced syntactic foams to address the effectual disposal of cenospheres for weight-sensitive applications.

1.11 MOTIVATION OF WORK

Fly ash is a waste byproduct produced in large quantities from the burning of coal in thermal power plants. It is mostly composed of silicon dioxide, iron oxide, and aluminum oxide. Fly ash is a serious hazard to the ecosystem since it pollutes air around it and requires the use of landfills for disposal. Economically and commercially, using fly ash as fillers in polymer composites is a sensible move. Studies have demonstrated that fly ash and polymers have excellent compatibility with each other. Further, naturally available HNTs possessing advantageous geometry ameliorate the properties of the polymers. The present work is emphasized studying the possibility of developing HNTs reinforced epoxy syntactic foams employing the conventional casting route.

Domain of nanoparticle reinforced syntactic foam composites present science and technology with a tremendous opportunity and also considerable challenges for future research in the polymer composite sector. These reinforced syntactic foam composites containing HNTs have desirable mechanical, thermal, and electrical properties, enhanced dimensional stability, and are cost-effective to be used for weight-sensitive structural applications. The reasons for exploring this topic are outlined below.

- Waste utilization.
- Reduction in environmental pollution.
- Utilization of naturally available nanoclay fillers.
- Eco-friendly processing.
- Reduction in consumption of polymers.

Based on the preceding considerations, objectives are formulated and presented in the following section.

1.12 OBJECTIVES AND SCOPE OF WORK

From the comprehensive literature review, it is clear that scientific studies on development of inexpensive secondary filler-reinforced syntactic foams are scarce. In light of this, the present study proposes the design and performance evaluation of a polymer resin system using naturally available nanoclay and low-cost fly ash. A complete and methodical investigation of these composites was conducted by experimental characterization for a variety of physical and mechanical properties. As a result, the work undertaken aims to study following objectives

- To develop halloysite nanotubes reinforced syntactic foam with cenospheres as a hollow filler in epoxy resin matrix at room temperature by open mold casting technique.
- To investigate the physical (density and void content), mechanical properties (tensile, compression, flexural), and dynamic mechanical properties of the developed reinforced syntactic foams.
- To study the micrographs of fractured samples for structure-property correlations.
- To investigate the effect of post-curing on thermal and mechanical properties of HNTs reinforced syntactic foam composites.
- To carry out water absorption studies on HNTs reinforced syntactic foam composites.

The scope of current study includes processing HNTs and their subsequent addition along varied content of cenospheres to produce reinforced syntactic foams by conventional casting method. Analytical testing techniques such as FTIR spectroscopy, X-ray diffractogram, and particle size analysis are carried out on fabricated syntactic foams. Fractured samples are studied using micrographs to infer the filler-matrix interaction. Testing outcomes of the fabricated syntactic foam composites concerning tensile, flexural, compressive, and viscoelastic response are discussed focusing on the effect of HNTs reinforcement and varied content of cenospheres in the epoxy matrix.

1.13 OUTLINE OF THESIS

The thesis presents the methodical investigation conducted concerning the aforementioned goals. Chapter 1 provides the essential introduction to the composites, syntactic foams, and reinforced syntactic foams composites, including a comprehensive literature review, followed by the purpose and objectives of the current research. The organization of Chapter 2 includes the material constituents, the fabrication route adopted, and the characterization techniques employed in the work. The mechanical behavior of the reinforced syntactic foams is presented in Chapter 3, which comprises tensile, flexural, and compression study of room temperature cured samples. Alongside this, the flexural and compressive response of post-cured samples is also detailed. Structure-property relations for the fractured samples are established by microscopy. The dynamic mechanical response along the thermal property characterization of the reinforced syntactic foam composites is presented in Chapter 4. Chapter 5 contains a brief summary and conclusions obtained from the study.

CHAPTER 2

2. MATERIALS, FABRICATION, AND CHARACTERIZATION TECHNIQUES

2.1 CONSTITUENTS

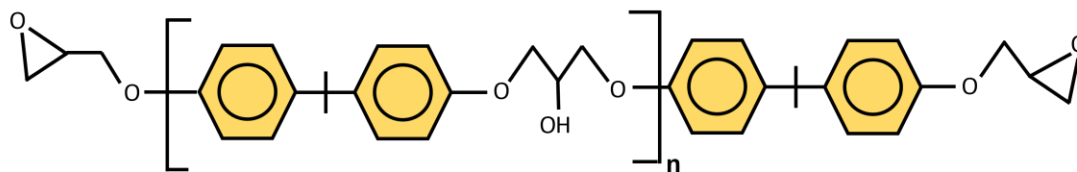
In the current study, hollow cenospheres were used as a micro filler, LY556-epoxy as a matrix, and halloysite nanotubes (HNTs) as a nanoscale reinforcement in the fabrication of lightweight reinforced syntactic foam composites. The details of the composite material's constituents will be covered in the sections that follow.

2.1.1 MATRIX

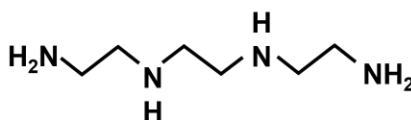
Figure 2.1 shows chemical structure of the epoxy resin LY556 and hardener HY951. The epoxy resin with hardener (shown in Figure 2.2c), procured from S. M. Composites, Chennai, India, was the matrix resin combination used in this study. The LY556 is an unmodified liquid resin with a moderate viscosity used to make structural composites with a variety of hardeners. Table 2.1. presents the compiled properties of epoxy and hardener.

Table 2.1. Properties of epoxy resin and hardener.

Property	Value	Unit
Epoxy resin (LY556)		
Epoxide index	5.30 – 5.45	Eq/kg
Viscosity at 25°C	10000 - 12000	mPa s
Density at 25°C	1.16 – 1.2	g/cm ³
Color	Clear liquid	
Hardener (HY951)		
Viscosity at 25°C	10 - 20	mPa s
Pot life at 25°C	5580	s
Gel time at 25°C	9600	s
Colour	Yellowish	



(a) Epoxy Resin (LY556)



(b) Epoxy Hardener (HY951)

Figure 2.1 Chemical structure of (a) epoxy resin (LY556) and (b) hardener (HY951).

2.1.2 REINFORCEMENT

The fly ash cenospheres with grade CIL 150 used as a micro filler were procured from Cenosphere India Limited, Kolkata, India. The cenospheres were utilized in their original as received state (Figure 2.2a), with no surface modification. These cenospheres comprise silica, alumina, calcium, and iron oxides. Further, Halloysite nanotubes, which are nanoscale fillers procured from Sigma Aldrich, USA, were employed in the fabrication of structurally reinforced syntactic foam. Figure 2.3 shows the morphological structure of the as-received cenospheres and HNTs, whereas Table 2.2 describes the properties of cenospheres and HNTs.

Table 2.2 Property details of cenospheres and halloysite nanotubes*.

		Cenosphere			
	Physical properties	Chemical analysis		Sieve analysis	
True particle density	920 kg/m ³	SiO ₂	52-62%	+ 30 # (500µm)	Nil
Bulk density	400 – 450 kg/m ³	Al ₂ O ₃	32-36%	+ 60 # (250µm)	Nil
Hardness (MOH)	5 – 6	CaO	0.1-0.5%	+100 # (150µm)	Nil
Compressive strength	180 – 280 kg/m ²	Fe ₂ O ₃	1-3%	+120 # (125µm)	Nil
Shape	Spherical	TiO ₂	0.8-1.3%	+150 # (106µm)	0-10%
Packing factor	60 - 65%	MgO	1-2.5%	+ 240 # (63µm)	70-95%

Wall thickness	5 - 10% of shell dia.	Na ₂ O	0.2-0.6%	- 240 #	0-30%
Color	Light grey – light buff	K ₂ O	1.2-3.2%		
Melting point	1200 – 1300 °C	CO ₂	70%		
pH in water	6 – 7	N ₂	30%		
Moisture	0.5% max.				
Loss on ignition	2% max.				
Sinkers	5% max.				
Oil absorption	16 - 18 g/100g				

Halloysite nanotubes

Color	white
Purity	99.9%
Diameter	30 – 150 nm
Length	1 – 3 μm
Density	2530 kg/m ³
Pore volume	1.26 – 1.34 ml/g

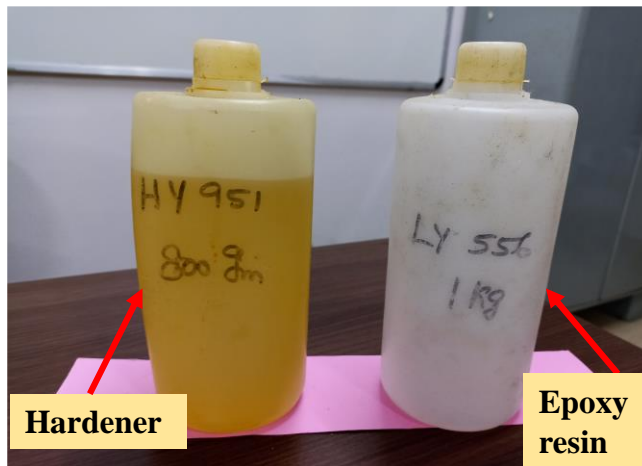
*As provided by the supplier.



(a)



(b)



(c)

Figure 2.2 (a) Cenospheres, (b) Halloysite nanotubes, and (c) Epoxy resin and hardener.

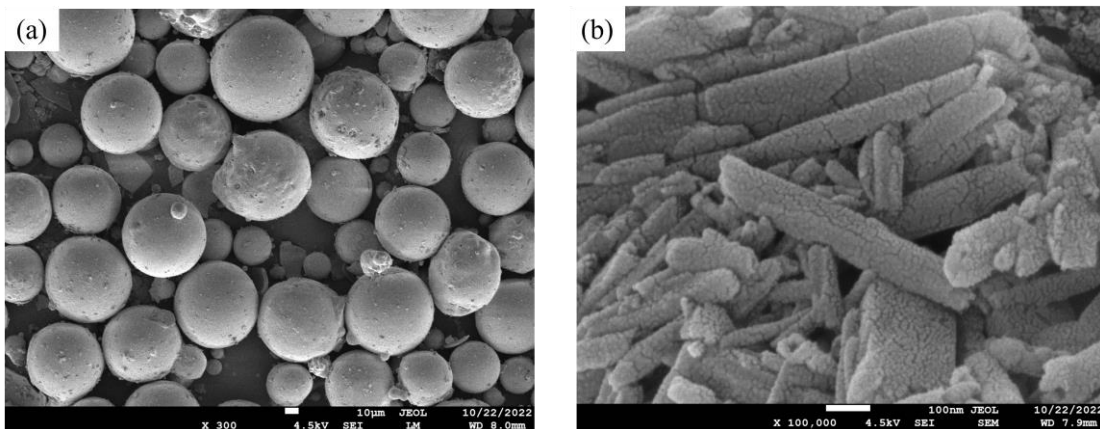


Figure 2.3 FESEM image of as-received (a) cenospheres and (b) HNTs.

2.2 PARTICLE SIZE ANALYSIS, FOURIER TRANSFORM INFRARED SPECTROSCOPY, AND X-RAY DIFFRACTION

In the particle size analysis, modulated laser lightens the particles while they were passed through a camera that captures images at 185 frames per second. The equivalent diameter was calculated as 36.13 μm . The diameter of a sphere with a projected area equal to the projection recorded by a camera, for each particle imaged. Each particle type was subjected to five runs, and the values were averaged across these runs, with weighting based on the quantity of particles in each run. Neat epoxy, syntactic foam, and HNTs reinforced syntactic foam were studied by FTIR analysis (Bruckers Karlsruhe, Equinox 55, Germany, Automated Reflection mode) by KBr pellet method to elucidate the possible interactions between neat epoxy matrix and the reinforcements. The FTIR spectra were recorded over a wavenumber range of 600 – 4000 cm^{-1} with a scan resolution of 2 cm^{-1} . The FTIR test setup is shown in Figure 2.4. X-ray diffraction (XRD) test was performed on amorphous neat-epoxy, pristine cenosphere, HNTs, and HNTs reinforced syntactic foams (HRSF) composite samples using Empyrean 3rd Gen, Malvern PANalytical, Netherland set up having a resolution of $2\theta \pm 0.01^\circ$. The crystalline peaks were noted for a scanning speed of 2 $^\circ/\text{min}$ Cu $K\alpha$ ($\lambda = 1.514 \text{ \AA}$) radiation source over a range of 5-80 $^\circ$. The XRD test setup is shown in Figure 2.5.



Figure 2.4 FTIR spectroscopy test setup.



Figure 2.5 XRD test setup.

2.3 DIFFERENTIAL SCANNING CALORIMETRY AND THERMOGRAVIMETRIC ANALYSIS

Differential scanning calorimetry (DSC) (DSC 600 machine Perkin Elmer, USA) test was carried out to examine the influence of post-curing and study the changes in the glass transition temperature (T_g) of the samples. The test was carried out by taking ~10 mg of the sample in an aluminum pan that was hermetically taped up in a nitrogen atmosphere purged at 50 mL/h as shown in Figure 2.6. The samples were operated over the temperature range of 0 – 140 °C at a heating rate of 5 °C/min. Thermogravimetric (TG) analysis was performed to investigate thermal stability of the RSF composites using TGA 4000, Perkin Elmer, Singapore, as shown in Figure 2.7. An average of 10 mg of the sample were considered to be operated from room temperature to 720 °C at a heating rate of 10 °C/min under an inert nitrogen atmosphere.



Figure 2.6 DSC test setup.



Figure 2.7 TG analysis setup.

2.4 SAMPLE PREPARATION

To keep the parameters affecting properties of composites minimum and for the ease of commercialization to manufacturing industries, no modifications in the HNTs nanofiller were considered. As received HNTs were first dried in an oven at 50 °C for 10 minutes to enhance the mechanical properties in epoxy composites (Ravichandran et al. 2019). Later, 1 vol.% of HNTs was added to 15 mL acetone to carry

ultrasonication using PROBE SONICATOR PKS-250FL (Power-250Watt), India, for 2 hours at 27°C and 55 W power maintaining pulse mode (10s ON / 5s OFF). The amount of acetone required for the sonication was to ensure that HNTs have sufficient medium to disperse. On the contrary, if an excess amount was taken, it should be ensured that acetone is entirely evaporated in order to avoid excessive dilution of the base matrix. The ice bath was used to cool beaker against the temperature rise during the sonication process. Once sonication process was completed, the dispersion was poured into uncured epoxy resin. This HNTs/uncured epoxy resin system was agitated to obtain a homogenous mixture by a mechanical stirrer at 800 rpm for 30 minutes. Then the mixture was kept under vacuum for a few minutes to remove entrapped air bubbles if any.

According to the literature (Gültekin et al. 2016; Zamani 2022), adding acetone to the resin nanoparticle mixture and then subjecting it to a sonication procedure resulted in a noticeable increase in mechanical properties of nanocomposites. However, the amount of epoxy used in current investigation was comparatively larger. Dispersing HNTs in the resin mixture under consideration can eventually demand additional time and energy. Further, the high viscosity of epoxy would prevent the dispersion of nanoparticles. For this reason, only acetone was utilized during sonication of HNTs, and mechanical stirring with the resin was subsequently carried out to achieve uniform dispersion. Furthermore, a known quantity of as-received cenospheres was added to the HNTs modified-epoxy mixture. The addition of cenospheres in the epoxy matrix varied from 20 - 50 vol% with a step-up of 10%. For every sample, the addition of cenospheres was executed in small amounts and gradually stirred by a glass rod. This enables maximum wettability of cenospheres in the syntactic foam and minimizes particle breakage due to friction (Gupta and Woldesenbet 2003; Kaur and Jayakumari 2016; Shahapurkar et al. 2017; Thakur and Chauhan 2014; Waddar et al. 2018). The time taken in manual stirring for 20 vol% cenospheres addition lasted 45 minutes, and for 40 vol%, it took 105 minutes to get wet completely. Based on the physical observation of immersing cenospheres, the stirring time was chosen for optimal fabrication. Further, the hardener was added in a ratio of 10:100 (hardener to epoxy resin ratio) to enable curing. Degassing was carried out to eject the entrapments included during mixing. The

acetone evaporation along with entrapment removal is essential for successful manufacturing. The weight of acetone to be added and resin mixed with fillers was recorded. In order to remove acetone from the degassed mixture, it was kept in a vacuum oven at a temperature of 50 °C. To ensure the acetone has completely evaporated, the weight of the mixture was frequently monitored. The solution casting method was employed to prepare all kinds of syntactic foam as it is much more feasible for the industrial-scale manufacturing process. Finally, the mixture of RSF was poured into an aluminum mold with dimensions $195 \times 145 \times 0.32 \text{ cm}^3$ as shown in Figure 2.8 and left for curing for about 24 hours. Once the curing was completed, the fabricated samples were machined for evaluation of tensile, flexural, compression, and dynamic mechanical properties.

The samples with varying amounts of cenospheres in the syntactic foam were coded as SFXX (XX = 20, 30, 40, 50), where ‘SF’ denotes syntactic foam, and ‘XX’ denotes vol. % addition of cenosphere. The RSF samples containing constant addition of 1 vol.% of HNTs throughout the fabrication were prefixed with ‘N’, i.e., NSFXX. Also, neat epoxy and four types of cenosphere epoxy syntactic foams (CESFs) without HNTs addition were fabricated for comparison study.

The density of all the syntactic foams was measured according to the ASTM D792-13 standard (“Standard Test Methods for Density and Specific Gravity (Relative Density) of Plastics by Displacement,” 2018). The rule of mixture was employed to estimate theoretical densities of all syntactic foam. The difference between the measured and theoretical densities was used to calculate the void content (% $\emptyset V$) and is given as follows (Saha and Nilufar 2009):

$$\emptyset V = \left[\frac{\rho_{th} - \rho_{exp}}{\rho_{th}} \right] * 100 \quad (2.1)$$

where, ρ_{th} and ρ_{exp} are the theoretical and experimentally measured densities, respectively. The theoretical density of CESF containing cenospheres and epoxy was calculated using the rule of mixture given in Eq. 2:

$$\rho_{th} = v_f \rho_f + v_m \rho_m \quad (2.2)$$

where, ρ_f , v_f and ρ_m , v_m were the density and volume fraction of the cenospheres and matrix, respectively. In the case of HNTs RSF, knowing the predetermined amount of HNTs in the composite, the volume fraction of HNTs was determined using the relation given:

$$vol. \% = \left(\frac{1}{1 + (\rho_n/\rho_m)(m_m/m_n)} \right) * 100 \quad (2.3)$$

where, ρ_m , m_m and ρ_n , m_n were the density and mass of the matrix and HNTs, respectively. Once the volume fractions of HNTs were determined, volume fractions of the cenospheres and matrix were found based on the remaining volume. Further, knowing the volume fractions, the density of HNTs reinforced HNTs RSF was estimated using the relation of the rule of mixture as given below:

$$\rho_{th} = v_f \rho_f + v_m \rho_m + v_n \rho_n \quad (2.4)$$

where, v_n is volume fraction of HNTs. The theoretical densities obtained were higher as compared to densities obtained by experiment, signifying the inclusion of air during the manual stirring approach employed.



Figure 2.8 Casting mold for the sample fabrication.

2.5 DENSITY MEASUREMENT

The density of all fabricated syntactic foam specimens was estimated according to the standard ASTM D792-13. A total of five specimens were considered for the measurement, and an average value was reported along the standard deviations of the specimens.

2.6 POST-CURING OF SYNTACTIC FOAMS

The syntactic foam samples fabricated at the ambient condition were called room temperature cured syntactic foams. Another set of samples with a similar formulation was fabricated at room temperature and then post-cured at 60 °C (which lies around T_g of the samples) for about 10 hours. The convention for post-cured samples followed was ‘SFXX_H’ and ‘NSFXX_H’, where suffix ‘_H’ denotes post-curing to the prepared samples. For example, post-cured neat epoxy was coded as SFO_H.

All the fabricated specimens were tested for mechanical characterization. The following section discusses the method used to determine the mechanical properties of the syntactic foam composite samples.

2.7 TENSILE TESTING

A tensile test was performed on samples in accordance with ASTM D638-14 (“Standard Test Method for Tensile Properties of Plastics” 2014) using a computerized universal testing machine (UTM) (H75KS, Tinius Olsen, UK) of 50 kN load capacity as shown in Figure 2.9. Samples with the dimension of overall length - 165 mm, overall width - 19 mm, length of narrow section - 57 mm, narrow width – 13 mm. The machine was operated with a crosshead displacement of 5 mm/min with a 50 mm gage length under displacement control mode. The test was carried out until the sample fractures. At least five representative specimens were tested at room temperature for each kind of sample, and average values were reported along the standard deviation. Tensile strength and modulus values were calculated from the obtained load-displacement data.

2.8 FLEXURAL TESTING

Flexural testing was carried out in three-point bending mode, maintaining a span-to-depth ratio of 16:1 on samples with dimensions 127 mm × 12.7 mm × 3.2 mm according to the ASTM D790-14 standard (“Standard Test Methods for Flexural Properties of Unreinforced and Reinforced Plastics and Electrical Insulating Materials”, 2017) using computerized UTM shown in Figure 2.10. Testing was performed at room temperature with a crosshead speed of 1.36 mm/min by taking five specimens of each fabricated sample. The average values were reported along the standard deviation. The tests were carried out until the specimen failed and stress-strain information was gathered. Flexural modulus was determined by,

$$E_{fm} = \left[\frac{L^3 t}{4bd^3} \right] \quad (2.5)$$

where L – support span (mm), b – width of the beam (mm), d – thickness of the beam (mm), and t – the slope of the tangent. Also, the flexural stress is given by (Garcia et al. 2017),

$$\sigma_{fs} = \left[\frac{3PL}{2bd^2} \right] \quad (2.6)$$

where P – load (N). The obtained values of flexural strength post-fracture were considered to illustrate a comparison between the samples.

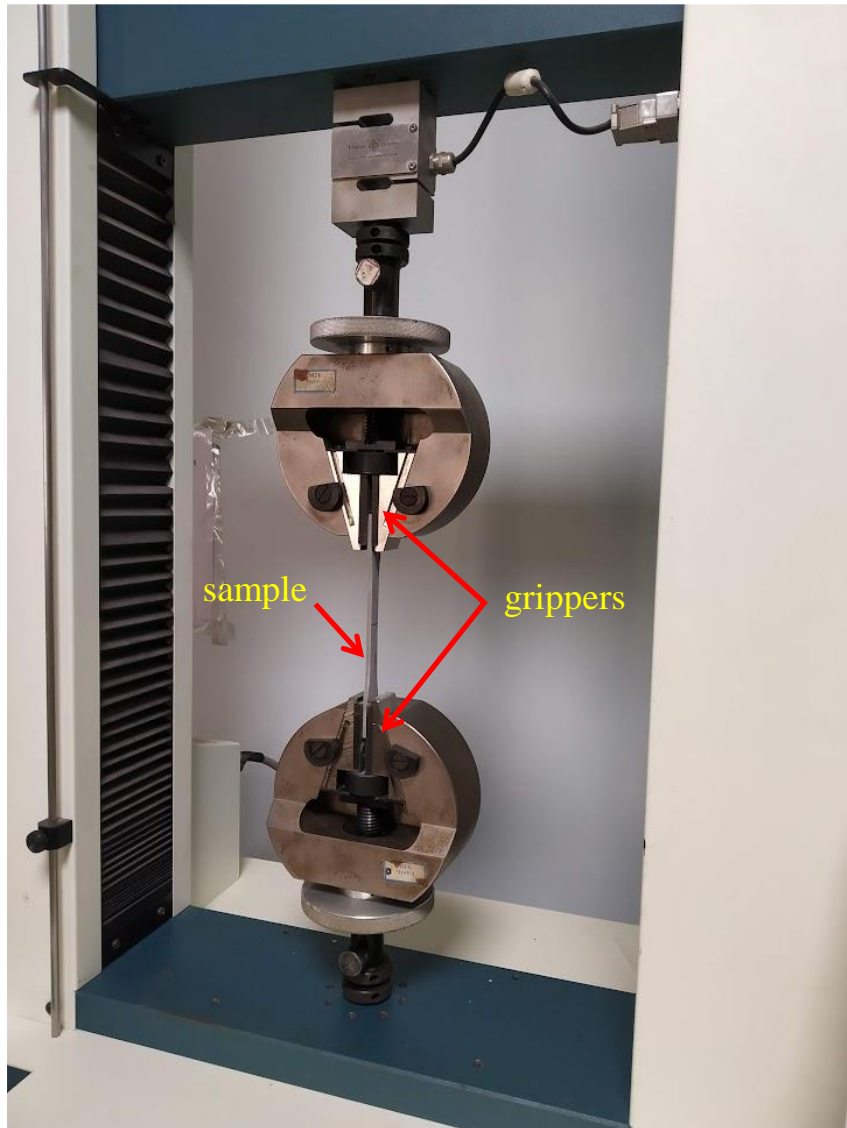


Figure 2.9 Tensile setup.

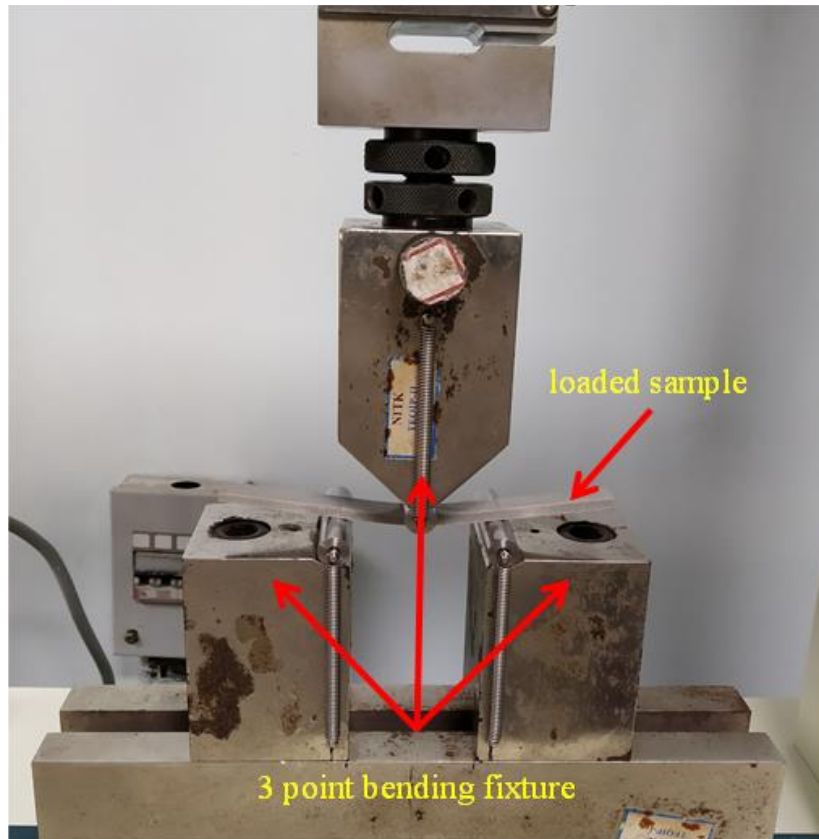


Figure 2.10 Three-point bending test setup.

2.9 COMPRESSION TESTING

Compression testing was performed on samples with edgewise loading having dimensions $25.4 \text{ mm} \times 12.7 \text{ mm} \times 12.7 \text{ mm}$ according to the ASTM D695 standard (“Standard Test Method for Compressive Properties of Rigid Plastics” 2015) using a computerized universal testing machine (UTM) (H75KS, Tinius Olsen, UK) of 50 kN load capacity. The load was applied on a $12.7 \text{ mm} \times 12 \text{ mm}$ face with a crosshead motion rate of 1.3 mm/min at the ambient condition, as shown in Figure 2.11. At least five specimens of each sample were considered, and their average values were presented. The testing continued until the specimen could support a load of 20 kN. Representative stress-strain curves were used to account for the compressive modulus and strength of the samples. At the end of an elastic region, the peak stress determines the compressive strength.

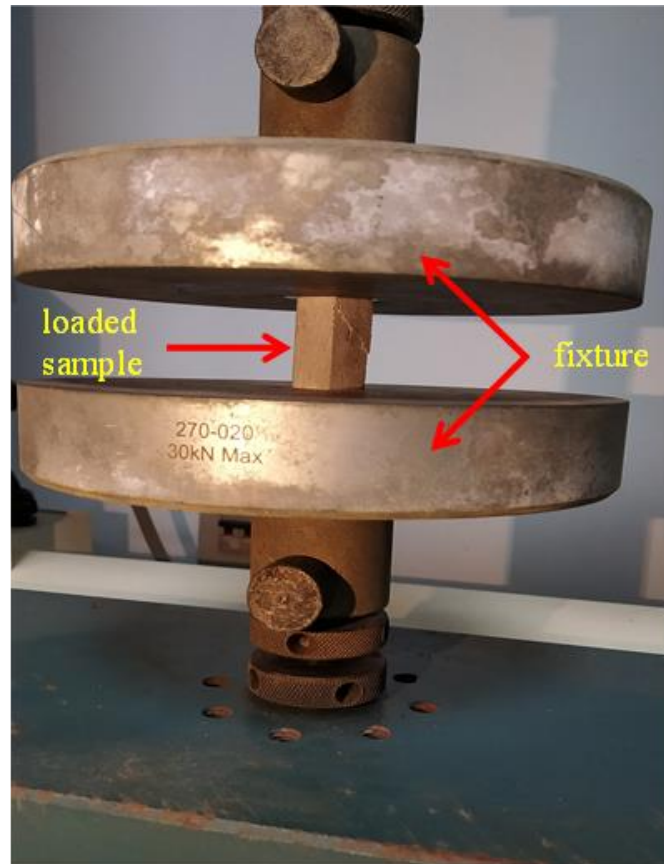


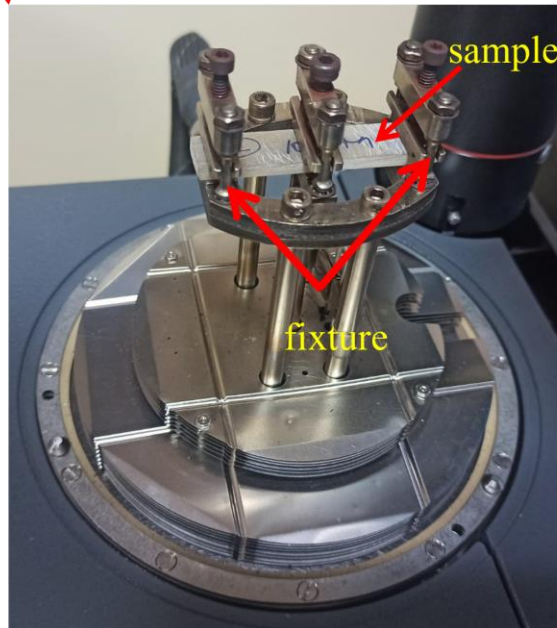
Figure 2.11 Compression test setup.

2.10 DYNAMIC MECHANICAL ANALYSIS

Dynamic mechanical tests were performed on syntactic foam samples with dimensions $55 \text{ mm} \times 13 \text{ mm} \times 3 \text{ mm}$ using Q800 DMA, New Castle, DE set up in a dual cantilever configuration as shown in Figure 2.12. The tests were performed in temperature ramp mode from room temperature to $140 \text{ }^\circ\text{C}$ to study the dynamic property variation at elevated temperatures of CESF and HNTs RSF composites. A constant heating rate of $2 \text{ }^\circ\text{C}/\text{min}$ with a constant frequency of deformation of 1 Hz was maintained throughout the test run with intending the difference of temperature lag to a minimum between the sample and environment. The significant outcomes from this test, such as storage modulus and loss modulus, were examined. A minimum of five representative specimens for each kind of sample were considered for the test, and their average values were reported. The test run was terminated once the storage modulus value reaches 20 MPa , to avoid polymer degradation on the clamps.



(a)



(b)

Figure 2.12 (a) DMA setup (b) test configuration.

2.11 MICROSCOPY

The morphology of microstructure of the fracture surfaces was examined using a scanning electron microscope (SEM) (JEOL JSM-6380LA, Japan) at an accelerating voltage of 20 kV. Before the investigation, samples were mounted on aluminum stubs and gold-sputtered to make their surfaces conduct. Field emission scanning electron

microscopy (FESEM) (Carl Zeiss Sigma) was used to study the interaction of HNTs in the samples. High-resolution transmission electron microscopy (HRTEM: JEOL/JEM 2100) with 200 kV voltage, LaB6 electron gun with a pointed resolution of 0.23 nm was used to examine the morphology of HNTs structure and to elucidate the dispersion in the matrix.

2.12 STANDARD DEVIATION AND ERROR MARGIN

Statistical analysis was performed on the experimentally obtained results with a 95% confidence interval and a significance of $p < 0.05$. The sample mean, standard deviation and margin error were evaluated using the following equations;

$$\text{➤ The sample mean, } \mu = \frac{\sum x_i}{n} \quad (2.7)$$

$$\text{➤ Standard deviation, } \sigma = \sqrt{\frac{\sum (x_i - \mu)^2}{n-1}} \quad (2.8)$$

Where, μ = the sample mean, σ = sample standard deviation, n = sample size, x_i = each value from the population

➤ Standard error of the mean for statistical significance $p < 0.05$ at a 95% confidence interval,

$$\mu \pm 1.96 * \frac{\sigma}{\sqrt{n}} \quad (2.9)$$

where, $\left[1.96 * \frac{\sigma}{\sqrt{n}}\right]$ gives the margin error for the standard error mean at a 95 % confidence level.

2.13 SUMMARY

This chapter encompasses the material constituents, fabrication methodology and the characterization techniques used in the current study. The microscopic images of as received cenospheres and halloysite nanotubes are presented to throw light on their received structural morphology. The technique of particle size analysis was carried to determine the average size of the particles. Using Archimedes principle, the density of the samples are found to observe the relative specific permormances of the syntactic foams. To evaluate the mechanical properties of the fabricated samples, mechanical testing such as, tensile, flexural, and compression were carried out. To quantify the thermal properties, differential scanning calorimetry and thermogravimetric analysis

were employed. The storage modulus, loss modulus and glass transition values are found from the viscoelastic study by the dynamic mechanical analyzer. The microscopy of the fractured specimens are studied to establish the structure-property correlations of the nanocomposite foams.

CHAPTER 3

3. MECHANICAL BEHAVIOR OF REINFORCED SYNTACTIC FOAM COMPOSITES

This chapter presents the outcomes of mechanical testing of reinforced syntactic foam (RSF) composites. The study analyzes the influence of cenospheres content and the effect of halloysite nanotubes (HNTs) reinforcement on mechanical properties of RSF composites. Mechanical testing such as tensile, flexural, and compression are carried out on the fabricated samples. Meanwhile, the analytical testing tools such as Fourier transform infrared (FTIR) spectroscopy and X-ray diffraction (XRD) are used for the qualitative study of composites.

3.1 FTIR STUDY

FTIR spectroscopy is used to elucidate the materials' specific components, miscibility if copolymers are blended, and interfacial bonding between the polymer and the fillers (Hong and Wu 1998; Kim et al. 2008; Riaz and Ashraf 2015). This spectroscopy also helps to monitor the progress of reaction in the polymer composites (Strankowski et al. 2016).

3.1.1 ANALYSIS OF FTIR SPECTRA OF ROOM TEMPERATURE CURED COMPOSITES

The samples initially were taken in powder form and by the KBr method they were made as pellets, ready for spectroscopy. Figure 3.1 shows the FTIR spectra of neat epoxy, cenosphere epoxy syntactic foam (CESF), and HNTs RSF composite. The peaks arising at 2965 cm^{-1} and 2930 cm^{-1} were attributed to asymmetrical C-H stretching vibration, while the peak appearing at 2869 cm^{-1} was corresponding to the aldehyde C-H stretching vibrations. Further, the peaks at 1607 and 1507 cm^{-1} were corresponding to N-H bending, C = C stretching of the aromatic ring, and CH_3 deformation vibration mode, respectively (Maharsia et al. 2006; Maharsia and Jerro 2007). Meanwhile, the peaks in the range of $1293 - 1028\text{ cm}^{-1}$ relate to C-H in-plane bending vibration. Also, the peaks at 825 cm^{-1} and 914 cm^{-1} correspond to C-H out-of-plane bending vibration, while a broad peak at 3390 cm^{-1} was attributed to the N-H stretching vibration.

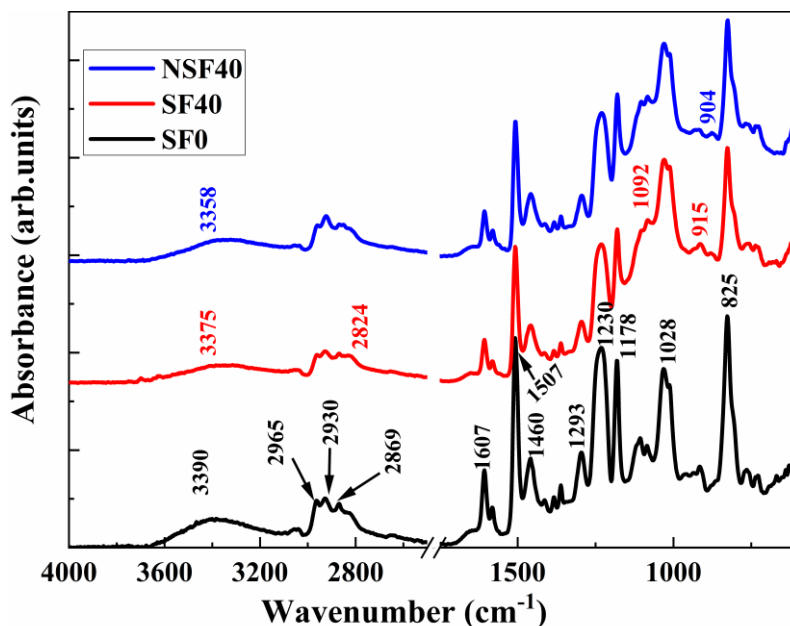


Figure 3.1 FTIR spectra of SF0, SF40, and NSF40 composites.

For CESF and HNTs RSF, the peak at 3390 cm^{-1} broadened and shifted towards the lower wavenumber, i.e., 3375 and 3358 cm^{-1} indicating a strong hydrogen bonding interaction between negatively charged oxygen atoms present in HNT and cenosphere with the N-H groups of epoxy matrix. Moreover, additional peaks observed were ascribed to the cenosphere (915 , 1092 , and 2824 cm^{-1}) that may correspond to Si–O–C bonds inferring bonding among the cenosphere, epoxy matrix (Maharsia et al. 2006; Maharsia and Jerro 2007) and HNT (904 cm^{-1}) Al_2OH bending band (Zhang et al. 2014a). The shifting of peaks and the arising of new peaks suggest that there existed a strong interaction between the epoxy matrix and incorporated fillers. Thus, the compatibility and strong bonding between the filler and epoxy lead to better stress transfer efficiency, which eventually resulted in enhancement of mechanical properties of the HNTs RSF over neat epoxy and CESF.

3.1.2 ANALYSIS OF FTIR SPECTRA OF POST-CURED COMPOSITES

FTIR spectra of thermally post-cured SF0_H, SF40_H, and NSF40_H are shown in Figure 3.2 in the wavenumber range of $4000 - 400\text{ cm}^{-1}$. The bands arising at 2959 and 2848 cm^{-1} correspond to asymmetric and symmetric $-\text{CH}_2$ stretching vibration, respectively. Further, it was observed that the bands in the wavenumber range of $650 - 750\text{ cm}^{-1}$ might be attributed to out-of-plane bending of aromatic rings. The

signature bands of oxirane rings were noticed at $\sim 3050\text{ cm}^{-1}$ and $\sim 825\text{ cm}^{-1}$. The C-O deformation of the oxirane group was identified at 823 cm^{-1} , and the weak band at $\sim 3050\text{ cm}^{-1}$ was noticed for C-H stretching vibration related to the methylene group. But it was difficult to quantify due to its weak intensity and close to the OH absorption. Particularly in NSF40_H, the characteristic bands of HNT at 3400 cm^{-1} , which attribute to the hydroxyl groups of inner surfaces of Al-OH groups shown to overlap with the C-H stretching band arising at 3050 cm^{-1} .

Further, in NSF40_H, the band at 1120 cm^{-1} and 1020 cm^{-1} correspond to Si-O band and Si-O-Si stretching vibration of HNT. The presence of these bands and the shifting of functional bands indicate an excellent interaction of HNT with epoxy groups. It was well-accepted that post-curing dramatically augments the crosslink density in epoxy. As a result, mechanical properties of the epoxy improve besides the glass transition temperature and reduce the residual stresses (Cañavate et al. 2000; Nikolic et al. 2010; Saif and Naveed 2021). An increase in the crosslinking density of epoxy can be predicted using FTIR analysis. Some of the bands remain unchanged, while the bands related to the linkages that participate in curing reactions vary during the crosslinking reaction. Hence, these bands were used for quantitative and qualitative analysis of the reaction progress and crosslink density. For instance, the band at 1609 and 1586 cm^{-1} attributed to benzene rings did not vary during the curing reaction. Instead, the absorption of bands at 3050 , 911 , and 823 cm^{-1} decreased during the reaction due to the epoxy ring opening. The quantitative analysis was somewhat tricky because of the low intensity and close vicinity of the C-H stretching band (3050 cm^{-1}) with the OH band. Hence, evaluation of the band area for the epoxy groups at 911 and 823 cm^{-1} was permitted to determine progress of the reaction. The bands arising at 1607 cm^{-1} and 911 cm^{-1} were deconvoluted (Gaussian fitting method), and their ratios were considered as an indicator of the progress of response while carrying out the analysis in absorbance mode (Figure 3.2(c)). The synergistic effect of fillers and post-cure heating significantly decreased the intensity of the bands arising at 911 and 823 cm^{-1} , indicating the progress of the curing reaction. For the post-cure heated samples, the ratio of absorbance of band area of 911 and 1607 cm^{-1} was lower than that of room temperature cured neat epoxy sample (SF0), which was 0.45 relatively. A significant

decrease in the absorbance ratio indicated an appreciable increase in crosslink density of the epoxy molecular network and confirmed the complete curing reaction of the epoxy.

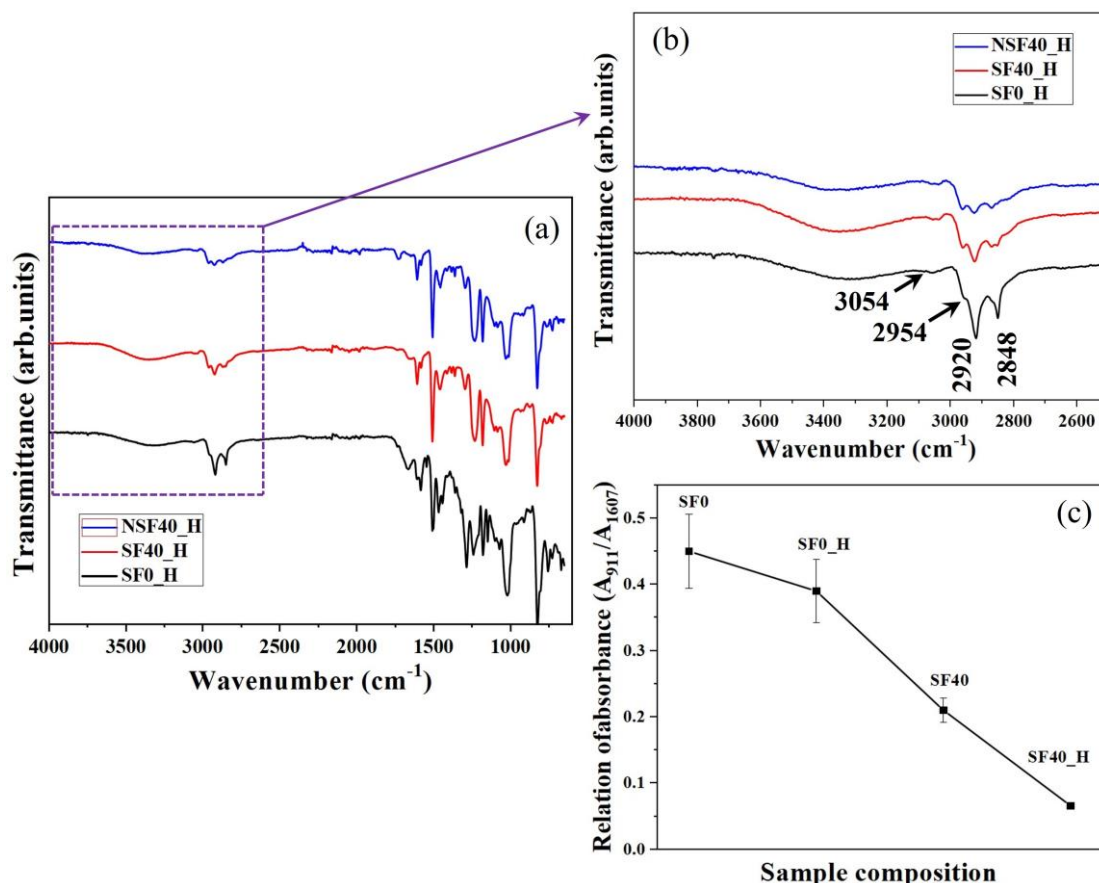


Figure 3.2 (a) FTIR spectra of neat epoxy and RSF composites, with an enlarged view reporting synergism between fillers and the epoxy as depicted in (b), and comparison of relative absorbance between the foams signifying advantage of post-cure treatment shown in (c).

3.2 XRD ANALYSIS

Figure 3.3(a) shows the XRD pattern of a neat epoxy matrix, pristine cenospheres with HNTs, and HNTs RSF composites. The neat epoxy matrix, which is amorphous, does not possess any crystalline peaks. A hump was observed over a range of 2θ value 10 – 30 degrees in XRD (Sathishkumar et al. 2018). The prominent crystalline peaks obtained in the cenosphere were at 2θ values: 16.40° (110), 26.17° (210), 31.00° (001), 35.20° (111), 40.86° (121), 60.67° (331) and 64.26° (002). The reported peaks in cenospheres were similar to mullite mineral with the chemical name

Aluminum Silicon Oxide, which is detailed in ICSD 0.7 - 079 - 153. Further, the intensity peaks arriving at 8.836° (001) showed 100% relative intensity. The peaks at 20.35° (100), 26.58° (003), 54.86° (006), and 62.78° (301) were also shown among the peaks of HNT, which followed the ICSD 00 - 029 - 1489 with the chemical name Aluminum Silicate Hydroxide Hydrate. The most significant XRD peak at 20.35° is related to the tube-like structure of HNT, which makes HNT distinguish itself from the class of platy clays called kaolinite (Saif and Naveed 2021). As mentioned earlier, the crystalline peaks in the HNTs RSF composite shown resemblance to that cenosphere. Interestingly, the absence of the halloysite peaks in the HNTs RSF composite infers that HNTs might have been finely dispersed within the epoxy matrix. Furthermore, Figure 3.3(b) presents the TEM image of HNT having the lumen filled with an epoxy matrix. The intensity of peaks of dispersed nanoparticles remained absent in the XRD spectrum of nanocomposites that might undergo intercalation and/or exfoliation (Tang et al. 2011).

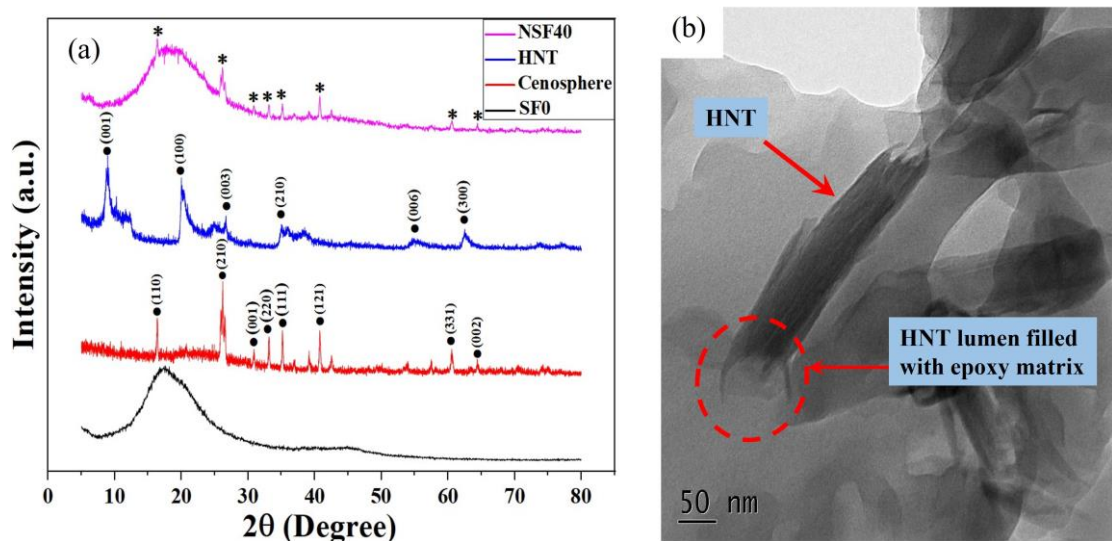


Figure 3.3 (a) XRD spectra of neat epoxy, pristine cenosphere, HNTs, and HNTs RSF composite, (b) TEM image depicting the occupancy of the epoxy network in the HNT lumen.

HNTs-polymer nanocomposites can be made reasonably quickly using standard processing techniques when compared to CNTs-base polymer composites. First, while the aspect ratio of CNTs is greater than that of HNTs also, HNTs have the proper aspect ratio (~ 10) for dispersion in the polymer matrix. Additionally, the shearing force used to disperse the nanotubes can be used to reduce the length of HNTs during processing.

Second, the HNTs' inter-tubular interactions are comparatively weak, making shearing during processing an effective means of achieving good dispersion. In Figure 3.4(c), the closely held HNTs correctly validate weak tube-tube interaction. Similar findings were reported in studies carried out by Liu et al. (2019). Thus, processing HNTs-polymer nanocomposites does not require surface pre-treatment of the HNTs. In the majority of polymer systems, raw HNTs successfully reinforce polymers (Liu et al. 2019b). The dispersion of nanofillers also affects the modulus value in polymer nanocomposites. The random dispersion i.e., planar, as shown in Figure 3.4(b) augmented the resultant properties of the polymer nanocomposites corroborating better reinforcing efficiency of nanotubes in the matrix. Similar outcomes concerned with the dispersion were elucidated by Šupová et al. (2011).

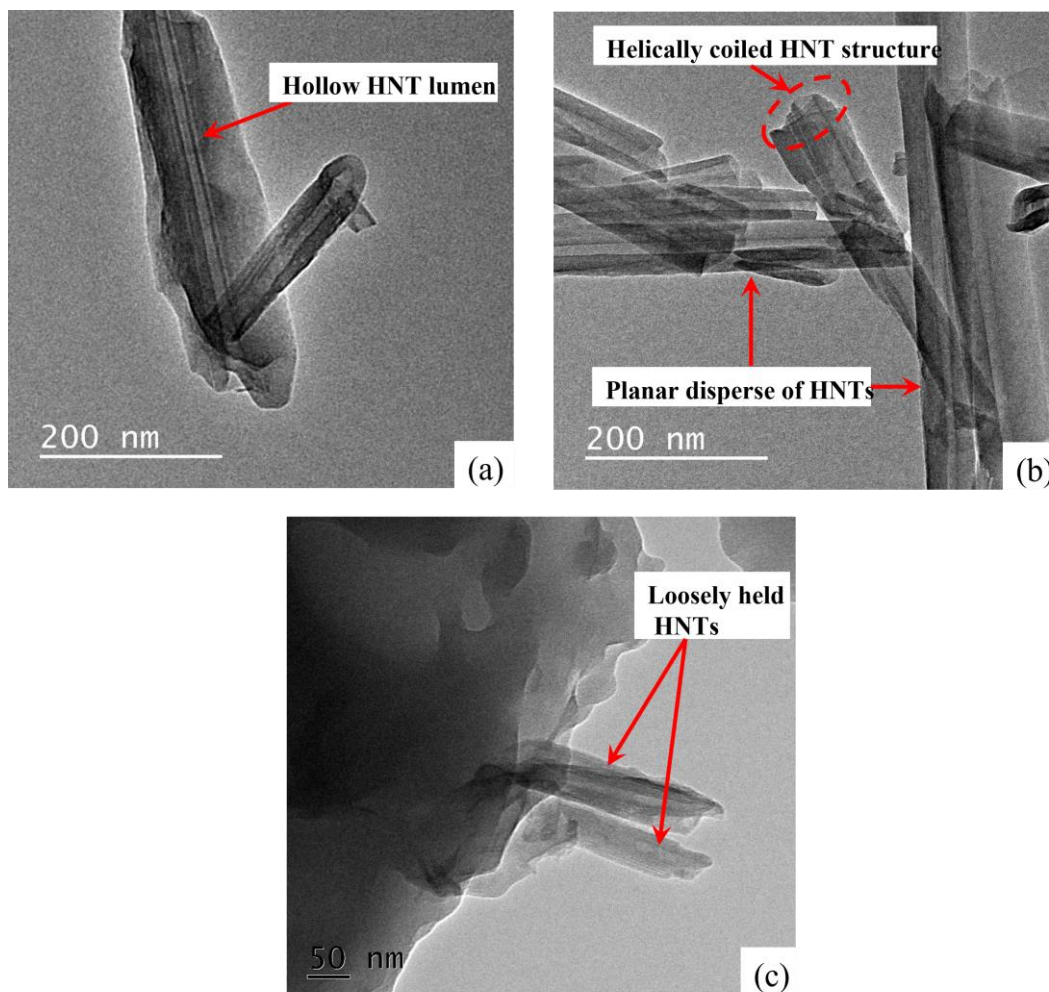


Figure 3.4 TEM images showing (a) HNTs hollow structure, (b) planar dispersion of HNTs, and (c) loosely held HNTs.

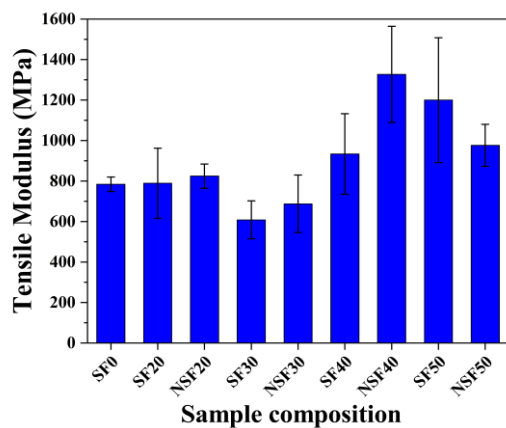
3.3 TENSILE RESPONSE

The tensile properties of neat epoxy, CESFs, and HNTs RSFs are listed in Table 3.1. It may be observed from this table that two types of comparison on the strength and modulus of all samples were presented. The first one was the effect of content of cenospheres volume fraction in the neat epoxy, and another was its comparison with the HNTs RSF with 1 vol.% HNTs reinforcement. In the case of tensile loading, the matrix being a continuous medium in all kinds of samples, carried most of the loads, as inferred by Wouterson et al. (2007). Thus, the tensile strength of neat epoxy was the highest (47.43 MPa) among all fabricated samples, as presented in Figure 3.5. With the increase of cenospheres content, the tensile strength decreased because of the lower strength of the cenospheres compared to the neat epoxy. Further, with the addition of HNTs, the tensile strength decreased over a range of 18 - 67% with respect to CESF. A similar trend of reduction in strength with HNTs reinforcement was reported by Dando and Salem (2017). However, adding cenospheres increased the tensile modulus over the range of 1 - 52% with respect to the neat epoxy matrix, except for SF30, wherein the cracks passed through significant voids during tensile loading may bring the modulus value down. It is also evident from Table 3.2 that the possible entrapments during the fabrication process resulted in voids. Hence, actual density deviated from the theoretically calculated ones.

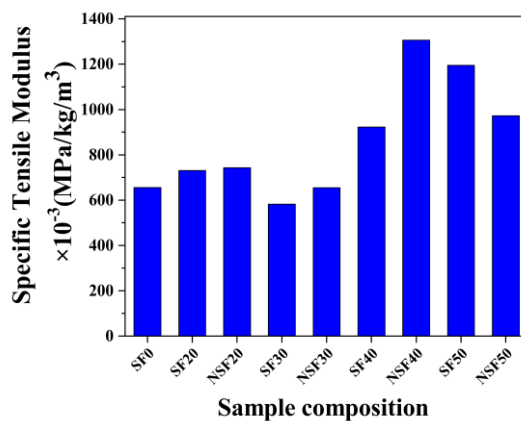
Table 3.1 Tensile modulus and strength properties of RSF composites.

Sample	Tensile	
	Modulus (GPa)	Strength (MPa)
SF0	784.33 ± 35.36	47.43 ± 6.10
SF20	789 ± 173.46	32.5 ± 5.06
NSF20	824.33 ± 59.69	22.1 ± 7.96
Variation (%)	+4	-32
SF30	608 ± 93.60	23.36 ± 5.26
NSF30	687.33 ± 142.01	11.09 ± 3.59
Variation (%)	+13	-52
SF40	933.33 ± 198.90	21.93 ± 2.81
NSF40	1326.67 ± 237.95	7.15 ± 1.26
Variation (%)	+42	-67.3
SF50	1199.66 ± 308.34	13.94 ± 5.75
NSF50	976.33 ± 103.83	16.49 ± 5.95
Variation (%)	-18	-18

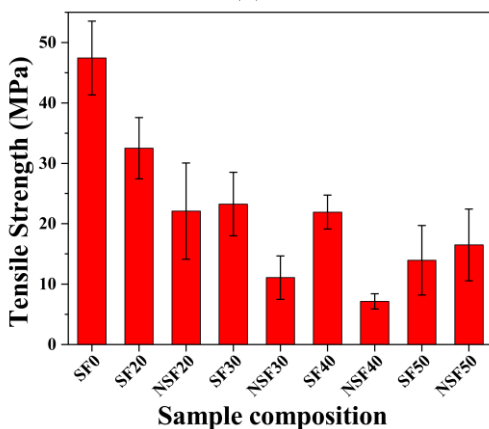
On the other hand, a maximum of 42% of enhancement in modulus was observed for NSF40 with reference to SF40 due to the presence of HNTs reinforcement in HNTs RSF. These HNTs increase the crosslinking tendency with neat epoxy, eventually resulting in better stress transfer within the molecular chains of neat epoxy microstructure. Such strengthening of neat epoxy was well supported by literature (Li et al. 2013a; Zhang et al. 2014a). It is evident from the FTIR spectra (Figure 3.1) that a hydrogen bonding existed between HNT and the chain of a neat epoxy matrix, causing HNTs RSF to exhibit superior mechanical properties relative to CESF samples. The NSF50 samples exhibited lower modulus values than NSF40 due to the possible cenospheres breakage with 50 vol.% cenospheres in NSF50. The neat epoxy registered maximum specific tensile strength of 39.67 MPa/Kg/m³ and NSF40 measured a maximum specific tensile modulus of 1360.29 MPa/Kg/m³ among all the fabricated samples.



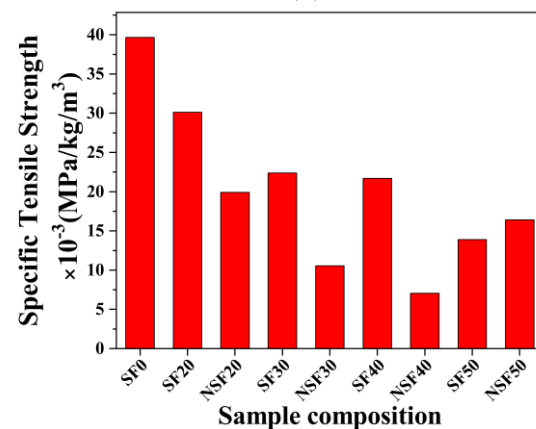
(a)



(b)



(c)



(d)

Figure 3.5 Experimentally measured (a) tensile modulus (b) specific tensile modulus (c) tensile strength and (d) specific tensile strength of RSF composites.

Table 3.2 Density and void content of room temperature cured RSF composites.

Sample type	ρ_{th} (g/cc)	ρ_{exp} (g/cc)	ϕ_v (%)	Weight saving potential w.r.t SF0
SF0	-	1.1955 \pm 0.018	0.37	-
SF20	1.1404	1.0793 \pm 0.023	5.35	4.6
NSF20	1.1565	1.1101 \pm 0.021	4.01	3.3
SF30	1.1128	1.0438 \pm 0.019	6.25	6.9
NSF30	1.1289	1.0493 \pm 0.017	7.05	5.6
SF40	1.0835	1.0116 \pm 0.023	6.79	9.2
NSF40	1.1014	1.0156 \pm 0.020	7.79	7.9
SF50	1.0577	1.0038 \pm 0.018	5.10	11.5
NSF50	1.0738	1.0040 \pm 0.021	6.50	10.2

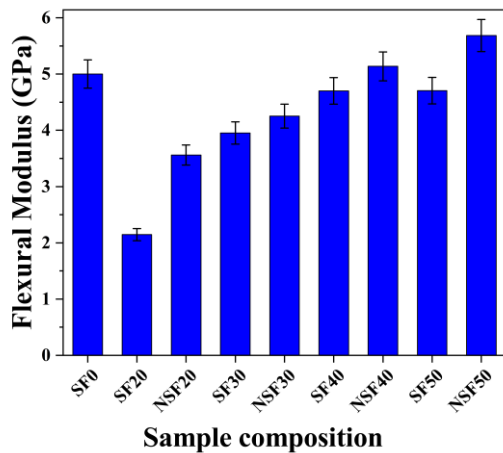
3.4 FLEXURAL RESPONSE OF ROOM TEMPERATURE CURED COMPOSITES

Figure 3.6 summarizes experimentally measured flexural properties obtained from the load-displacement data of the test. The flexural strength (111 MPa) and modulus (5 GPa) of neat epoxy reported in Figure 3.6 were the highest among all composite samples. All the CESFs registered flexural strength and modulus values less than the neat epoxy, as presented in Table 3.3. With the addition of cenospheres in neat epoxy matrix, the flexural modulus was enhanced with the range of 2.14 - 4.70 GPa. Similar results were reported in earlier work (Labella et al. 2014). In the case of HNTs RSFs, the flexural strength enhancement by 58% and 31% in NSF20 and NSF50 were reported, respectively, over their counter CESFs. However, the maximum decrease in strength of 30% is witnessed for NSF30. It may be because of improper load transfer due to the possible clustering of HNTs. The flexural modulus of NSF50 was measured at 13% higher than all the samples, including a neat epoxy matrix. Further, a 7 - 66% of improvement in flexural modulus in HNTs RSFs was observed against the CESF. NSF20 records 3.56 GPa which is 66% higher than the SF20 sample. The increase in flexural modulus by HNTs reinforcement may be attributed to efficient stress transfer from HNTs to the epoxy matrix, which is evident by FTIR analysis as shown in Figure 3.1. Similar improvement in flexural modulus by HNTs in the epoxy matrix was

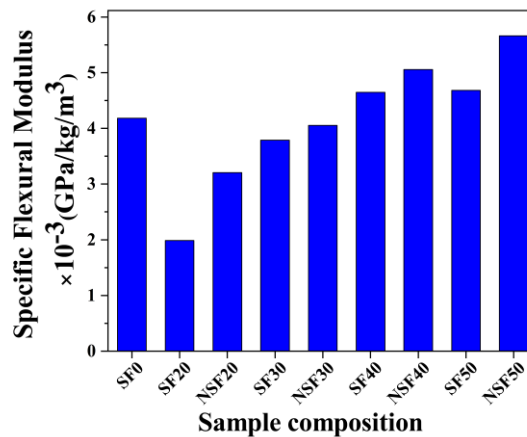
obtained in earlier studies (Dando and Salem 2017; Maharsia et al. 2006; Peter and Woldesenbet 2008). The specific flexural strength for SF0 was 92.84 MPa/Kg/m³, and NSF50 reported a maximum specific flexural modulus of 5.6 GPa among all the fabricated samples.

Table 3.1 Flexural modulus and strength properties of RSF composites.

Sample	Flexural	
	Modulus (GPa)	Strength (MPa)
SF0	5 ± 0.58	111 ± 1
SF20	2.14 ± 0.12	29.83 ± 4.42
NSF20	3.56 ± 0.35	47.23 ± 1.59
change (%)	+66	+58
SF30	3.95 ± 0.41	50.26 ± 2.1
NSF30	4.25 ± 0.54	35.1 ± 5.66
change (%)	+7	-30
SF40	4.7 ± 0.23	46.26 ± 4.27
NSF40	5.13 ± 0.30	35.06 ± 0.94
change (%)	+9	-24
SF50	4.70 ± 0.37	26.9 ± 1.2
NSF50	5.68 ± 0.36	35.43 ± 2.11
change (%)	+20	+31



(a)



(b)

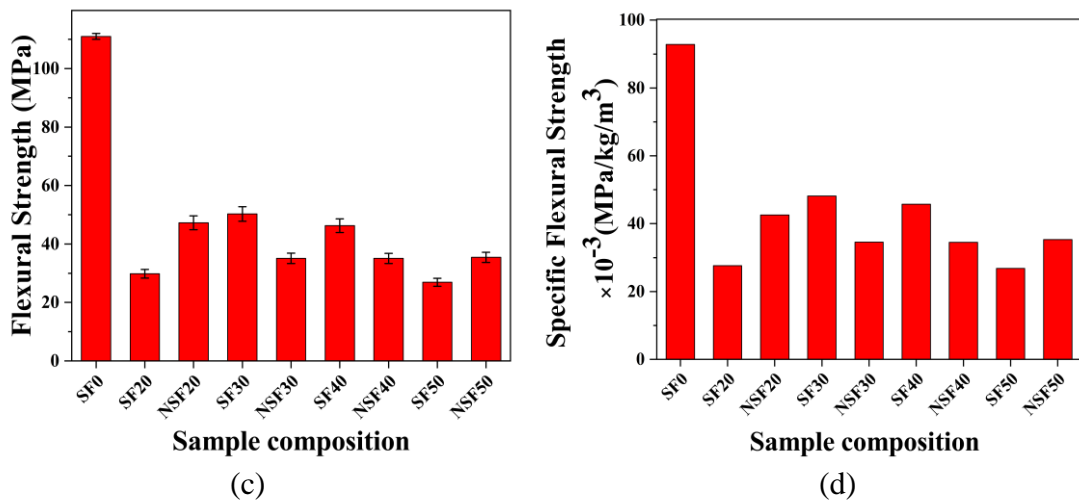


Figure 3.6 Experimentally measured (a) flexural modulus (b) specific flexural modulus (c) flexural strength and (d) specific flexural strength of RSF composites.

3.4.1 SPECTROSCOPY OF FRACTURE FEATURES OF POST-FLEXURAL TEST SPECIMENS

Fracture characteristics of composites containing 20 and 50 vol.% of cenospheres with and without HNTs reinforcement are analyzed and are shown in Figure 3.7 and Figure 3.8, respectively. The micrographs were taken with gold sputtering on post-flexural fracture surface of the specimens. All micrographs in Figure 3.7 and Figure 3.8 show less amount of debris, indicating a tensile fracture of all samples, which is evident from previous studies (Chan et al. 2011; Dando, Kerrick R. 2019; Ravichandran et al. 2019). The crack initiates from the specimen's tensile side, reaching the compression side where major cenospheres crushing was witnessed. Moreover, the micrographs of higher magnification revealed cenospheres debonding during the fracture process, implying that the matrix material carried most of the stress during the loading process. The extensive plastic deformations were noticed for the neat epoxy devoid of debris, as depicted in Fig. 3.7(a). In Figure 3.7(b), the cracks were observed with weak interfacial bonding between cenospheres and the matrix, whereas in Figure 3.7(c), good adhesion of cenospheres is noticed due to the HNTs reinforcement. A similar morphology is observed in Figure 3.8 with a little more cenospheres breakage due to particle-particle collision at 50 vol.% cenospheres addition. The intactness of cenospheres is enhanced due to hydrogen bonding provided

by the reinforcement of HNTs in the matrix. Consequently, with better stress transfer, superior mechanical properties in HNTs RSFs were obtained as compared to CESFs.

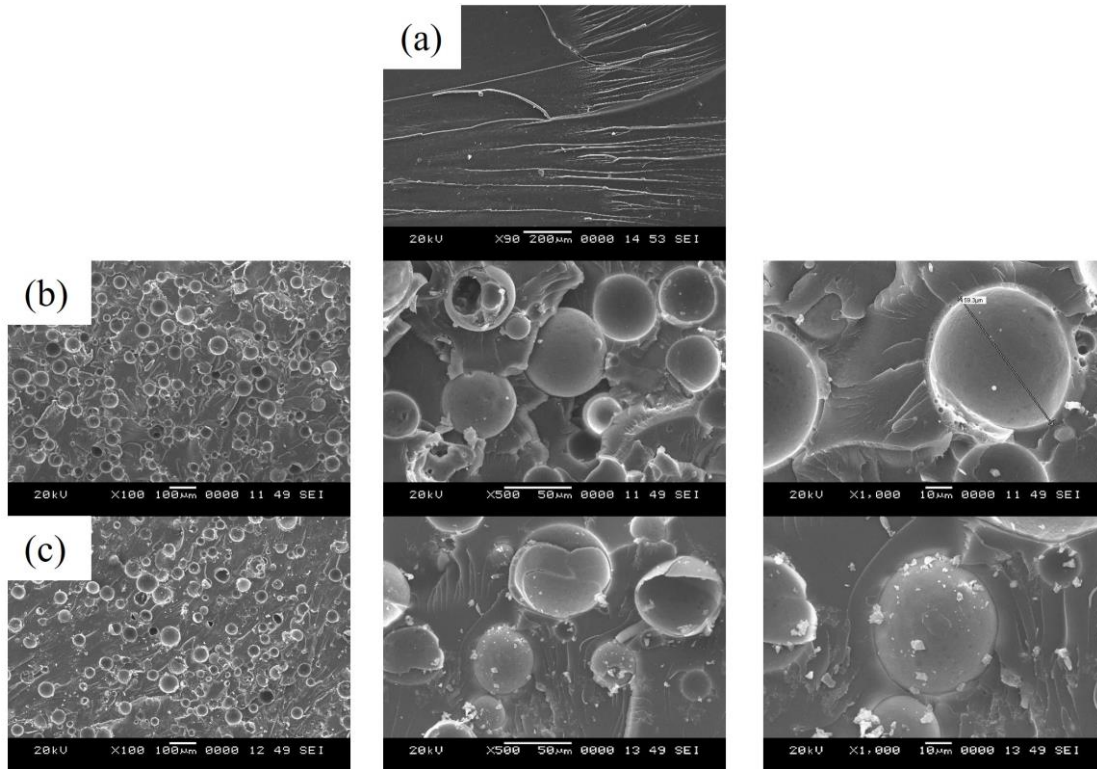


Figure 3.7 Morphology of post flexural test specimens (a) Neat Epoxy (b) SF20, showing rough matrix failure (c) NSF20, displaying intactness of cenospheres within the matrix.

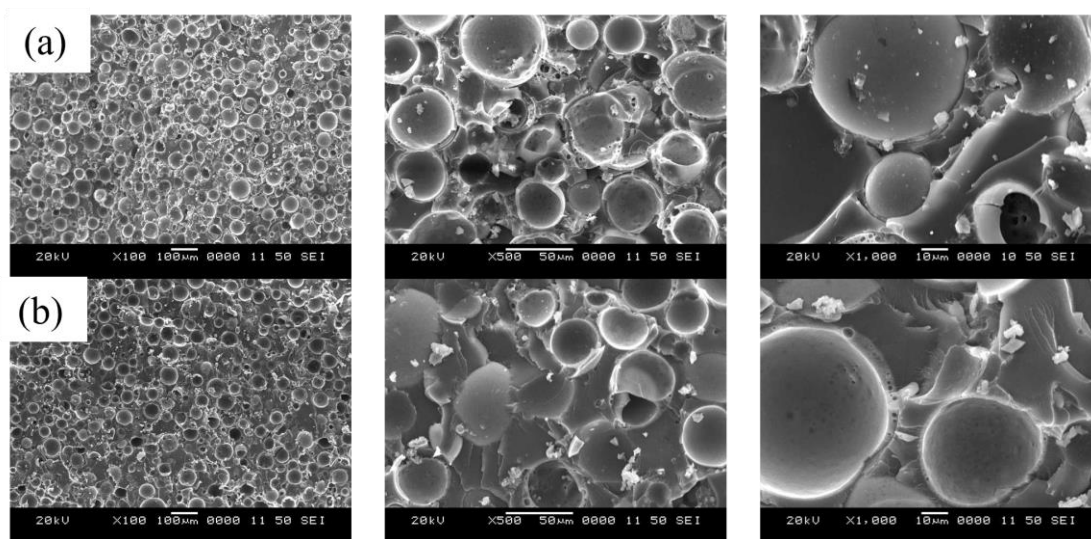


Figure 3.8 Morphology of post flexural test specimens (a) SF50, showing poor bondage and breakage of cenospheres in the matrix (b) NSF50, showing cenospheres intact with the matrix.

Fracture features for a representative sample comprising 40 vol.% of cenospheres with and without HNTs reinforcement can be observed in Figure 3.9 and Figure 3.10, respectively. Micrographs of post-flexural fracture specimens were considered for the study. Identical features of fracture were noticed for both CESFs and HNTs RSFs. Analogous to the CESF sample, the tensile fracture was also recorded in HNTs reinforced HNTs RSFs. The tension side of the surface depicted retaining of cenospheres, whereas, on the compression side, the breakage/crushing of cenospheres resulted in more debris.

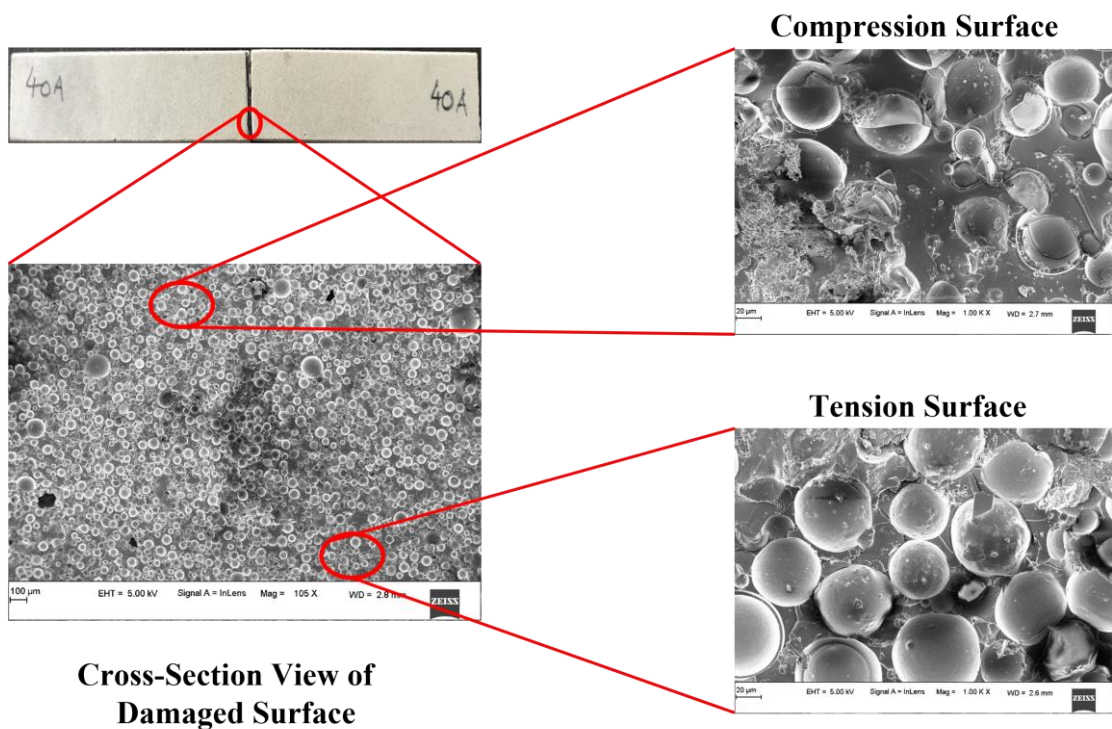


Figure 3.9 Schematic micrographs of SF40 post-flexural test specimen.

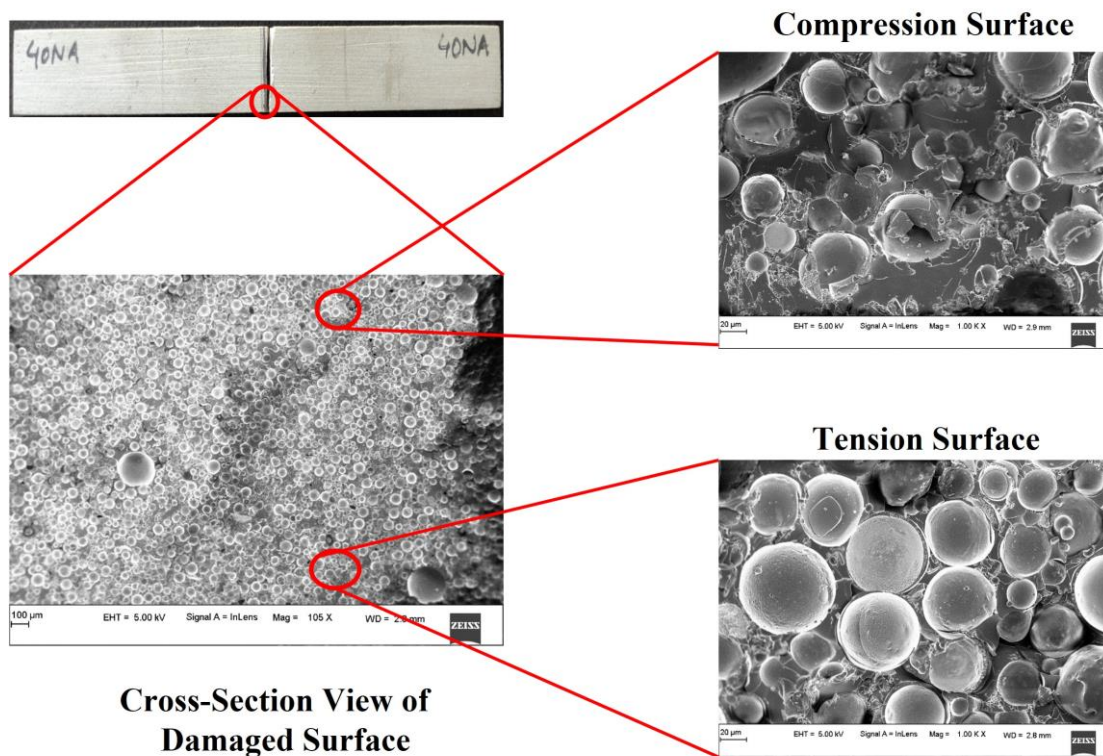


Figure 3.10 Schematic micrographs of NSF40 post-flexural test specimen.

Figure 3.11 elucidated peculiar features of the fracture surface of the NSF40 specimen. It may be understood from Figure 3.11(a) that cenospheres failure occurred by crushing under flexural loading. The higher magnification of Figure 3.11(a) confirmed in-built porosity within the thin wall of cenospheres, which was also supported by Garcia et al. (2018) as shown in Figure 3.11(b). Figure 3.11(c) shows a representative void introduced due to the entrapped air during the fabrication process. The presence of voids may reduce the density of composites making a lightweight structure. Moreover, excess voids may adversely influence the intended mechanical properties. These voids with coalescence may protrude as a potential crack in upbrining the failure of the material well below its strength. This may be one of the reasons for deviations in modulus and strength values of the fabricated specimens. As shown in Figures 3.11(d) and 3.11(e), HNTs can be seen on the fracture surfaces within the matrix. It is clear from the figures that the presence of HNT offers resistance to crack propagation, consequently deflecting the crack and bridging it. Meanwhile, HNTs reinforcement toughened the microstructure of epoxy matrix with strong crosslinking of hydrogen bonds, delivering the required strength to inhibit the crack.

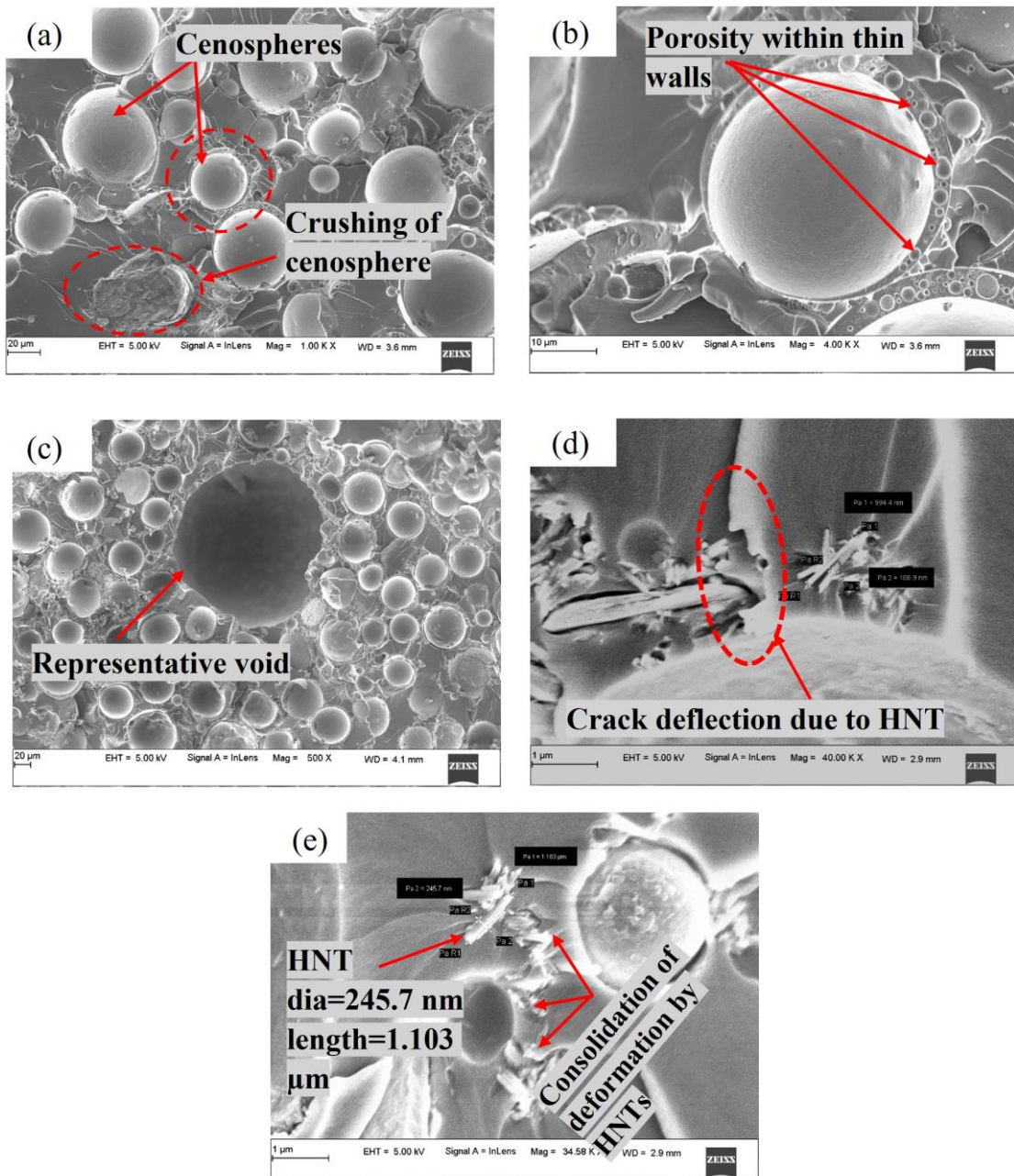


Figure 3.11 Morphology of NSF40 post-flexural test specimens depicting (a) Crushing of fly ash cenosphere, (b) Presence of porosity within thin cenosphere walls, (c) Representative void introduced by entrapped volatiles, (d) Crack deflection in the matrix due to HNTs, and (e) deformation consolidation by HNTs.

3.5 FLEXURAL RESPONSE OF POST-CURED COMPOSITES

The post-cured RSF composites undergo a density reduction due to the evolution of entrapped particles during the process, as shown in Figure 3.12. Figure 3.13 shows representative flexural stress-strain curves of post-cure heated RSF

composites. The curves portray a linear behavior and then a sudden drop after reaching peak stress which was recorded as flexural strength of the composites. Table 3.4 compares the flexural properties of room temperature cured and post-cured heated samples. When the flexural load was applied to the composites, major load-carrying member was the broad network of epoxy matrix. Therefore, SF0 entered a maximum flexural modulus value of 3.15 GPa and 101 MPa flexural strength among all the samples. With addition of cenospheres, the flexural modulus has increased. SF40_H witnessed 3.58 GPa of flexural modulus, which was 76.31% higher than that of SF20_H. It may be attributed to the cushioning effect of cenospheres rendered to epoxies (Jha et al. 2011). In addition, with HNTs reinforcement, the flexural modulus enhancement was obtained over 11.73% - 60.10% concerning their corresponding post-cured CESF composites. The HNTs addition did not follow a similar trend in increasing the flexural strength, unlike the cenospheres.

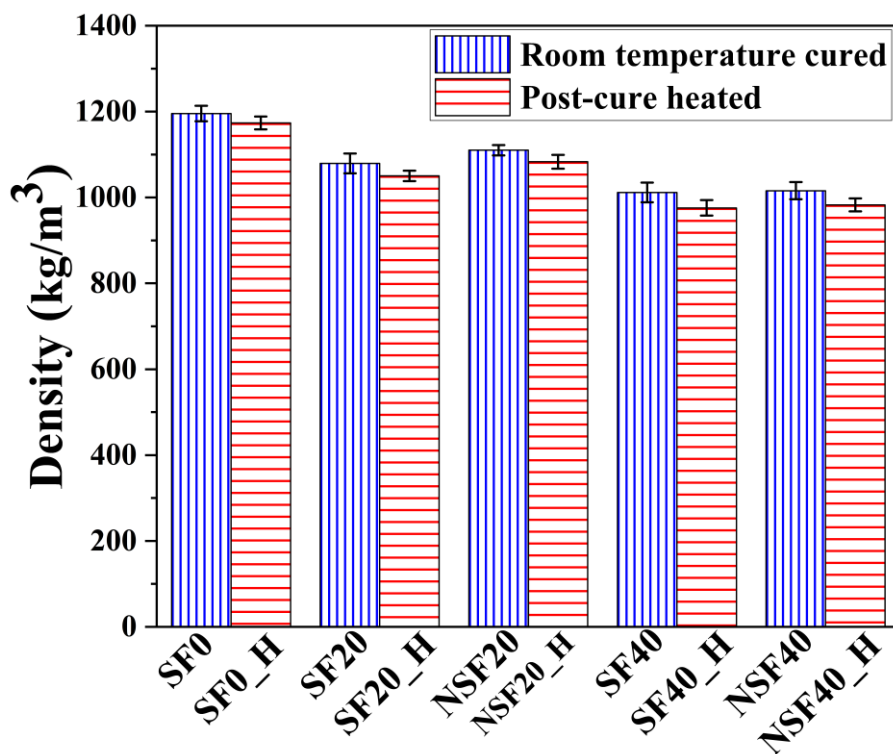


Figure 3.12 The density of the RSF composites.

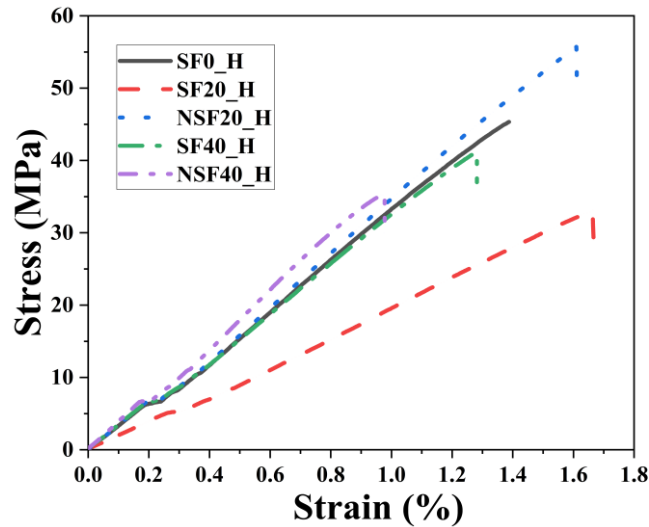


Figure 3.13 Flexural stress-strain curve of post-cure heated RSF composites.

It was interesting to note the reduction in the flexural properties when post-cure treatment was carried out. From Table 3.4, it can be inferred that the neat epoxy matrix (SF0_H) showed a 58.73% reduction in flexural modulus concerning its corresponding room temperature cured sample (SF0). Also, all other fabricated composites undergo a similar reduction in flexural modulus over a range of 5.40% - 31.20%. The reason for the comparative lower modulus reduction in RSF than the neat epoxy was due to synergism between the fillers in RSF, rendering thermal stability. In the case of flexural loading, the main deformation mechanism of laminated composites is presumed, wherein a portion of the loaded specimen undergoes compression and the other in tension. So, when a thermally exposed sample was loaded, the tension side of specimen was easily prone to open up shear cracks. Hence this made the material bear lower loads before failure (Birger et al. 1989; Kandare et al. 2010). When the crack progresses from the tension side of the specimen, cenospheres being spherical stood less significant to arrest it. Whereas HNTs with advantageous nanoscale size, uniformly dispersed throughout the epoxy matrix, counters a while in such events. SF0_H registered a flexural specific modulus value of 2.675×10^{-3} GPa/kg/m³ that was 37.19 % and 52.19 % lower than that of SF40_H and NSF40_H, respectively, as shown in Figure 3.14. However, all the RSF composites exhibited a specific flexural strength value lesser than SF0_H, i.e., 8.60×10^{-2} MPa/kg/m³ (Figure 3.14(d)), which remains a future concern of the study to balance even the strengths along with modulus enhancement.

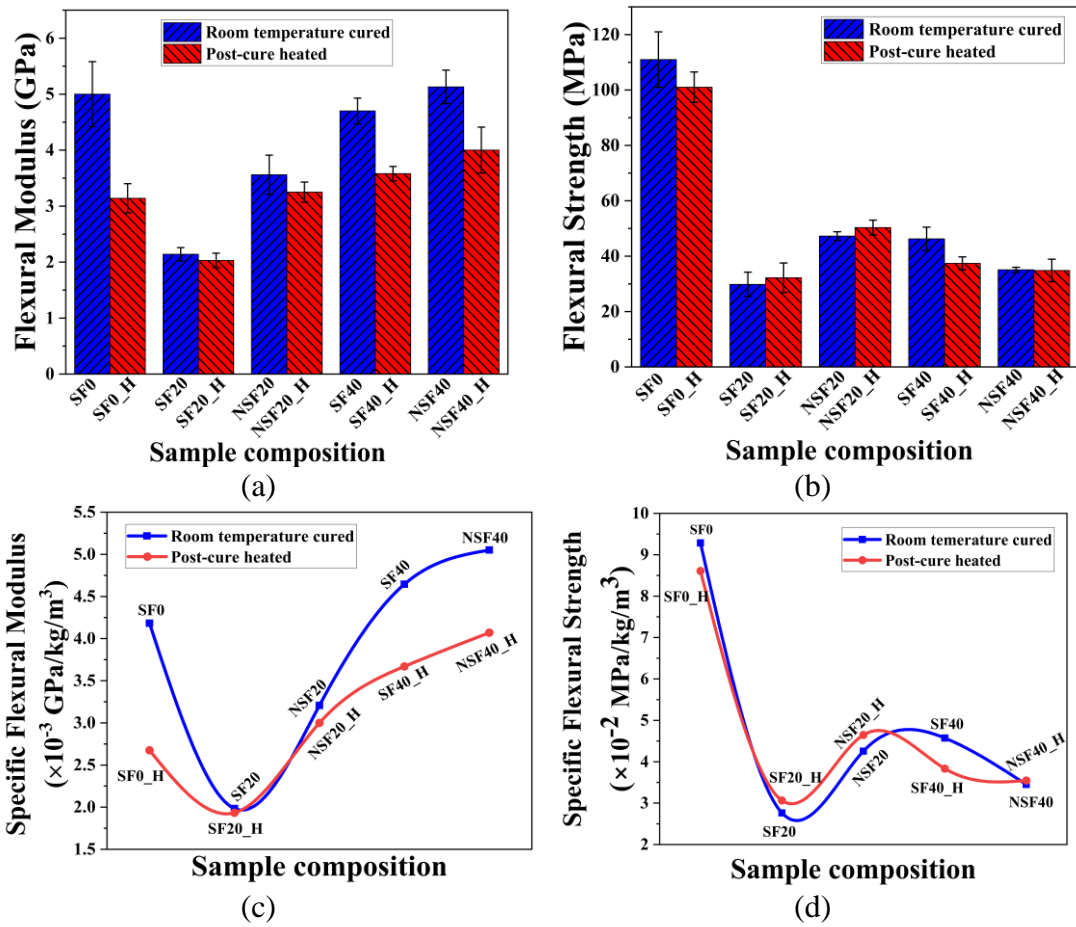


Figure 3.14 Shows (a) flexural modulus (b) flexural strength (c) specific flexural modulus (d) specific flexural strength, for room temperature cured and post-cure heated RSF composites.

Table 3.2 Flexural modulus and strength of room temperature cured and post-cure heated RSF composites.

Room temperature cured samples					Post-cure heated samples				
Sample	Modulus (GPa)	Error Margin (%)	Strength (MPa)	Error Margin (%)	Sample	Modulus (GPa)	Error Margin (%)	Strength (MPa)	Error Margin (%)
SF0	5.00 ± 0.58	± 9.52	111.0 ± 1	±12.83	SF0_H	3.15± 0.26	± 8.45	101.0 ± 5.50	±14.50
SF20	2.14 ± 0.12	±11.17	29.83 ± 4.42	±21.27	SF20_H	2.03 ± 0.13	±3.91	32.2 ± 5.32	±23.66
NSF20	3.56 ± 0.36	±16.69	47.23 ± 1.59	±9.82	NSF20_H	3.25 ± 0.18	±7.22	50.33 ± 2.68	±12.53
% change	+ 66.0	—	+ 58.0	—	% change	+ 60.1	—	+ 56.3	—
SF40	4.70 ± 0.23	±7.73	46.26 ± 4.27	±19.35	SF40_H	3.58 ± 0.13	±13.77	37.40 ± 2.33	±19.07
NSF40	5.13 ± 0.30	±13.18	35.06 ± 0.94	±5.19	NSF40_H	4.00 ± 0.41	±10.22	34.83 ± 4.07	±16.67
% change	+ 9	—	-24	—	% change	+ 11.73	—	- 6.8	—

3.6 COMPRESSIVE RESPONSE OF ROOM TEMPERATURE CURED AND POST-CURED COMPOSITES

The representative stress-strain curves of the current study are presented in Figure 3.15. This typical compression response curve consisted of three regions as similarly reported by (Li and Nettles 2010; Shahapurkar et al. 2018). Linear behavior of the RSF undergoing elastic deformation was termed region-1. As region-1 gradually ends, the stress drops slightly, indicating the yield point of the RSF. This region is called the plateau region or region-2. Typically, region-2 displays the energy consumption by RSF; meanwhile, crushing of the cenospheres occurs. The crushed cenosphere which has a hollow cavity within, gets occupied by the fractured moiety. The densification region (region-3) starts with a substantial amount of progressive cenospheres crushing where the curve takes an upward trend, as shown in Figures 3.15 (a, b). The obtained stress-strain behavior is analogous to the results reported by Bunn and Mottram (1993).

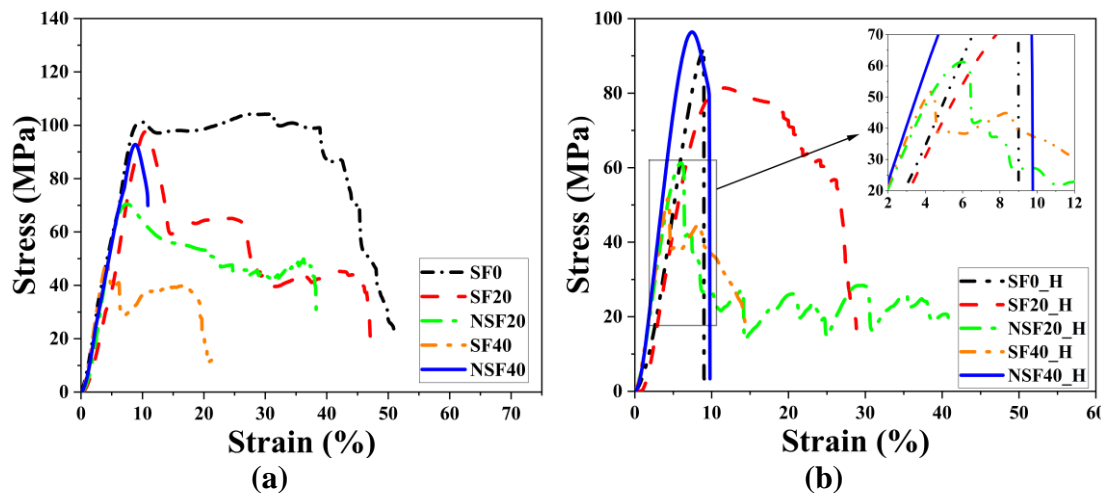


Figure 3.15 Compression stress-strain curves of (a) room temperature cured and (b) post-cure heated RSF composites.

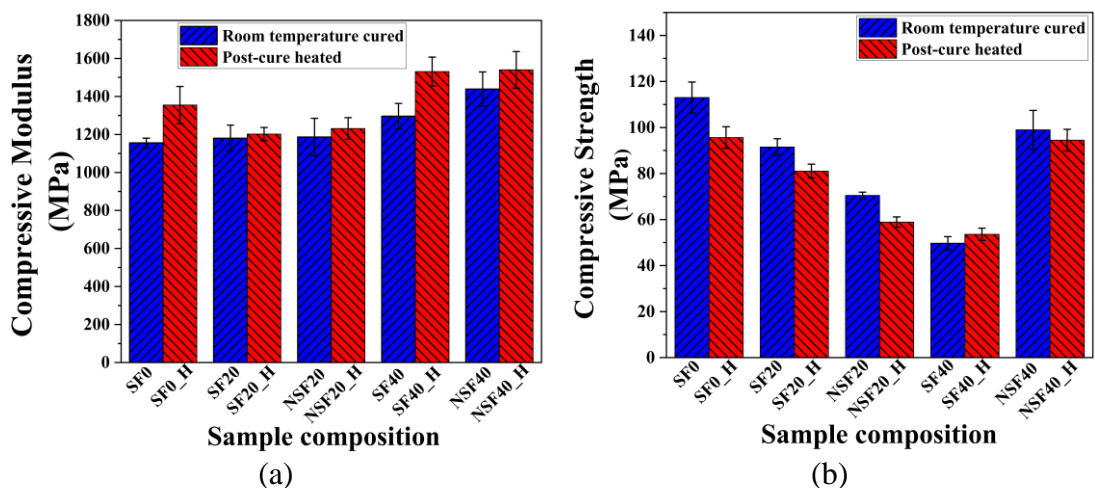
Compression modulus is obtained from the linear part of region-1 (elastic region) of the stress-strain curve. The results reported that the compressive modulus increased with an increase in the cenospheres content. Also, the compressive modulus of SF0 was lower than all the RSF composites. Further, with the addition of HNTs, compressive modulus enhancement in the range of 0.54% – 9.91% is noticed with respect to corresponding CESF composites. Furthermore, a maximum of 1.417

MPa/kg/m³ of specific compressive modulus was achieved by NSF40, which stands at 10.6% and 46.6% higher than that of SF40 and SF0, respectively. Hence, significant weight savings and better performance were achieved with the synergy of dispersed fillers within the matrix. The structure of RSF composites, when tailored with different amounts of filler addition, eventually brings out an increment in compressive properties. Specifically, the modulus (mechanical property) is enhanced. The crosslinking of HNTs with the base epoxy matrix is one of the reasons for modulus improvement which is evident in Figure 3.1 (FTIR study). The compressive strength is determined as the first peak-stress value of the curves from Figure 3.15. With the addition of cenospheres, the compressive strength of the RSF composites was reduced. Table 3.5 shows that SF0 exhibits the highest compressive strength among all samples, with a value of 113 MPa. The decrease in strength with such hollow inclusions is also reported earlier (Patil et al. 2019; Zhang and Ma 2010). Nevertheless, NSF40 exhibited a specific compressive strength value of 9.74×10^{-2} MPa/kg/m³, which was 11.57% higher than SF0.

Table 3.3 Compressive modulus and strength of room temperature cured and post-cure heated RSF composites.

Room temperature cured samples					Post-cure heated samples				
Sample	Modulus (MPa)	Error Margin (%)	Strength (MPa)	Error Margin (%)	Sample	Modulus (MPa)	Error Margin (%)	Strength (MPa)	Error Margin (%)
SF0	1155.5 ± 25.2	±4.82	113.0 ± 6.74	±2.11	SF0_H	1354.6 ± 97.8	±21.56	95.61 ± 4.71	±6.65
SF20	1180.2 ± 69.1	±11.71	91.5 ± 3.6	±3.20	SF20_H	1202.0 ± 34.5	±8.38	81.04 ± 3.02	±4.08
NSF20	1186.6 ± 98.1	±19.57	70.48 ± 1.42	±0.89	NSF20_H	1231.1 ± 57.4	±12.33	58.90 ± 2.21	±7.72
% change	+ 0.54	—	- 21.02	—	% change	+ 2.36	—	- 27.3	—
SF40	1296.0 ± 67.2	±9.35	49.7 ± 2.85	±2.93	SF40_H	1530.8 ± 76.4	±7.28	53.58 ± 2.69	±9.23
NSF40	1438.7 ± 89.8	±7.99	98.98 ± 8.42	±11.48	NSF40_H	1540.0 ± 96.3	±9.07	94.46 ± 4.75	±7.49
% change	+ 9.91	—	+ 49.78	—	% change	+ 0.597	—	+ 43.27	—

Figure 3.15(b) shows the representative compressive stress-strain curve of post-cure heated RSF composites which followed a similar pattern as Figure 3.15(a). It can be seen from Table 3.5 that the compressive modulus of all samples increased with the thermal treatment. In the case of SF0_H, the modulus obtained after post-cure heat treatment was 1354.6 MPa, which stood 17.2% higher than SF0 with a value of 1155.5 MPa. Interestingly, there existed a synergy between HNTs introduction and the thermal treatment in upbrining of the compressive properties of these RSF composites. The specific compressive modulus of NSF40_H exhibited 1.567 MPa/kg/m³, which was 7.0, 35.7, and 33.3% higher than NSF40, SF0_H, and SF0, respectively, as shown in Figure 3.16(c). Also, NSF40_H registered a specific compressive strength value of 9.61×10^{-2} MPa/kg/m³, which was 1.3% lower than NSF40 and 17.9% higher than SF0_H, as shown in Figure 3.16(d). These advantageous outcomes are suitable for compressive loading applications. Two main reasons can support the increase in modulus by thermal post-curing. One is the conversion of epoxies and enhanced crosslinking (Mgbemena et al. 2018) within the epoxy matrix and constituents, which is corroborated by the above FTIR study (Figure 3.2). Secondly, that the T_g is enhanced concerning the corresponding room temperature cured samples with post-cure heating. The increase in T_g may arise owing to the subdued plasticization. Thus, plasticization helps in improving compressive properties of the HNTs RSF composites (Yuan et al. 2020).



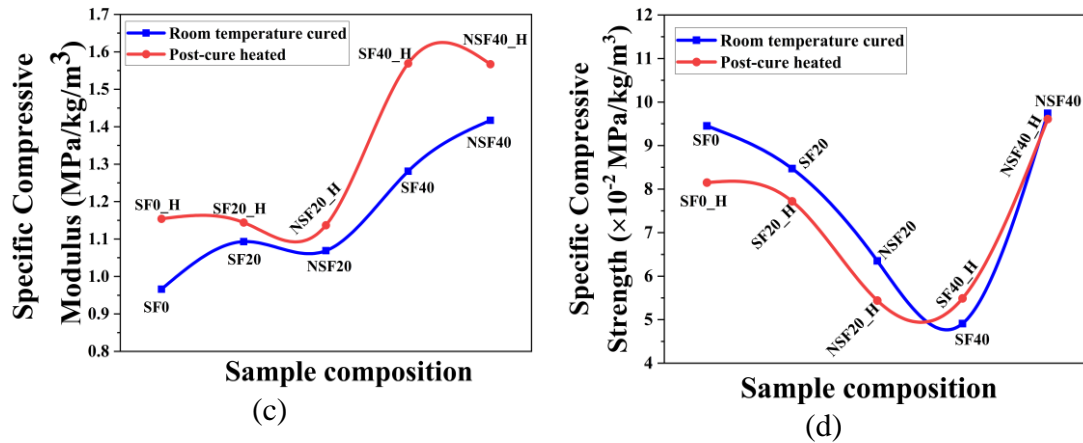


Figure 3.16 Shows (a) compressive modulus (b) compressive strength (c) specific compressive modulus (d) specific compressive strength, for room temperature cured and post-cure heated RSF composites.

3.6.1 MICROGRAPHIC IMAGE ANALYSIS OF POST-COMPRESSION TEST SPECIMENS

Figure 3.17 shows the fractured surfaces of the post-compression test of RSF composites. In Figure 3.17(a), SF0 possesses rough exteriors upon its fracture. Not much debris is found on the surfaces, which imply the matrix failed in a brittle manner. From Figure 3.17(b), it was observed that CESF exhibits breakage of the cenosphere. The matrix eventually takes more load during compression because it contains a low percentage of cenosphere. From Figure 3.17(d), it is noticed that with a higher amount of cenospheres addition, retention in the morphology is witnessed with minimum matrix debris on the fracture surface. But in Figure 3.17(c and e), the HNTs reinforcement improved the load-bearing compressive properties making the surface appear relatively more intact with the cenospheres.

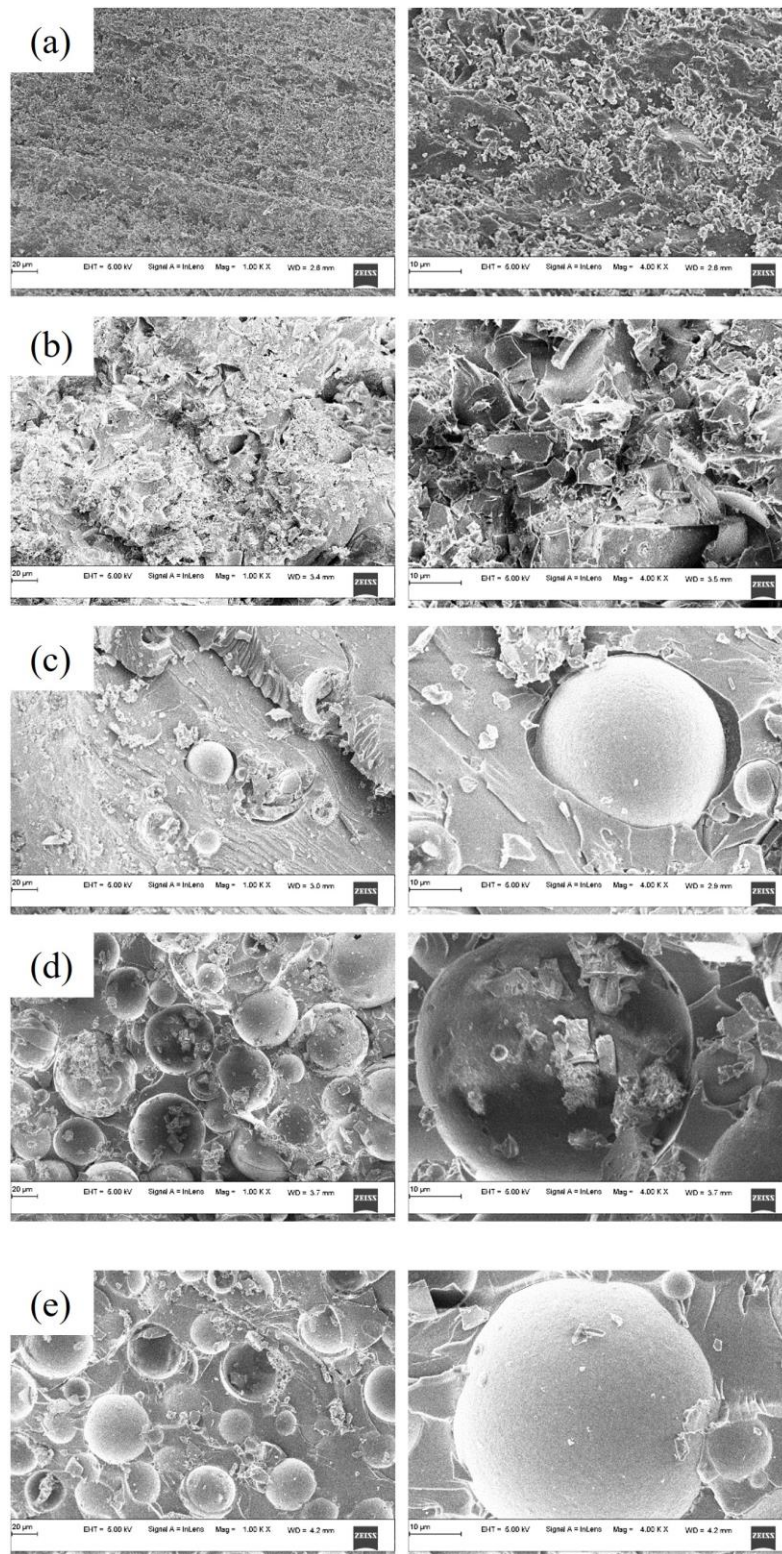


Figure 3.17 Morphology of (a) SF0, (b) SF20, (c) NSF20, (d) SF40, and (e) NSF40 post-compression test samples show the modification of matrix properties by HNTs inclusion.

Figure 3.18 shows fracture features of the surface of specimen subjected to compression loading depicting a load transfer from matrix to HNTs. There are two possible ways in which the applied load to polymer nanocomposites might be distributed to the reinforcement. One is the load transfer between nanoparticles via polymer matrix, while other is the load transfer from matrix to nanotubes. This is known as the "load transfer mechanism", which is also reported in similar studies (D. Qian and E. C. Dickey 2001; Naraghi et al., 2010; Schadler et al., 1998). Additionally, HNTs yield to the applied stress, which causes the nanotube to pull out from microstructure and permits the dissipation of additional energy. Thus, proportionate load bearing is shouldered by appreciable bonding between the HNTs and epoxy. The nanofiller reinforcing mechanisms such as load transfer and pull-out mechanism, crack-pinning make the material bear more load before its failure attributing to enhanced mechanical properties of the composites as previously reported.(Hasan NajiMehr et al. 2022; Zamani et al. 2021)

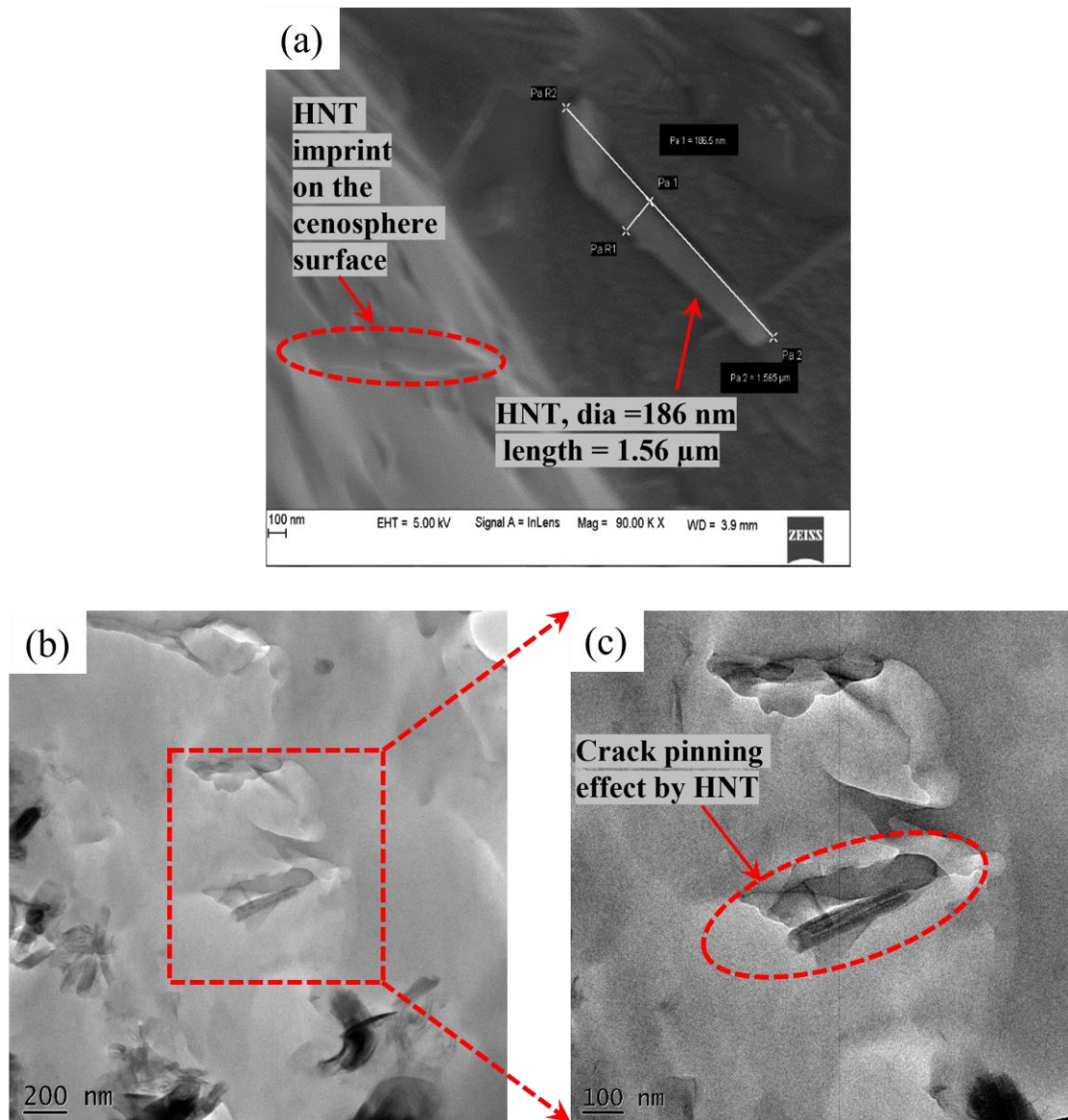


Figure 3.18 (a) SEM image of NSF40 post-compression test sample showing pull-out mechanism and (b) showing crack pinning mechanism of the HNT in the reinforced composites.

Besides the thermal and mechanical property enhancement by fillers, there were a few challenges in reinforcing composites, as shown in Figure 3.19, affecting the mechanical performance negatively. The unavoidable voids resulting from entrapments in the matrix around the cenospheres degrade mechanical properties, as it may become a potential site for crack initiation. Also, loosely bonded cenospheres and improperly wetted cenospheres debond and break easily in the initial part of the loading. Agglomeration of HNTs shown in Figure 3.19(d) poses the issue of non-uniform stress

transfer within the matrix, which is detrimental to mechanical performance of the nanofiller reinforced composites.

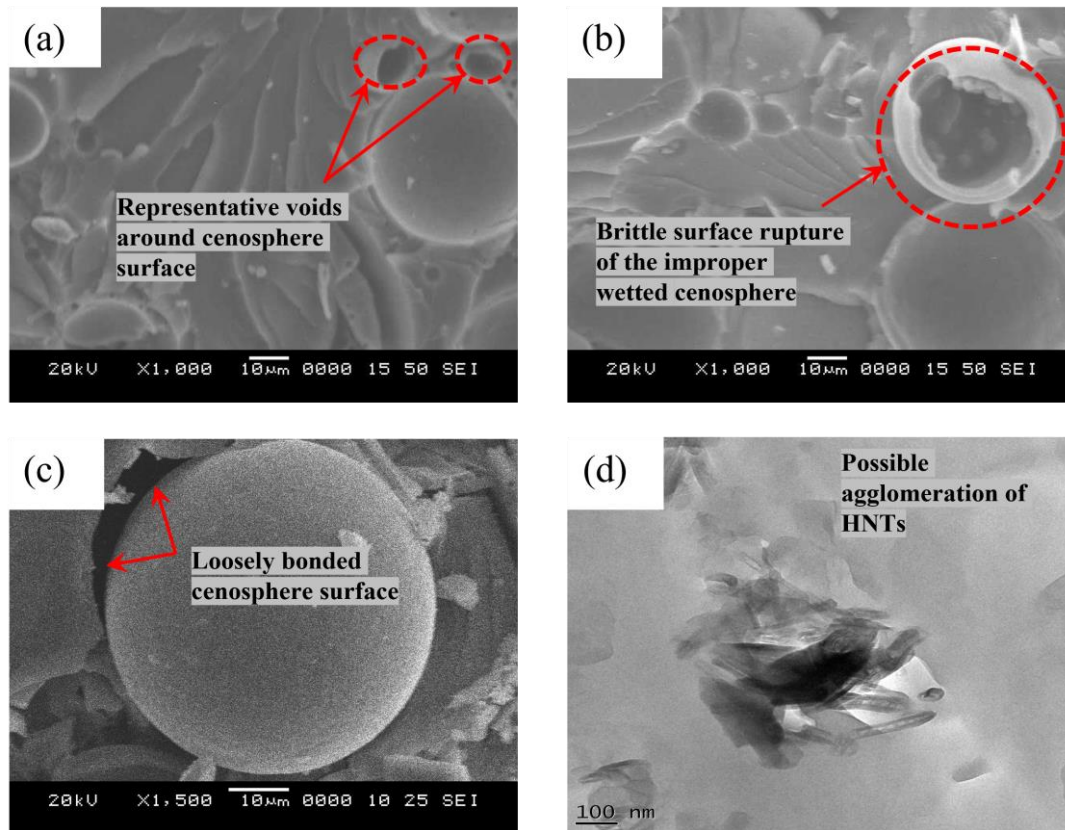


Figure 3.19 Fracture features of post-compression test depicting possible fabrication challenges of the HNTs RSF composites.

3.7 WATER ABSORPTION STUDIES

The major application of lightweight composites is in marine structures possessing buoyant properties (Guz et al. 2017). Marine floatation modules deploy composites owing to their tailored density of the composites which are water sensitive. Figures 3.20. and 3.21 show the water absorption and consequent thickness swelling characteristics respectively of neat epoxy and reinforced composites. An increase in the percentage additions of cenospheres in the epoxy matrix augmented the water ingress and thickness swelling characteristics. The neat epoxy slightly imbibed water of 0.36%, resulting in a swelling thickness of 0.67%. The SF40_W absorbed a maximum of water at 5.92% among all the samples, thus resulting in a swelling thickness of 3.45%. The inclusion of cenospheres gives a chance for the entrapments,

which may form potential sites for water ingress. The total void content in a sample may not necessarily imply a proportionate increase in water absorption. The number of voids present on the surface allows easy water entry into the molecular structure of the matrix and begins the initial phase of degradation. It is clear from Figure 3.20 that the inclusion of HNTs resists water absorption in both NSF20_W and NSF40_W samples. The reason for this resistance was offered by the tubular structure of the HNTs creating a tortuous path in the matrix (Alamri and Low 2012; Frigione and Lettieri 2020; Tham et al. 2016a; Wang et al. 2020).

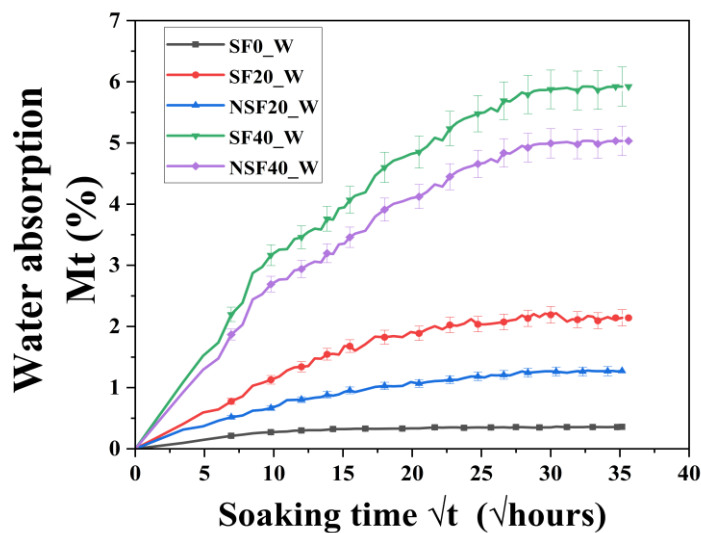


Figure 3.20 Water absorption of neat epoxy and reinforced composites.

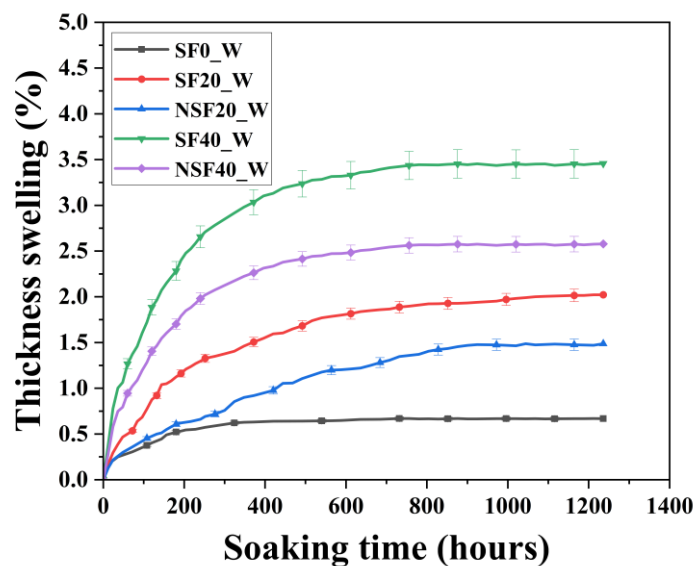


Figure 3.21 Swelling thickness of neat epoxy and reinforced composites.

3.7.1 TRANSPORTATION COEFFICIENTS

The diffusion coefficient (D), a kinetic parameter, is determined by Eq. (3.1) (Almansour et al. 2017):

$$D = \pi \left(\frac{kh}{4M_{\infty}} \right)^2 \quad (3.1)$$

where k – is the initial slope of water absorption curve (Mt vs \sqrt{t}), h – represents the initial thickness of the sample (mm), M_{∞} - the equilibrium moisture uptake mass (%). The coefficient of diffusion describes the ability of water molecules to diffuse through a polymer structure. Table 3.6 presents the diffusion coefficients for neat epoxy and reinforced composites. The diffusion coefficients increased with increase in filler content. Also, the outcomes of the current study were in agreement with those reported by earlier studies (Poveda et al. 2013; Tagliavia et al. 2012a).

Diffusion of water in the composites depends initially upon the pores/voids available at the surface leading to sorption in composites. Therefore, the sorption coefficient (S) was used to calculate the permeability (P). Equation (3.2) is used to compute the equilibrium absorption sorption coefficient (S) (Nosbi et al. 2010):

$$S = \frac{M_{\infty}}{M_p} \quad (3.2)$$

Where, M_{∞} - the equilibrium moisture uptake mass (%) and M_p – specimen mass before sorption test. The gross influence of the coefficient of diffusion (D) and coefficient of sorption (S) as given in Equation (3.3) as:

$$P = D \times S \quad (3.3)$$

The values of S and P of neat epoxy and reinforced composites with the water absorption behavior are presented in Table 3.6. From Table 3.6, it is evident that the SF40_W reported the highest permeability than all other composite samples as well as neat epoxy. Secondly, the permeability of the composites was reduced with the reinforcement of HNTs. With the introduction of HNTs, a tortuous path is created to resist the major water ingress in the molecular structure of the matrix.

Table 3.4 The maximum moisture absorption, diffusion coefficient, and permeability of neat epoxy and reinforced composites.

Sample	Saturation moisture uptake M_t (%)	Diffusion coefficient $D \times 10^{-8}$ (m^2/s)	Sorption coefficient $S \times 10^{-3}$ (g/g)	Permeability coefficient $P \times 10^{-12}$ (m^2/s)
SF0_W	0.36	1.18	0.85	10.09
SF20_W	2.14	8.94	5.19	46.4
NSF20_W	1.27	5.98	2.53	15.16
SF40_W	5.92	9.66	15.02	145.19
NSF40_W	5.03	9.59	12.55	120.36

3.7.2 ANALYSIS OF FTIR SPECTRA FOR WATER ABSORPTION

The FTIR spectra of wet and dry, neat, and composites samples were recorded over a range of 2500 – 3800 cm^{-1} . The spectra presented in Figure 3.22 displays the relative absorption bands of hydroxyl ions present in composite samples. It was noticed that the band around 3040 cm^{-1} corresponded to the stretching vibration of hydroxyl groups of free and hydrogen-bonded hydroxyl (OH) groups (Alamri and Low 2012). This peak is an indicator of water content in the materials since it shows water linked to the hydroxyl group directly or indirectly (Lasagabáster et al. 2009). It was observed that the peak in the neat epoxy sample presented lower absorption due to its intact molecular structure and lesser porosity available on the surface. It is evident from Figure 3.22 that the relative absorption of samples followed a relation as SF0_W < NSF40_W < SF40_W. This is because inclusion of HNTs inhibited water absorption in the structure of composites (Alamri and Low 2012).

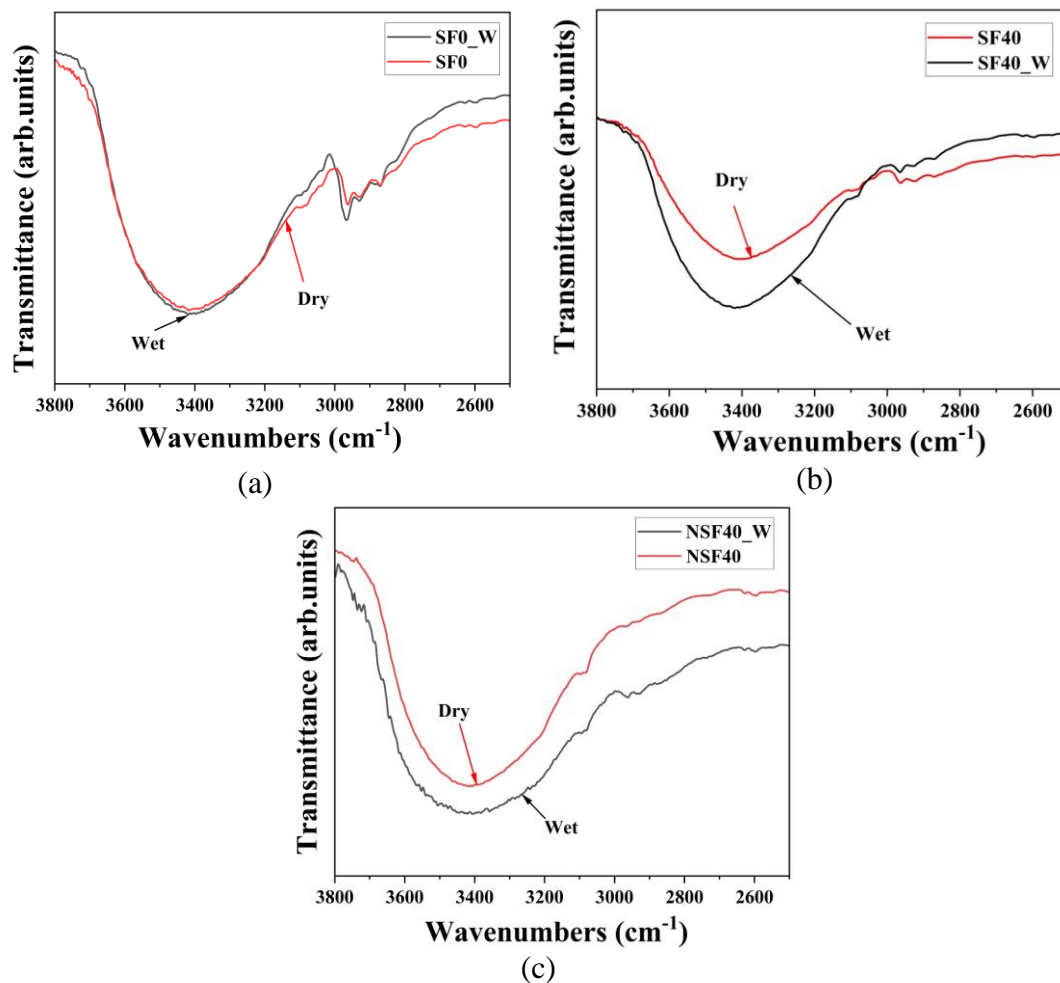


Figure 3.22 FTIR spectra of (a) neat epoxy, (b) SF40, and (c) NSF40 dry and wet samples.

3.7.3 COMPRESSION BEHAVIOR OF WATER-IMMERSED RSF COMPOSITES

Figure 3.23 shows the representative stress-strain curve of neat epoxy and RSF samples immersed in distilled water. The obtained curves are similar in trend to that obtained for room temperature cured samples (dry samples). It is evident from Table 3.7 that the neat epoxy registered a compressive modulus value of 1024 MPa, which is 131 MPa lower than the dry sample. A maximum impact of absorption was noticed in the SF40_W sample which undergoes a reduction of 628.3 MPa in its modulus (Figure 3.24(a)). This may be due to the possible entrapments that were included in the fabrication of high percentage addition of cenospheres. The superficial pores/voids that were open to the surface percolation easily paved the way for higher water ingress.

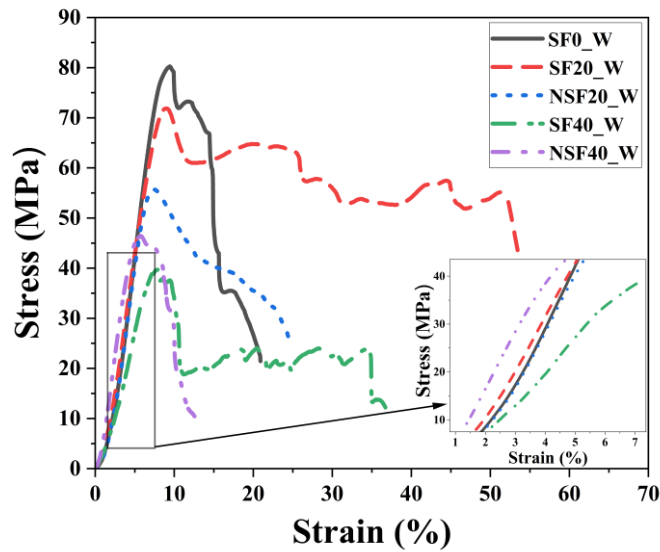


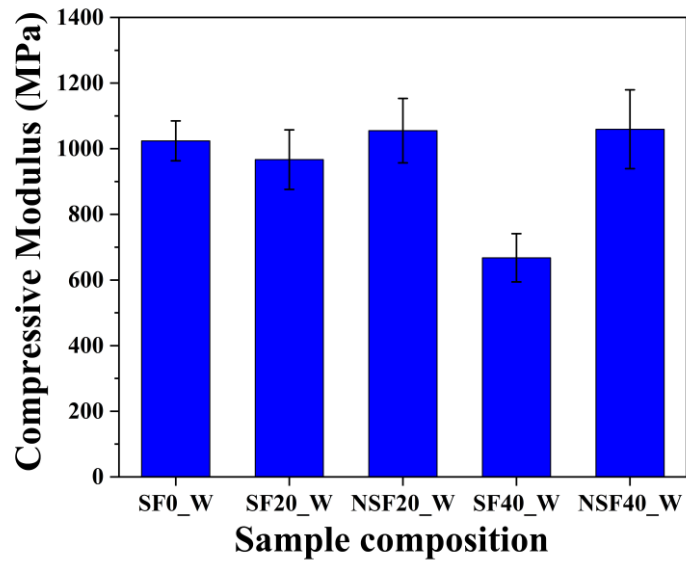
Figure 3.23 Compressive stress-strain curve of wet RSF composites.

Table 3.5 Compressive modulus and strength of dry and wet RSF composites.

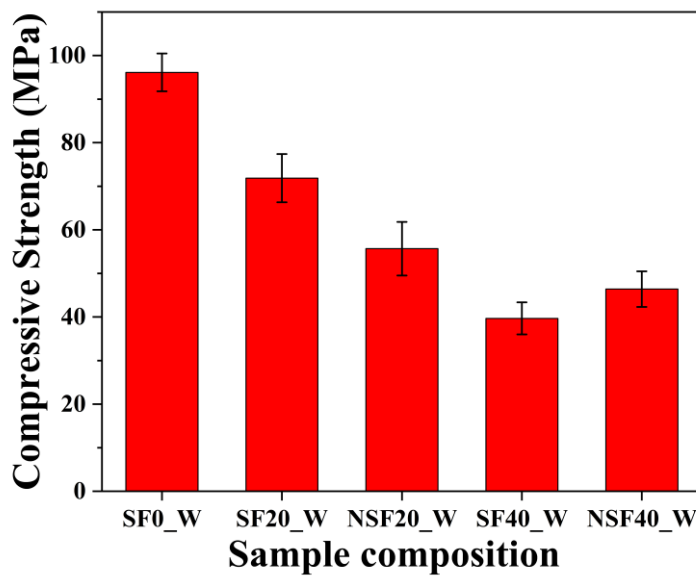
Sample	Room temperature cured		Sample	Water immersed	
	Modulus (MPa)	Strength (MPa)		Modulus (MPa)	Strength (MPa)
SF0	1155.5 ± 25.2	113.0 ± 6.74	SF0_W	1024 ± 60.65	96.14 ± 4.33
SF20	1180.2 ± 69.1	91.5 ± 3.6	SF20_W	966.8 ± 90.55	71.86 ± 5.53
NSF20	1186.6 ± 98.1	70.48 ± 1.42	NSF20_W	1055.12 ± 98.26	55.67 ± 6.13
SF40	1296.0 ± 67.2	49.7 ± 2.85	SF40_W	667 ± 73.44	39.67 ± 3.68
NSF40	1438.7 ± 89.8	98.98 ± 8.42	NSF40_W	1059.3 ± 120.3	46.4 ± 4.08

The reduction in modulus values was due to plasticization effect introduced by the water absorption (Alamri et al., 2012). Notably, a relative decrease in the compressive modulus with HNTs reinforcement was significantly lower in both HNTs RSF samples. This is due to the tortuous path created by the HNTs in the foams that inhibited water ingress in the molecular structure. Also, the compressive strength, as shown in Figure 3.24(b), depicted a reduction in strength for all samples. The dispersion of fillers at the nanoscale aided to resist incoming water molecules. Similar outcomes were reported by other researchers (Abdullah et al. 2019; Alamri and Low

2012; Balakrishnan et al. 2011). This fact can be further corroborated by the FTIR study carried out for dry and wet samples.



(a)



(b)

Figure 3.24 Experimentally measured (a) Compressive modulus and (b) compressive strength of wet RSF composites.

3.7.4 SPECTROSCOPY

The fracture features of neat epoxy, CESF, and RSF composites were analyzed after the post-compression test, as shown in Figure 3.25. The neat epoxy sample commonly depicted river flow deformation without imbibing much water, as evident

from the water absorption studies. The composites containing 40 vol% of cenospheres witnessed matrix collapse. This resulted due to plasticization owing to the ingress of the water in the structure of composites (Alamri and Low 2012; De'n~ve and Shanahan 1993; Han and Drzal 2003; Prolongo et al. 2012). However, NSF40_W possessed a smooth and brittle fracture surface relative to other samples. This was due to the HNTs reinforcement that allows lower water absorption and enables better mechanical properties compared to unreinforced foams.

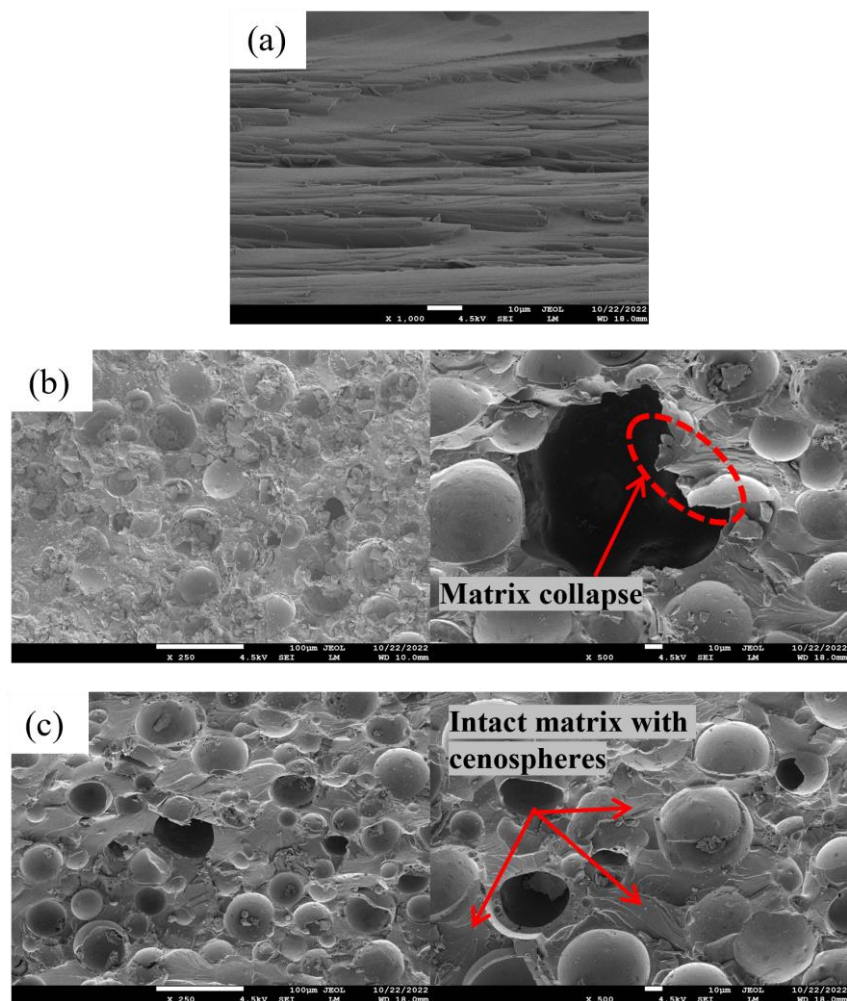


Figure 3.25 Fracture features of (a) SF0_W, (b) SF40_W, and (c) NSF40_W RSF composites.

3.8 SUMMARY

The tensile property of room temperature cured composites, and flexural and compressive properties of the room temperature cured and post-cured composites were

discussed in this chapter. It was reported that the HNTs reinforcement manifested augmentation in the modulus of the reinforced syntactic foams. Additionally, with an increase in the cenospheres content, improvement in the modulus values was reported. For the post-cured samples, the thermal treatment enhanced load-bearing characteristics in the case of compressive behavior of the RSF composites, whereas flexural properties degraded with post-curing effect. The post-curing study showed maximum degradation for a neat epoxy matrix. But due to HNTs reinforcement, the degradation was reduced in RSF composites. A significant increase in specific properties is registered by HNTs RSF composites enabling them for weight-sensitive structural applications. The water absorption study revealed the efficacy of HNTs reinforcement in the RSF composites. The diffusion coefficient, sorption coefficient, and permeability of the RSF composites were appreciably reduced due to the presence of HNTs. The compressive modulus of wet HNTs RSF composite was 58.7% higher than the corresponding sample without HNTs. This behavior of the HNTs RSF composites suits them for lightweight marine applications.

CHAPTER 4

4. VISCOELASTIC AND THERMAL STUDIES ON REINFORCED SYNTACTIC FOAMS COMPOSITES

All kinds of polymeric materials comprise different proportions of elastic, plastic, and viscous nature depending upon their lattice arrangement. When stressed, the polymer composites store, dissipate, and recover some part of the input energy (Ferry 1980). The viscoelastic response of such materials is contingent upon several factors, such as operating temperature, strain amplitude, frequency of excitation, ambient temperature, etc. (Javidan and Kim 2020). The following section presents the dynamic mechanical properties of reinforced syntactic foam (RSF) composites.

4.1 DYNAMIC MECHANICAL ANALYSIS (DMA)

Dynamic mechanical properties of polymer composites depend upon filler characteristics and the base matrix in which they are reinforced. Additionally, the effect of interface phase linked to particulate reinforcements also governs viscoelastic response in syntactic foams (Gu et al. 2009).

4.1.1 STORAGE MODULUS

A typical area of the plots comprises three distinct regions, as presented in Figure 4.1. It is noticed from Figure 4.1 that in a region I, as temperature sweeps, the storage modulus gradually decreases. Region II shows the storage modulus notably reduced with an increase in temperature which was attributed to the samples attaining their glass transition temperature (T_g). Lastly, region III represents a plastic-flow region where storage modulus values show the least variation with sweep compared to region I.

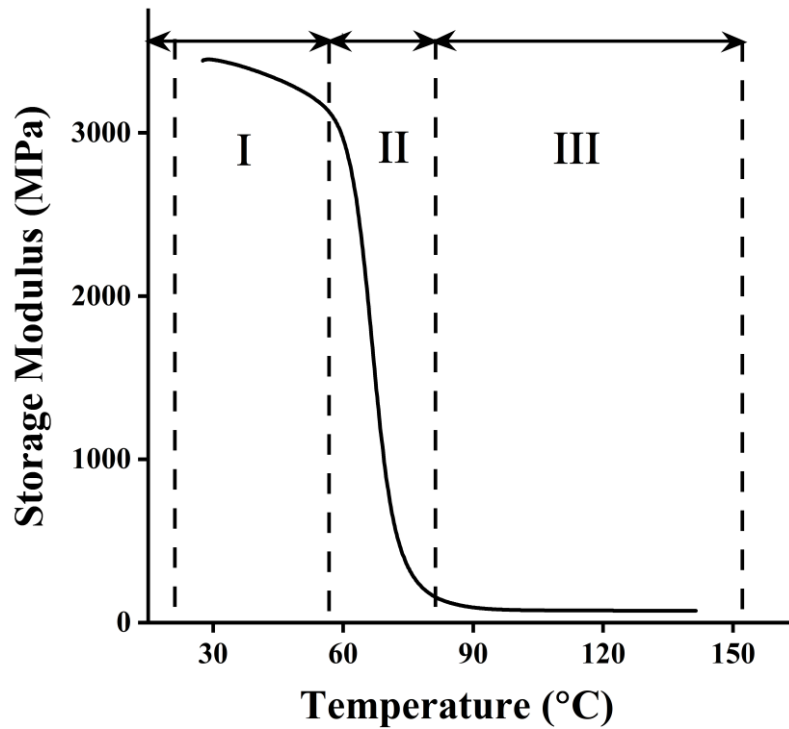


Figure 4.1 Schematic representation of the variation of storage modulus against temperature.

To elucidate the variation of storage modulus with respect to temperature, the storage modulus values at 30, 60, 80, and 140 °C are shown in Table 4.1. The selection of typical temperatures was based on the following observation.

- 27 °C was regarded as room temperature in the current study, which is significant for a broad spectrum of applications.
- Region I: Here, the variation of storage modulus remained quite linear, and thus the graphs are distinct within the range of 27 - 60 °C. This enables the selection of a representative temperature of 60 °C to portray the reliance of storage modulus on cenospheres content and modification by HNTs in syntactic foams.
- Region II: In this region, a radical drop in storage modulus after the T_g value, around 80 °C.
- Region III: It can be noticed from Figure 4.1 that there is a least variation in values of storage modulus within the temperature range of 80 - 140 °C. The maximum test temperature for the study considered was 140 °C.

Figure 4.2(a, b) depicts the storage modulus of cenosphere epoxy syntactic foams (CESFs), and halloysite nanotubes reinforced syntactic foams (HNTs RSFs), respectively, with respect to temperature. In the temperature range of 27 - 60 °C, the storage modulus drops gradually but reduces sharply post 60 °C. The neat epoxy registers a lower storage modulus value than the other syntactic foam at 30 °C. The addition of cenospheres causes an increase in storage modulus value content in the neat epoxy. Moreover, SF50 and NSF50 exhibit maximum storage modulus values in CESFs and HNTs RSFs. This may be attributed to the constrained molecular motion of neat epoxy lattice due to the addition of stiff cenospheres. Figure 4.2(b) shows that the storage modulus of HNTs RSFs in a region I measure higher values than neat epoxy. It may be observed that similar outcomes of enhancement in storage modulus of neat epoxy with HNTs reinforcement were also reported earlier (M. Liu et al., 2008b; Peter & Woldesenbet, 2008).

Interestingly, storage modulus values of HNTs RSFs with reference to their counter CESFs decreased. This can be attributed to free volume enlargement among the HNT, neat epoxy, and cenosphere that increases polymer chain mobility and thus causes a reduction of modulus in the HNTs RSFs. It was also observed that the storage modulus enhancement of up to 52% and 36% for CESF and HNTs RSF, respectively, was obtained concerning neat epoxy.

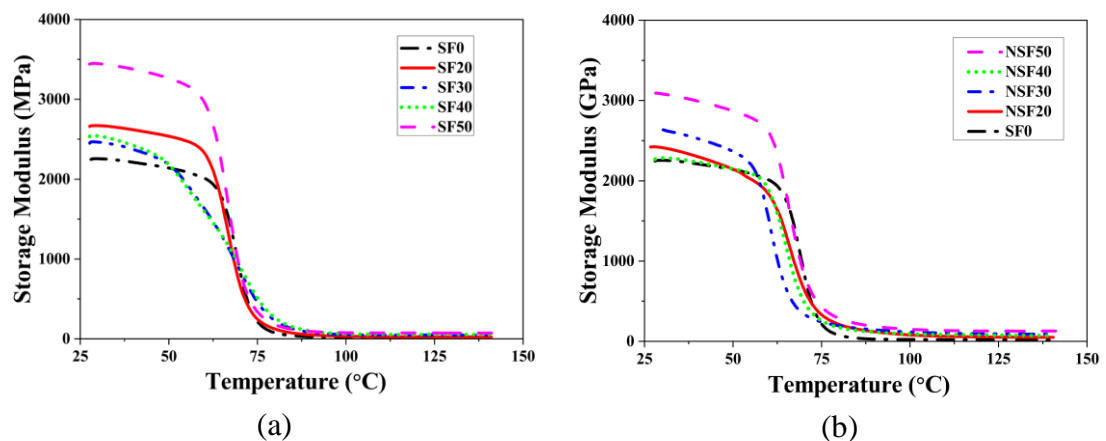


Figure 4.2 Experimentally measured storage modulus values of (a) CESF and (b) HNTs RSF composites.

Table 4.1 Comparison of storage modulus at four representative temperatures.

Sample	Storage Modulus (MPa)			
	30 °C	60 °C	80 °C	140 °C
SF0	2255.56 ± 56.38	2010.37 ± 50.25	75.25 ± 1.88	15.01 ± 0.379
SF20	2670.16 ± 65.41	2330.73 ± 57.10	121.36 ± 2.97	22.95 ± 0.56
SF30	2464.77 ± 110.91	2246.21 ± 101.07	1661.53 ± 74.76	61.00 ± 2.74
SF40	2546.67 ± 129.88	2306.52 ± 117.63	1695.32 ± 86.46	75.91 ± 3.87
SF50	3446.73 ± 180.26	2960.19 ± 154.81	174.78 ± 9.14	72.69 ± 3.87
NSF20	2412.10 ± 101.30	1832.75 ± 76.97	209.32 ± 8.78	50.49 ± 2.12
NSF30	2635.25 ± 126.49	1504.96 ± 72.23	194.39 ± 9.33	88.10 ± 4.22
NSF40	2282.41 ± 111.83	1881.78 ± 92.20	172.27 ± 8.44	71.44 ± 8.44
NSF50	3082.13 ± 169.51	2601.87 ± 143.10	283.04 ± 15.57	128.35 ± 7.06

In region II, all composite samples attained T_g , and eventually, a drastic drop in the storage modulus was witnessed. Meanwhile, the material undergoes a phase variation from an elastic-glassy to a plastic-rubbery state. However, region III was distinguished by the lowest storage modulus for the neat epoxy. Further, the recorded improvement in CESFs and HNTs RSFs were in the range of 52 - 405% and 236 - 755%, respectively, higher than the neat epoxy. In comparison, a 44 - 120% increase in storage modulus of HNTs RSF was observed over the CESF samples. The retaining of storage modulus values by HNTs RSFs, even at elevated temperatures, makes them a promising material in designing structures for high-temperature applications with lightweight embedment.

4.1.2 LOSS MODULUS

Figure 4.3(a, b) depicts the experimentally measured loss modulus values of CESF and HNTs RSF composites with respect to temperature sweep. The characteristic temperature at the maximum loss modulus value is named T_g of the sample. The loss modulus curve attained a peak at the T_g and then surged nearer to zero. The maximum loss modulus, room temperature loss modulus, and T_g values of all the samples are presented in Table 4.2. The T_g of SF0 was 70.32 °C which is equal to T_g of SF40 and also higher than all the other samples. The T_g of CESF increased with cenospheres

content except for SF50. It may be due to enhanced crosslinking of cenospheres with neat epoxy, as presented in Figure 3.1. The T_g value of HNTs RSFs reduced as compared to their corresponding CESFs. This can be attributed to the adsorption of epoxy matrix into nanotubes, as inferred by Zhang et al. (2014a) and Miyagawa and Drzal (2004).

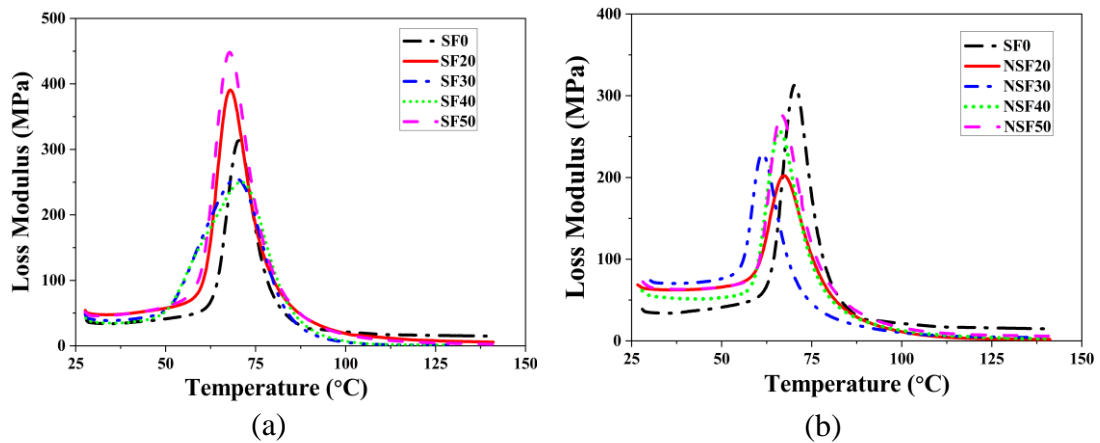


Figure 4.3 Experimentally measured loss modulus values of (a) CESF and (b) HNTs RSF composites.

The noteworthy trends in the loss modulus curves were observed as follows:

- Region I: The loss modulus of neat epoxy was the lowest of all the composite samples shown in Figure 4.3(a), while SF20 registered maximum loss modulus in CESFs due to lower sliding between cenosphere particles and epoxy matrix. As the cenospheres content increases, frictional energy dissipation overcomes the effect of matrix viscoelasticity. Thus, leading to a decrease in loss modulus owing to chain hindrance caused by minimal molecular movement within the matrix. Figure 4.3(b) depicts that the loss modulus values of HNTs RSF increase over a range of 30 - 84% compared to the CESFs. This improvement in loss modulus may be due to enhanced energy dissipation by HNTs in the epoxy matrix.
- However, the loss modulus of HNTs RSFs at temperature post 60 °C measured to be lower than the CESFs.

Table 4.2 Maximum loss modulus, room temperature loss modulus, and glass transition temperature (T_g) of all samples.

Sample	Loss modulus at 30 °C (MPa)	Maximum loss modulus (MPa)	Glass transition temperature T_g (°C)
SF0	34.82 ± 0.94	313.61 ± 8.46	70.32
SF20	48.50 ± 1.18	390.78 ± 9.54	67.93
SF30	40.04 ± 1.80	255.43 ± 11.49	69.42
SF40	36.53 ± 1.93	250.25 ± 12.76	70.33
SF50	45.78 ± 2.39	448.22 ± 23.43	67.67
NSF20	63.50 ± 2.66	202.15 ± 8.49	67.26
NSF30	73.77 ± 3.54	229.33 ± 11.00	61.34
NSF40	55.50 ± 2.71	256.03 ± 12.54	66.11
NSF50	65.94 ± 3.62	276.03 ± 15.81	67.72

4.1.3 FRACTURE FEATURES OF DMA-TESTED SAMPLES

The morphology of post-DMA test samples was considered for the analysis. The samples after temperature sweep were freeze fractured, and micrographs of the fracture surface were studied. The neat epoxy undergoes extensive plastic deformation due to its viscoelasticity, as presented in Figure 4.4(a). However, with addition of cenospheres, such a phenomenon was slightly reduced, as shown in Figure 4.4(b). Similar improvement with higher cenospheres content can be noticed in Figure 4.4(d). Further, due to the reinforcement of HNTs in RSF composites, the matrix becomes stiffer, resisting plastic deformation as depicted in Figure 4.4(c, e). This may be attributed to better crosslinking and efficient stress transfer by HNTs in the matrix with its rigid silicate nanotube structure, enabling the material to become stiff and thus absorb higher energy at elevated temperatures.

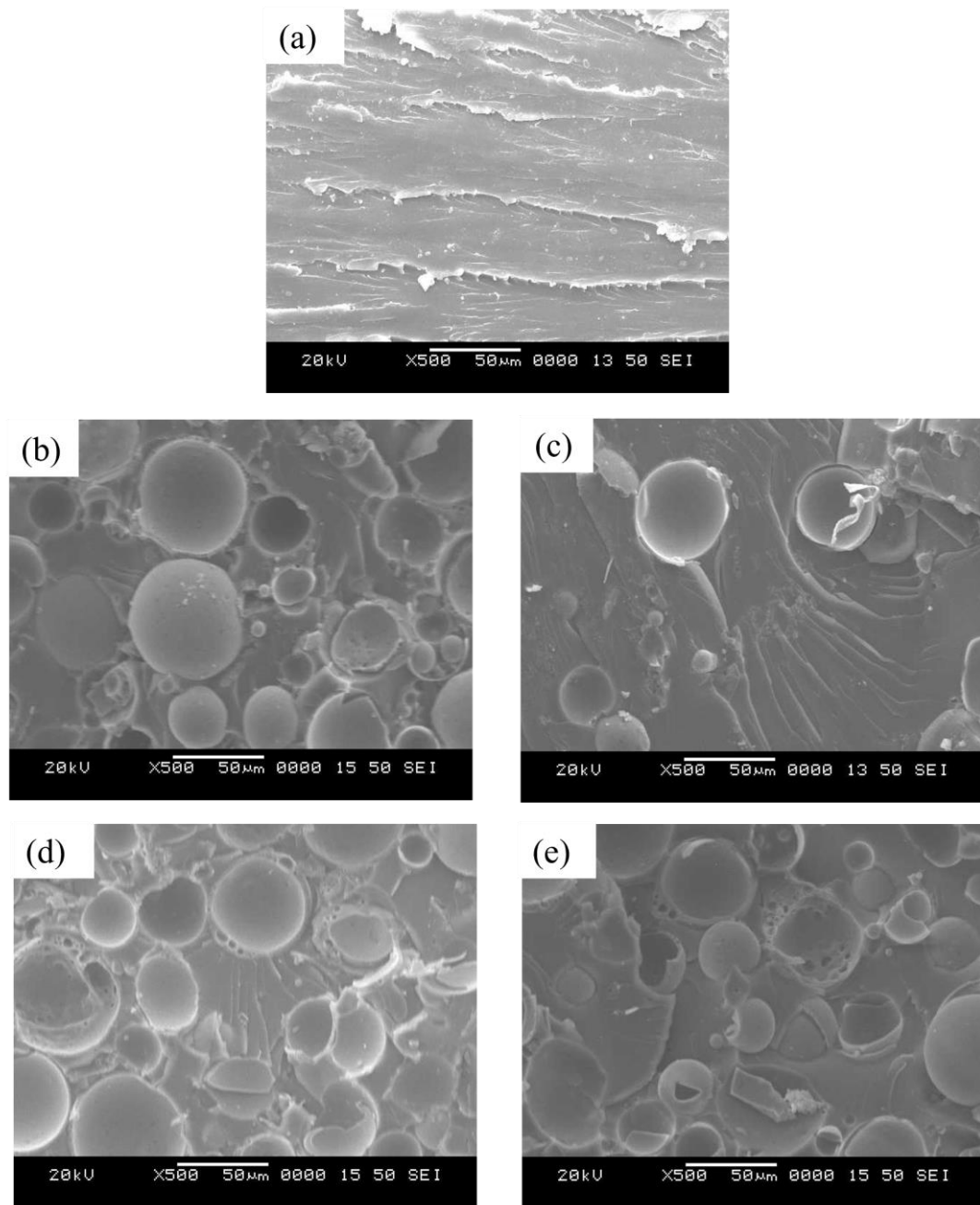


Figure 4.4 Micrographs display fracture features of (a) Neat epoxy (b) SF20 (c) NSF20 (d) SF50 and (e) NSF50 post-DMA tests.

4.2 THERMOGRAVIMETRIC ANALYSIS (TGA)

Figure 4.5 shows thermogravimetric analysis (TGA) curves in which the degraded RSF composite samples follow a single-step pattern. The novel HNTs reinforcement in the formulated syntactic foam composites offered excellent thermal

stability (Prashantha et al. 2011b) with the epoxy chain network, as shown in FTIR analysis (Figure 3.1). As presented in Table 4.3, upon the addition of HNTs, the thermal degradation temperature increased, which could be attributed to the hindrance effect of chain scissoring of epoxy. Furthermore, it is essential to note that the residual mass remaining at 700 °C of neat epoxy was 0.62%. Also, a maximum increase of 11.47% residual mass was reported for NSF20 compared to SF20. However, a petite contribution of HNTs was noticed in the initial decomposition. Similar results were conveyed in earlier studies (Dean et al. 2007; Liu et al. 2008). Nevertheless, the synergy of HNTs along with cenospheres enabled tailoring the dimensional and thermal stability of syntactic foams with a negligible increase in density.

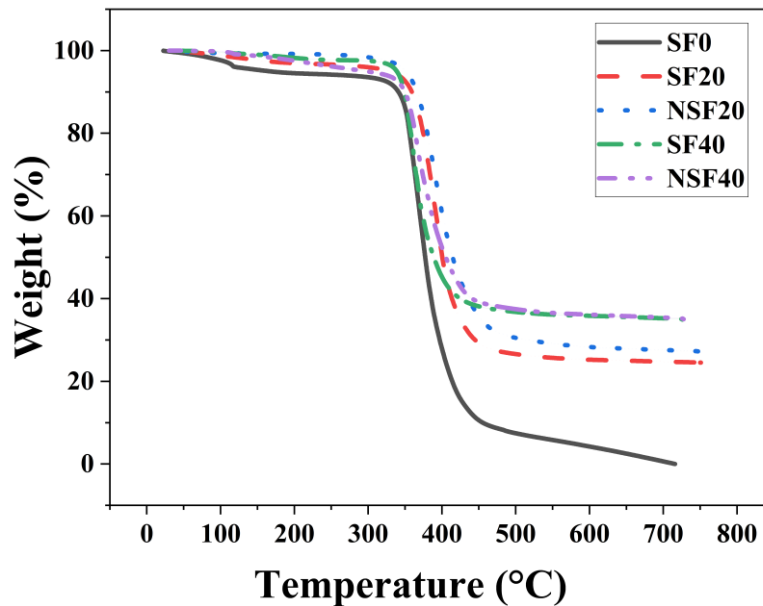


Figure 4.5 TGA curves of room temperature cured RSF composites.

Table 4.3 Degradation temperature values for 10, 30, and 50% mass loss in RSF composites.

Sample	Degradation temperature (°C)			Residual mass (%) at 700 °C
	T ₉₀	T ₇₀	T ₅₀	
SF0	341	363	377	0.62
SF20	359	383	400	24.75
NSF20	366	390	413	27.59
SF40	349	365	388	35.23
NSF40	350	373	405	35.42

4.3 DIFFERENTIAL SCANNING CALORIMETRY (DSC) ANALYSIS

The DSC test was carried out to study the influence of reinforcement in an epoxy matrix and determined thermal behavior, particularly glass transition temperature (T_g). The T_g value of a nanocomposite signifies its deployment in actual service conditions (Yeasmin et al. 2021). The T_g value variation obtained from the DSC thermogram shown in Figure 4.6, is tabulated in Table 4.4. It can be observed from Table 4.4 that improvements in T_g values obtained by post-cure heat treatment in RSF composites are in the range of 1.83 – 24.34% with respect to room temperature cured syntactic foams. The phenomenon of post-curing enables increased chances of cooperative movements of the epoxy molecular network, enabling the material to be utilized for higher operating temperatures. Similar studies were reported on the governance of T_g in composites by post-cure heat treatments (Pattanaik et al. 2019a; Yeasmin et al. 2021).

The analysis of thermogram results is carried out in two folds. Firstly, with post-curing, epoxy conversion eventually enhances this result in better crosslinking with improved T_g value. A similar outcome was also corroborated by the FTIR study presented in the previous chapter (Figure 3.2), indicating that the crosslinking of epoxies gets enhanced with post-cure heating effect in RSF composites. Secondly, as observed in Table 4.4, the T_g value dropped with addition of reinforcement. Together, HNTs addition to syntactic foam hinders the epoxy network, eventually restricting chain mobility of the matrix. The drop in T_g value was attributed to the possible adsorption of epoxy resin into the tubes (lumen space) of HNT. The lumen filled with epoxy matrix is also shown in Figure 3.3(b). This synergy of fillers and post-cure treatment produces thermally stable syntactic foam composites for thermally sensitive applications.

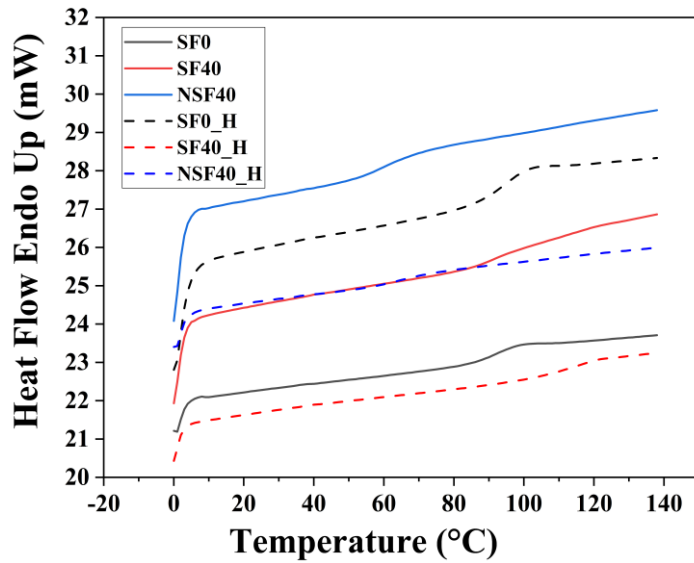


Figure 4.6 DSC curves of room temperature cured and post-cure heated RSF composites.

Table 4.4 Glass transition temperature values obtained from DSC analysis signifying the advantage of post-cure heating effect in RSF composites.

Sample	Glass transition, T _g (°C)	T _g enhancement w.r.t room temperature cured samples (°C)
SF0	92.91	-
SF0_H	94.74	1.83
SF40	91.74	-
SF40_H	116.08	24.34
NSF40	98.32	-
NSF40_H	105.58	7.26

4.4 SUMMARY

The thermal and viscoelastic properties of the CESF and HNTs RSF composites were investigated in this chapter. The storage modulus increased with an increase in cenospheres content in the epoxy matrix. Further, with incorporation of HNTs, the storage modulus obtained was higher than that of neat epoxy but still lower than CESFs. This is due to enlargement in free volume among the HNTs, epoxy, and cenosphere. The storage modulus of CESF and HNTs RSFs was up to 52 and 36% higher than SF0. The improvement in loss modulus of HNTs RSFs was obtained by 59 – 113% and 30 – 84% over the neat epoxy and CESFs due to better energy dissipation by HNTs within

the epoxy matrix. The glass transition temperature (T_g) values shifted to higher temperatures due to the addition of cenospheres in the epoxy matrix. It is because of enhanced crosslinking of cenospheres with epoxy matrix. Owing to the adsorption of the epoxy matrix into the tubular structure of HNT, the T_g values slightly decrease compared with the unreinforced CESFs. The T_g value amelioration obtained in neat epoxy and NSF40 by post-curing is 1.83 °C and 7.26 °C, respectively. In addition, relatively high char content retainment and delayed degradation temperature rendered by HNTs to syntactic foams allow them the flexibility to be operated from moderate to high-temperature lightweight applications.

CHAPTER 5

5. SUMMARY AND CONCLUSIONS

5.1 SUMMARY

A thorough investigation was conducted to prepare and characterize reinforced epoxy syntactic foam composites using cenospheres and halloysite nanotubes (HNTs). Utilizing cenospheres in weight-sensitive structural applications might lessen the load on landfills and aid in addressing the environmental issue of fly ash disposal. In the present work, reinforced epoxy syntactic foam composite specimens were fabricated using manual stir casting, and their mechanical, thermal, and viscoelastic properties were investigated. The effects of halloysite nanotube reinforcement, cenospheres volume fraction, and post-curing on composites were investigated.

Experiments were conducted to extract the properties of RSF composites and evaluate the efficacy of reinforcing HNTs and cenospheres. Tensile, flexural, compressive, and viscoelastic responses were studied for room temperature cured composites. Further, flexural and compressive behavior was characterized by post-cured specimens. To evaluate the structure-property correlations and failure processes, extensive scanning electron microscopy, field emission scanning electron microscopy, and transmission electron microscopy were carried out.

5.2 CONCLUSIONS

The significant conclusions are summarized as follows:

Density:

- When cenospheres are mechanically mixed into the resin, a decrease in the density of composites was observed compared to the theoretical values, which accounted for the trapping of air in the matrix.
- Reinforced syntactic foams (RSFs) containing HNTs were found to slightly increase the density of cenosphere epoxy syntactic foams (CESFs), thereby not affecting much the weight-saving potential of composite foams suiting lightweight applications.

- The post-curing effect marginally reduced the RSF composites' density, thus enhancing the weight-saving capability of RSF composites.

Tensile, flexural, and compressive behavior of room temperature cured specimens

- An increase in the content of cenospheres enhanced the tensile modulus of the RSF composites.
- The HNTs reinforcement augmented the tensile modulus of RSF composites by a maximum of 42% relative to the cenosphere epoxy syntactic foam (CESF) composites.
- In NSF40 sample, the specific tensile modulus was 107% higher than the SF40 and 7.9% lighter than neat epoxy sample.
- Neat epoxy samples registered maximum strength, and the strength was reduced with the addition of reinforcements.
- The tensile strength of RSF composites diminished with the HNTs addition.
- The neat epoxy sample registered maximum flexural modulus and strength values of 5 GPa and 111 MPa among all the samples, respectively.
- With the addition of cenospheres, the flexural modulus increased in CESF composites.
- The addition of HNTs in the RSF composites reported an increment in the flexural modulus over a range of 7 - 66% with respect to the CESF composites.
- NSF50 sample registered a specific flexural modulus value 35.17% higher than SF50 and has 10.2% weight-saving potential than the neat epoxy sample.
- The addition of cenospheres and HNTs ameliorated the compressive modulus of the RSF composites.
- NSF40 sample registered a 9.91% improvement in the compressive modulus compared to the SF40 sample.
- Furthermore, a maximum of 1.417 MPa/kg/m³ of specific compressive modulus was achieved by NSF40, which stands at 10.6% and 46.6% higher than SF40 and SF0, respectively.

Flexural and compressive behavior of post-cured specimens

- The neat epoxy sample, SF0_H, suffered a reduction of 58.73% in flexural modulus compared to the SF0. Similarly, all other samples exhibited a modulus reduction of over 11.73 – 60.10%. This comparatively lower reduction in RSF composites was due to synergism and thermal stability of the fillers.
- With the HNTs reinforcement, the flexural modulus enhancement obtained was over 11.73 – 60.10% concerning their corresponding post-cured CESF composites.
- The post-curing effect positively influenced the compressive properties in that the neat epoxy sample observed a 17.2% amelioration in the modulus values.
- The specific compressive modulus of NSF40_H exhibited 1.567 MPa/ kg/m³, which was 7.0%, 35.7%, and 33.3% higher than NSF40, SF0_H, and SF0, respectively.

Water absorption study

- The neat epoxy sample, SF0_W, registered 0.36% of least water absorption and consequent swelling thickness of 0.67%.
- The addition of cenospheres attracting air entrapments during its fabrication permitted higher water ingress. The sample, SF40_W, exhibited a maximum water ingress of 5.92%.
- HNTs, due to their advantageous geometry, create a tortuous path inhibiting the water intake in the RSF composites.
- The permeability coefficient (P) value was observed to reduce over 17.12 – 67.33% due to HNTs reinforcement with respect to CESF composites.
- The neat epoxy registered a compressive modulus value of 1024 MPa, which was 131 MPa lower than the dry sample.
- The maximum impact of water absorption was noticed in the SF40_W sample, which undergoes a reduction of 628.3 MPa in its compressive modulus.
- The compressive modulus of NSF40_W was 58.7% higher than the corresponding sample without HNTs. This may be attributed to the hindrance in the ingress path created by tubular HNTs.

Dynamic mechanical analysis and thermal behavior

- The storage modulus increased as the cenospheres content in the epoxy matrix increased, whereas the storage modulus achieved with the addition of HNTs was greater than that of pure epoxy but still less than that of CESFs. This may be because the free volume in the matrix containing HNTs, epoxy, and cenospheres has enlarged.
- The storage modulus of CESF and HNTs RSFs was 52 and 36% higher than SF0. The improvement in loss modulus of HNTs RSFs was obtained by 59 – 113% and 30 – 84% over the neat epoxy and CESFs due to better energy dissipation by HNTs within the epoxy matrix.
- The glass transition temperature (T_g) values shifted to higher temperatures due to the addition of cenospheres in the epoxy matrix because of the enhanced crosslinking of cenospheres with the epoxy matrix. Owing to the adsorption of the epoxy matrix into the tubular structure of HNT, the T_g values slightly decreased compared with the unreinforced PSFs.
- The T_g value amelioration obtained in neat epoxy and NSF40 by post-curing was 1.83 °C and 7.26 °C, respectively. It was attributed to the improvement in crosslinking by the HNTs addition and post-curing effect validated by FTIR studies.
- The thermal stability with retarded degradation temperature manifested by HNTs to syntactic foams allows them the flexibility to be operated from moderate to high temperature weight-sensitive structural applications.

The present work successfully illustrates the possibility of a manual stirring method for developing halloysite nanotube reinforced thermosetting syntactic foam composites based on cenospheres. These composites are lightweight, eco-friendly, and provide 11.5% weight-saving potential. In addition, the use of cenospheres decreases landfill waste and environmental concerns. Experiments are carried out to examine the effect of adding the HNTs and cenospheres content over a wide spectrum of mechanical characteristics and temperature profiles. The experimental outcomes reported in the current investigation can help industry professionals develop reinforced syntactic foams for significant weight-sensitive structural applications.

SCOPE OF FUTURE WORK

The present work demonstrates feasibility of the manual stirring technique in developing reinforced syntactic foam composites. Variation in the content of HNTs along with the cenospheres affecting the thermal and mechanical properties needs to be studied. Further, the effect of surface functionalization of HNTs needs to be investigated to bring out better mechanical properties. The rubber particles may be reinforced along the nanofillers to examine and ameliorate the strain characteristics of the reinforced syntactic foam composites. Developing the micro-mechanical models considering the interfacial interaction between the fillers in the syntactic foam composites is worth investigating to arrive at optimized designs for materials. Also, the fatigue analysis of these syntactic foams is significant to investigate, as it will be crucial in designing aerospace applications.

REFERENCES

- Abdullah, Z. W., Dong, Y., Han, N., and Liu, S. (2019). "Water and gas barrier properties of polyvinyl alcohol (PVA)/starch (ST)/ glycerol (GL)/halloysite nanotube (HNT) bionanocomposite films: Experimental characterisation and modelling approach." *Compos B Eng*, 174.
- Agrawal, A., and Satapathy, A. (2019). "Thermal, mechanical, and dielectric properties of aluminium oxide and solid glass microsphere-reinforced epoxy composite for electronic packaging application." *Polym Compos*, 40(7), 2573–2581.
- Ahmadi, H., Liaghat, G., and Charandabi, S. C. (2020). "High velocity impact on composite sandwich panels with nano-reinforced syntactic foam core." *Thin-Walled Structures*, 148.
- Alamri, H., and Low, I. M. (2012). "Effect of water absorption on the mechanical properties of nano-filler reinforced epoxy nanocomposites." *Mater Des*, 42, 214–222.
- Alhuthali, A., and Low, I. M. (2013). "Water absorption, mechanical, and thermal properties of halloysite nanotube reinforced vinyl-ester nanocomposites." *J Mater Sci*, 48(12), 4260–4273.
- Arza Seidel. (2012). *Polymer Science and Technology Fourth Edition*.
- Bai, S., Sun, X., Wu, M., Shi, X., Chen, X., Yu, X., and Zhang, Q. (2020). "Effects of pure and intercalated halloysites on thermal properties of phthalonitrile resin nanocomposites." *Polym Degrad Stab*, 177.
- Bakshi, M. S., and Kattimani, S. (2021). "Study of mechanical and dynamic mechanical behavior of halloysite nanotube-reinforced multiscale syntactic foam." *J Appl Polym Sci*, 138(7), 49855.
- Bakshi, M. S., and Kattimani, S. (2022). "Probing the effect of post-curing and halloysite nanotube reinforcement on thermo-mechanical properties of lightweight epoxy syntactic foam composites." *Proceedings of the Institution of Mechanical Engineers, Part L: Journal of Materials: Design and Applications*, 237(3), 697-713

Balakrishnan, H., Azman, •, Muhammad, H. •, Mat, I. •, and Wahit, U. (2011). “Aging of Toughened Polylactic Acid Nanocomposites: Water Absorption, Hygrothermal Degradation and Soil Burial Analysis.” 19, 863–875.

Bao, F., Wang, J., Wang, J., Zeng, S., and Guo, X. (2020). “Static and impact responses of syntactic foam composites reinforced by multi-walled carbon nanotubes.” *Journal of Materials Research and Technology*, 9(6), 12391–12403.

Barbero, E. J. (2018). “Introduction to Composite Materials Design (3rd Editio).” *Boca Raton*.

Bardella, L., and Genna, F. (2001). “On the elastic behavior of syntactic foams.” *Int J Solids Struct*, 38(40–41), 7235–7260.

Bhanushali, R., Ayre, D., and Nezhad, H. Y. (2017). “Tensile Response of Adhesively Bonded Composite-to-composite Single-lap Joints in the Presence of Bond Deficiency.” *Procedia CIRP*, 59, 139–143.

Bharath Kumar, B. R., Zeltmann, S. E., Doddamani, M., Gupta, N., Uzma, Gurupadu, S., and Sailaja, R. R. N. (2016). “Effect of cenosphere surface treatment and blending method on the tensile properties of thermoplastic matrix syntactic foams.” *J Appl Polym Sci*, 133(35).

Bilyeu, B., Brostow, W., and Menard, K. P. (1999). *Epoxy thermosets and their applications: chemical structures and applications*. *Journal of Materials Education*.

Birger, S., Moshonov, A., and Kenig, S. (1989). “The effects of thermal and hygrothermal ageing on the failure mechanisms of graphite-fabric epoxy composites subjected to flexural loading.” *Composites*, 20(4), 341–348.

Bittmann, B., Hauptert, F., and Schlarb, A. K. (2009). “Ultrasonic dispersion of inorganic nanoparticles in epoxy resin.” *Ultrason Sonochem*, 16(5), 622–628.

Bunn, P., and Mottram, J. T. (1993). “Manufacture and compression properties of syntactic foams.” *Composites*, 24(7), 565–571.

- Campana, C., Leger, R., Sonnier, R., Ferry, L., and Ienny, P. (2018). "Effect of post curing temperature on mechanical properties of a flax fiber reinforced epoxy composite." *Compos Part A Appl Sci Manuf*, 107, 171–179.
- Cañavate, J., Colom, X., Pagès, P., and Carrasco, F. (2000). "Study of the curing process of an epoxy resin by FTIR spectroscopy." *Polym Plast Technol Eng*, 39(5), 937–943.
- Chan, L. C., Naé, H. N., and Gillham, J. K. (1984). "Time-temperature–transformation (TTT) diagrams of high Tg epoxy systems: Competition between cure and thermal degradation." *J Appl Polym Sci*, 29(11), 3307–3327.
- Chan, M. L., Lau, K. T., Wong, T. T., and Cardona, F. (2011). "Interfacial bonding characteristic of nanoclay/polymer composites." *Appl Surf Sci*, 258(2), 860–864.
- Chauhan, V., Kärki, T., and Varis, J. (2022). "Review of natural fiber-reinforced engineering plastic composites, their applications in the transportation sector and processing techniques." *Journal of Thermoplastic Composite Materials*, SAGE Publications Ltd.
- Curtis, A. R., Shortall, A. C., Marquis, P. M., and Palin, W. M. (2008). "Water uptake and strength characteristics of a nanofilled resin-based composite." *J Dent*, 36(3), 186–193.
- Czerwinski, F. (2021). "Current trends in automotive lightweighting strategies and materials." *Materials*, 14(21).
- D. Qian and E. C. Dickey. (2001). "In-situ transmission electron microscopy studies of polymer-carbon nanotube composite deformation." *J Microsc*, 204(1), 39–45.
- Dando, K. R., and Salem, D. R. (2017). "The effect of nano-additive reinforcements on thermoplastic microballoon epoxy syntactic foam mechanical properties." *J Compos Mater*, 52(7), 971–980.
- Dando, Kerrick R., S. R. D. (2019). "Nano-additive reinforcement of mixture epoxy syntactic foams." *Journal of Thermoplastic Composite Materials*.

Danish, A., and Mosaberpanah, M. A. (2020). “Formation mechanism and applications of cenospheres: a review.” *J Mater Sci*, Springer.

Das, A., and Satapathy, B. K. (2011). “Structural, thermal, mechanical and dynamic mechanical properties of cenosphere filled polypropylene composites.” *Mater Des*, 32(3), 1477–1484.

Dean, K., Krstina, J., Tian, W., and Varley, R. J. (2007). “Effect of ultrasonic dispersion methods on thermal and mechanical properties of organoclay epoxy nanocomposites.” *Macromol Mater Eng*, 292(4), 415–427.

De’n~ve, B., and Shanahan, M. E. R. (1993). *Water absorption by an epoxy resin and its effect on the mechanical properties and infra-red spectra*.

Deng, S., Zhang, J., and Ye, L. (2009). “Halloysite-epoxy nanocomposites with improved particle dispersion through ball mill homogenisation and chemical treatments.” *Compos Sci Technol*, 69(14), 2497–2505.

Dhanasekar, S., Stella, T. J., Thenmozhi, A., Bharathi, N. D., Thiyagarajan, K., Singh, P., Reddy, Y. S., Srinivas, G., and Jayakumar, M. (2022). “Study of Polymer Matrix Composites for Electronics Applications.” *J Nanomater*, 2022.

Doddamani, M. (2020). “Dynamic mechanical analysis of 3D printed eco-friendly lightweight composite.” *Composites Communications*, 19, 177–181.

Dogan, A. (2021). “Low-velocity impact, bending, and compression response of carbon fiber/epoxy-based sandwich composites with different types of core materials.” *Journal of Sandwich Structures and Materials*, 23(6), 1956–1971.

Du, M., Guo, B., and Jia, D. (2010). “Newly emerging applications of halloysite nanotubes: A review.” *Polym Int*, 59(5), 574–582.

Feldman, D. (1993). “Handbook of polymeric foams and foam technology, by D. Klepner and KC Frisch (editors), hanser publishers, Munich, 442 pp. DM 228.00.” Wiley Online Library.

Ferry, J. D. (1980). *Viscoelastic Properties of Polymers*. John Wiley & Sons, Inc.

Fiore, V., Bella, G. di, and Valenza, A. (2011). “Glass-basalt/epoxy hybrid composites for marine applications.” *Mater Des*, 32(4), 2091–2099.

Forintos, N., and Czigany, T. (2019). “Multifunctional application of carbon fiber reinforced polymer composites: Electrical properties of the reinforcing carbon fibers – A short review.” *Compos B Eng*, Elsevier Ltd.

Frigione, M., and Lettieri, M. (2020). “Recent advances and trends of nanofilled/nanostructured epoxies.” *Materials*, MDPI AG.

Gangwar, S., and Pathak, V. K. (2021). “A critical review on tribological properties, thermal behavior, and different applications of industrial waste reinforcement for composites.” *Proceedings of the Institution of Mechanical Engineers, Part L: Journal of Materials: Design and Applications*, SAGE Publications Ltd.

Garcia, C. D., Shahapurkar, K., Doddamani, M., Kumar, G. C. M., and Prabhakar, P. (2018). “Effect of arctic environment on flexural behavior of fly ash cenosphere reinforced epoxy syntactic foams.” *Compos B Eng*, 151, 265–273.

Gauthier, M. M. (1995). *Engineered materials handbook*. ASM International.

Ghamsari, A. K., Zegeye, E., and Woldesenbet, E. (2015). “Viscoelastic properties of syntactic foam reinforced with short sisal fibers.” *J Compos Mater*, 49(1), 27–34.

Gokhale, A. A., Ravi Kumar, N. v., Sudhakar, B., Sahu, S. N., Basumatary, H., and Dhara, S. (2011). “Cellular metals and ceramics for defence applications.” *Def Sci J*, 61(6), 567–575.

González, C., Vilatela, J. J., Molina-Aldareguía, J. M., Lopes, C. S., and LLorca, J. (2017). “Structural composites for multifunctional applications: Current challenges and future trends.” *Prog Mater Sci*, Elsevier Ltd.

“Govt notifies norms for fly ash utilisation by coal-fired power plants - The Hindu BusinessLine.” (2022).

Gu, J., Wu, G., and Zhao, X. (2009). “Effect of Surface-Modification on the Dynamic Behaviors of Fly Ash Cenospheres Filled Epoxy Composites.” *Polym Compos*, 233–238.

Gültekin, K., Akpınar, S., Gürses, A., Eroglu, Z., Cam, S., Akbulut, H., Keskin, Z., and Ozel, A. (2016). “The effects of graphene nanostructure reinforcement on the adhesive method and the graphene reinforcement ratio on the failure load in adhesively bonded joints.” *Compos B Eng*, 98, 362–369.

Gupta, N., Kishore, Woldesenbet, E., and Sankaran, S. (2001). “Studies on compressive failure features in syntactic foam material.” *J Mater Sci*, 36(18), 4485–4491.

Gupta, N., and Nagorny, R. (2006). “Tensile properties of glass microballoon-epoxy resin syntactic foams.” *J Appl Polym Sci*, 102(2), 1254–1261.

Gupta, N., Pinisetty, D., and Shunmugasamy, V. C. (2013). *Reinforced Polymer Matrix Syntactic Foams Effect of Nano and Micro-Scale Reinforcement*. Springer Cham Heidelberg New York Dordrecht London.

Gupta, N., and Woldesenbet, E. (2003). “Hygrothermal studies on syntactic foams and compressive strength determination.” *Compos Struct*, 61(4), 311–320.

Gupta, N., and Woldesenbet, E. (2005). “Characterization of flexural properties of syntactic foam core sandwich composites and effect of density variation.” *J Compos Mater*, 39(24), 2197–2212.

Gupta, N., Woldesenbet, E., and Mensah, P. (2004). “Compression properties of syntactic foams: Effect of cenosphere radius ratio and specimen aspect ratio.” *Compos Part A Appl Sci Manuf*, 35(1), 103–111.

Gupta, N., Zeltmann, S. E., Shunmugasamy, V. C., and Pinisetty, D. (2014). “Applications of polymer matrix syntactic foams.” *Jom*, 66(2), 245–254.

Gupta, V. B., Drzal, L. T., Lee, C. Y. -C, and Rich, M. J. (1985). “The temperature-dependence of some mechanical properties of a cured epoxy resin system.” *Polym Eng Sci*, 25(13), 812–823.

Guz, I. A., Menshykova, M., and Kee Paik, J. (2017). “Ships and Offshore Structures Thick-walled composite tubes for offshore applications: an example of stress and failure analysis for filament-wound multi-layered pipes”, 12(3), 304–322.

- H S, B., Bonthu, D., Prabhakar, P., and Doddamani, M. (2020). “Three-dimensional printed lightweight composite foams.” *ACS Omega*, 5(35), 22536–22550.
- Han, S. O., and Drzal, L. T. (2003). “Water absorption effects on hydrophilic polymer matrix of carboxyl functionalized glucose resin and epoxy resin.” *Eur Polym J*, 39(9), 1791–1799.
- Hasan NajiMehr, , , Danial Ghahremani Moghadam, Mahmoud Shariati, Pedram Zamani, and Lucas F. M. da Silva. (2022). “Investigating on the influence of multi-walled carbon nanotube and graphene nanoplatelet additives on residual strength of bonded joints subjected to partial fatigue loading.” *J Appl Polym Sci*, 139(18).
- Hodge, A. J., Kaul, R. K., McMahon, W. M., and Reinarts, T. (2000). *Sandwich composite, syntactic foam core based, application for space structures*.
- Hong, S.-G., and Wu, C.-S. (1998). *DSC and FTIR analysis of the curing behaviors of epoxy/DICY/solvent open systems*.
- Hu, G., and Yu, D. (2011). “Tensile, thermal and dynamic mechanical properties of hollow polymer particle-filled epoxy syntactic foam.” *Materials Science and Engineering A*, 528(15), 5177–5183.
- Huang, Y. J., Vaikhanski, L., and Nutt, S. R. (2006). “3D long fiber-reinforced syntactic foam based on hollow polymeric microspheres.” *Compos Part A Appl Sci Manuf*, 37(3), 488–496.
- Javidan, M. M., and Kim, J. (2020). “Experimental and Numerical Sensitivity Assessment of Viscoelasticity for Polymer Composite Materials.” *Sci Rep*, 10(1).
- Jayavardhan, M. L., and Doddamani, M. (2018). “Quasi-static compressive response of compression molded glass microballoon/HDPE syntactic foam.” *Compos B Eng*, 149, 165–177.
- Jena, H., Pandit, M. K., and Pradhan, A. K. (2013). “Effect of cenosphere on mechanical properties of bamboo-epoxy composites.” *Journal of Reinforced Plastics and Composites*, 32(11), 794–801.

Jha, N., Badkul, A., Mondal, D. P., Das, S., and Singh, M. (2011). "Sliding wear behaviour of aluminum syntactic foam: A comparison with Al10 wt% SiC composites." *Tribol Int*, 44(3), 220–231.

Kandare, E., Kandola, B. K., Myler, P., and Edwards, G. (2010). "Thermo-mechanical responses of fiber-reinforced epoxy composites exposed to high temperature environments. Part I: Experimental data acquisition." *J Compos Mater*, 44(26), 3093–3114.

Kaur, M., and Jayakumari, L. S. (2016). "Eco-friendly cardanol-based phenalkamine cured epoxy-cenosphere syntactic foams: Fabrication and characterisation." *J Appl Polym Sci*, 133(46).

Kaur, M., and Jayakumari, L. S. (2019). "Consequence of cenosphere loading on hygrothermal, thermal, and mechanical properties of epoxy syntactic foams." *Journal of Cellular Plastics*, 55(3), 297–318.

Khan, L. A., Mahmood, A. H., and Khan, Z. (2013). "Post curing effect of poly epoxy on visco-elastic and mechanical properties of different sandwich structures." *Polym Compos*, 34(4), 477–481.

Kim, J., Seidler, P., Fill, C., and Wan, L. S. (2008). "Investigations of the effect of curing conditions on the structure and stability of amino-functionalized organic films on silicon substrates by Fourier transform infrared spectroscopy, ellipsometry, and fluorescence microscopy." *Surf Sci*, 602(21), 3323–3330.

Kong, E. S.-W. (1986). "Physical aging in epoxy matrices and composites." 125–171.

Kumar, M., and Jena, H. (2022). "Water absorption behaviour of glass fibre-reinforced polymer composite with clamshell and cenosphere fillers." *Proceedings of the Institution of Mechanical Engineers, Part E: Journal of Process Mechanical Engineering*.

Kumar, S. J. A., and Ahmed, K. S. (2016). "Effects of ageing on mechanical properties of stiffened syntactic foam core sandwich composites for marine applications." *Journal of Cellular Plastics*, 52(5), 503–532.

- Labella, M., Zeltmann, S. E., Shunmugasamy, V. C., Gupta, N., and Rohatgi, P. K. (2014). “Mechanical and thermal properties of fly ash/vinyl ester syntactic foams.” *Fuel*, 121, 240–249.
- Lasagabáster, A., Abad, M. J., Barral, L., Ares, A., and Bouza, R. (2009). “Application of FTIR spectroscopy to determine transport properties and water-polymer interactions in polypropylene (PP)/poly (ethylene-co-vinyl alcohol) (EVOH) blend films: Effect of poly (ethylene-co-vinyl alcohol) content and water activity.” *Polymer (Guildf)*, 50(13), 2981–2989.
- Lee, M., Paria, S., Mondal, S., Lee, G. B., Shin, B., Kim, S., Park, S., and Nah, C. (2022). “Amphiphilic block co-polymer and silica reinforced epoxy composite with excellent toughness and delamination resistance for durable electronic packaging application.” *Polymer (Guildf)*, 245.
- Li, G., and Jones, N. (2007). “Development of rubberized syntactic foam.” *Compos Part A Appl Sci Manuf*, 38(6), 1483–1492.
- Li, G., and Muthyala, V. D. (2008). “Impact characterization of sandwich structures with an integrated orthogrid stiffened syntactic foam core.” *Compos Sci Technol*, 68(9), 2078–2084.
- Li, G., and Nettles, D. (2010). “Thermomechanical characterization of a shape memory polymer based self-repairing syntactic foam.” *Polymer (Guildf)*, 51(3), 755–762.
- Li, J., Wu, Z., Huang, C., Chen, Z., Huang, R., and Li, L. (2013a). “Plasma functionalization for improving dispersion and interfacial bonding of multi-wall carbon nanotubes in cyanate ester/epoxy nanocomposites.” *Colloids Surf Physicochem Eng Asp*, 433, 173–180.
- Li, W., Dichiara, A., and Bai, J. (2013b). “Carbon nanotube-graphene nanoplatelet hybrids as high-performance multifunctional reinforcements in epoxy composites.” *Compos Sci Technol*, 74, 221–227.
- Liang, C., Gu, Z., Zhang, Y., Ma, Z., Qiu, H., and Gu, J. (2021). “Structural Design Strategies of Polymer Matrix Composites for Electromagnetic Interference Shielding: A Review.” *Nanomicro Lett*, Springer Science and Business Media B.V.

- Liu, H., Su, X., Tao, J., Fu, R., You, C., and Chen, X. (2019a). "Effect of SiO₂ nanoparticles-decorated SCF on mechanical and tribological properties of cenosphere / SCF / PEEK composites." 48749, 1–10.
- Liu, M., Cao, X., Liu, H., Yang, X., and Zhou, C. (2019b). *Halloysite-Based Polymer Nanocomposites. Nanomaterials from Clay Minerals*, Elsevier Inc.
- Liu, M., Guo, B., Du, M., Cai, X., and Jia, D. (2007). "Properties of halloysite nanotube-epoxy resin hybrids and the interfacial reactions in the systems." *Nanotechnology*, 18(45).
- Liu, M., Guo, B., Du, M., Lei, Y., and Jia, D. (2008). "Natural inorganic nanotubes reinforced epoxy resin nanocomposites." *Journal of Polymer Research*, 15(3), 205–212.
- Liu, Y., Du, H., Liu, L., and Leng, J. (2014). "Shape memory polymers and their composites in aerospace applications: A review." *Smart Mater Struct*, 23(2).
- Lvov, Y., Wang, W., Zhang, L., and Fakhrullin, R. (2016). "Halloysite Clay Nanotubes for Loading and Sustained Release of Functional Compounds." *Advanced Materials*, 28(6), 1227–1250.
- Maharsia, R., Gupta, N., and Jerro, H. D. (2006). "Investigation of flexural strength properties of rubber and nanoclay reinforced hybrid syntactic foams." *Materials Science and Engineering A*, 417, 249–258.
- Maharsia, R. R., and Jerro, H. D. (2007). "Enhancing tensile strength and toughness in syntactic foams through nanoclay reinforcement." *Materials Science and Engineering A*, 454–455, 416–422.
- Mahrholz, T., Stängle, J., and Sinapius, M. (2009). "Quantitation of the reinforcement effect of silica nanoparticles in epoxy resins used in liquid composite moulding processes." *Compos Part A Appl Sci Manuf*, 40(3), 235–243.
- Mallik, S., Ekere, N., Best, C., and Bhatti, R. (2011). "Investigation of thermal management materials for automotive electronic control units." *Appl Therm Eng*, 31(2–3), 355–362.

- Mgbemena, C. O., Li, D., Lin, M. F., Liddel, P. D., Katnam, K. B., Kumar, V. T., and Nezhad, H. Y. (2018). "Accelerated microwave curing of fibre-reinforced thermoset polymer composites for structural applications: A review of scientific challenges." *Compos Part A Appl Sci Manuf*, Elsevier Ltd.
- Miyagawa, H., and Drzal, L. T. (2004). "Thermo-physical and impact properties of epoxy nanocomposites reinforced by single-wall carbon nanotubes." *Polymer (Guildf)*, 45(15), 5163–5170.
- Moller, J. C., Berry, R. J., and Foster, H. A. (2020). "On the nature of epoxy resin post-curing." *Polymers (Basel)*, 12(2).
- Mondal, D. P., Datta Majumder, J., Jha, N., Badkul, A., Das, S., Patel, A., and Gupta, G. (2012). "Titanium-cenosphere syntactic foam made through powder metallurgy route." *Mater Des*, 34, 82–89.
- Naraghi, M., Filleter, T., Moravsky, A., Locascio, M., Loutfy, R. O., and Espinosa, H. D. (2010). "A Multiscale Study of High Performance Double-Walled Nanotube Polymer Fibers."
- Nielsen, L. E. (1966). "Simple theory of stress-strain properties of filled polymers." *J Appl Polym Sci*, 10(1), 97–103.
- Nikolic, G., Zlatkovic, S., Cakic, M., Cakic, S., Lacnjevac, C., and Rajic, Z. (2010). "Fast fourier transform IR characterization of epoxy GY systems crosslinked with aliphatic and cycloaliphatic EH polyamine adducts." *Sensors*, 10(1), 684–696.
- Nosbi, N., Akil, H. M., Ishak, Z. A. M., and Bakar, A. A. (2010). "Degradation of compressive properties of pultruded kenaf fiber reinforced composites after immersion in various solutions." *Mater Des*, 31(10), 4960–4964.
- Nunes, J. P., and Silva, J. F. (2016). "Sandwiched composites in aerospace engineering." *Advanced Composite Materials for Aerospace Engineering*, Elsevier, 129–174.

- Omar, M. Y., Xiang, C., Gupta, N., Strbik, O. M., and Cho, K. (2015). "Syntactic foam core metal matrix sandwich composite under bending conditions." *Mater Des*, 86, 536–544.
- Pareta, A. S., Gupta, R., and Panda, S. K. (2020). "Experimental investigation on fly ash particulate reinforcement for property enhancement of PU foam core FRP sandwich composites." *Compos Sci Technol*, 195.
- Patil, B., Bharath Kumar, B. R., and Doddamani, M. (2019). "Compressive behavior of fly ash based 3D printed syntactic foam composite." *Mater Lett*, 254, 246–249.
- Pattanaik, A., Mukherjee, M., and Mishra, S. B. (2019a). "Influence of curing condition on thermo-mechanical properties of fly ash reinforced epoxy composite." *Compos B Eng*, 176.
- Pattanaik, A., Mukherjee, M., and Mishra, S. B. (2019b). "Influence of curing condition on thermo-mechanical properties of fly ash reinforced epoxy composite." *Compos B Eng*, 176.
- Pervaiz, M., Panthapulakkal, S., KC, B., Sain, M., and Tjong, J. (2016a). "Emerging Trends in Automotive Lightweighting through Novel Composite Materials." *Materials Sciences and Applications*, 07(01), 26–38.
- Pervaiz, M., Panthapulakkal, S., KC, B., Sain, M., and Tjong, J. (2016b). "Emerging Trends in Automotive Lightweighting through Novel Composite Materials." *Materials Sciences and Applications*, 07(01), 26–38.
- Peter, S., and Woldesenbet, E. (2008). "Nanoclay syntactic foam composites-High strain rate properties." *Materials Science and Engineering A*, 494(1–2), 179–187.
- Platzer, N. (1988). "Handbook of fillers for plastics, Harry S. Katz and John V. Milewski, Eds., Van Nostrand Reinhold, New York, 1987, 467 pp." *Journal of Polymer Science: Polymer Letters Edition*, 26(6), 274.
- Popescu, M. C., Dogaru, B. I., and Popescu, C. M. (2020). "Effect of cellulose nanocrystals nanofiller on the structure and sorption properties of carboxymethyl cellulose-glycerol-cellulose nanocrystals nanocomposite systems." *Materials*, 13(13).

- Poveda, R. L., Achar, S., and Gupta, N. (2014). “Viscoelastic properties of carbon nanofiber reinforced multiscale syntactic foam.” *Compos B Eng*, 58, 208–216.
- Poveda, R. L., Dorogokupets, G., and Gupta, N. (2013). “Carbon nanofiber reinforced syntactic foams: Degradation mechanism for long term moisture exposure and residual compressive properties.” *Polym Degrad Stab*, 98(10), 2041–2053.
- Prashantha, K., Lacrampe, M. F., and Krawczak, P. (2011a). “Processing and characterization of halloysite nanotubes filled polypropylene nanocomposites based on a masterbatch route: Effect of halloysites treatment on structural and mechanical properties.” *Express Polym Lett*, 5(4), 295–307.
- Prashantha, K., Schmitt, H., Lacrampe, M. F., and Krawczak, P. (2011b). “Mechanical behaviour and essential work of fracture of halloysite nanotubes filled polyamide 6 nanocomposites.” *Compos Sci Technol*, 71(16), 1859–1866.
- Prolongo, S. G., Gude, M. R., and Ureña, A. (2012). “Water uptake of epoxy composites reinforced with carbon nanofillers.” *Compos Part A Appl Sci Manuf*, 43(12), 2169–2175.
- Ravichandran, G., Rathnakar, G., and Santhosh, N. (2019). “Effect of heat treated HNT on physico-mechanical properties of epoxy nanocomposites.” *Composites Communications*, 13(February), 42–46.
- Ren, S., Tao, X., Ma, X., Liu, J., Du, H., Guo, A., and Xu, J. (2018). “Fabrication of fly ash cenospheres-hollow glass microspheres / borosilicate glass composites for high temperature application.” *Ceram Int*, 44(1), 1147–1155.
- Riaz, U., and Ashraf, S. M. (2015). *Characterization of Polymer Blends: Miscibility, Morphology and Interfaces*.
- Rooj, S., Das, A., Thakur, V., Mahaling, R. N., Bhowmick, A. K., and Heinrich, G. (2010). “Preparation and properties of natural nanocomposites based on natural rubber and naturally occurring halloysite nanotubes.” *Mater Des*, 31(4), 2151–2156.
- Saha, M. C., and Nilufar, S. (2009). “Nanoclay-Reinforced Syntactic Foams: Flexure and Thermal Behavior.” *Polym Compos*, 31(8), 1332–1342.

Saif, M. J., and Naveed, M. (2021). “Effect of pristine halloysite nanotubes on dynamic mechanical and thermal behavior of reinforced epoxy nanocomposites.” *Iranian Polymer Journal (English Edition)*.

Samsudin, S. S., Ariff, Z. M., Zakaria, Z., and Bakar, A. A. (2011). “Development and characterization of epoxy syntactic foam filled with epoxy hollow spheres.” *Express Polym Lett*, 5(7), 653–660.

Sankaran, S., Sekhar, K. R., Raju, G., and Kumar, M. N. J. (2006). “Characterization of epoxy syntactic foams by dynamic mechanical analysis.” *J Mater Sci*, 4041–4046.

Sathishkumar, G. K., Rajkumar, G., Srinivasan, K., and Umapathy, M. J. (2018). “Structural analysis and mechanical properties of lignite fly-ash-added jute–epoxy polymer matrix composite.” *Journal of Reinforced Plastics and Composites*, 37(2), 90–104.

Schadler, L. S., Giannaris, S. C., and Ajayan, P. M. (1998). “Load transfer in carbon nanotube epoxy composites.” *Appl Phys Lett*, 73(26), 3842–3844.

Seretis, G. v., Nitodas, S. F., Mimigianni, P. D., Kouzilos, G. N., Manolakos, D. E., and Provatidis, C. G. (2018). “On the post-curing of graphene nanoplatelets reinforced hand lay-up glass fabric/epoxy nanocomposites.” *Compos B Eng*, 140(November 2017), 133–138.

Shahapurkar, K., Doddamani, M., Mohan Kumar, G. C., and Gupta, N. (2019). “Effect of cenosphere filler surface treatment on the erosion behavior of epoxy matrix syntactic foams.” *Polym Compos*, 40(6), 2109–2118.

Shahapurkar, K., Garcia, C. D., Doddamani, M., Kumar, M., and Prabhakar, P. (2017). *Compressive behavior of Cenosphere/Epoxy syntactic foams in Arctic Conditions*.

Shahapurkar, K., Garcia, C. D., Doddamani, M., Mohan Kumar, G. C., and Prabhakar, P. (2018). “Compressive behavior of cenosphere/epoxy syntactic foams in arctic conditions.” *Compos B Eng*, 135(October 2017), 253–262.

Shakil, U. A., Hassan, S. B. A., Yahya, M. Y., and Nauman, S. (2020). “Mechanical properties of electrospun nanofiber reinforced/interleaved epoxy matrix composites—A review.” *Polym Compos*, John Wiley and Sons Inc.

Sharma, B., Chhibber, R., and Mehta, R. (2019a). “Effect of mixing parameters, postcuring, and stoichiometry on mechanical properties of fiber reinforced epoxy–clay nanocomposites.” *Proceedings of the Institution of Mechanical Engineers, Part L: Journal of Materials: Design and Applications*, 233(7), 1363–1374.

Sharma, S., Sudhakara, P., Misra, S. K., and Singh, J. (2019b). “A comprehensive review of current developments on the waste-reinforced polymer-matrix composites for automotive, sports goods and construction applications: Materials, processes and properties.” *Mater Today Proc*, Elsevier Ltd, 1671–1679.

Shekhar, B. (2012). “Roadmap to 13 Million Tons.” *Plastindia in-house journal*, 37, 6–11.

Simon, F. (1931). “The state of supercooled liquids and glasses.” *Z. Anorg. Allgem. Chem.*, 203, 219–227.

Srivastava, S., and Pandey, A. (2019). “Mechanical behavior and thermal stability of ultrasonically synthesized halloysite-epoxy composite.” *Composites Communications*, 11, 39–44.

“Standard Test Method for Compressive Properties of Rigid Plastics 1.” (2015). 1–8.

“Standard Test Method for Tensile Properties of Plastics 1.” (2014). 1–17.

“Standard Test Methods for Density and Specific Gravity (Relative Density) of Plastics by Displacement 1.” (2018). 1–6.

“Standard Test Methods for Flexural Properties of Unreinforced and Reinforced Plastics and Electrical Insulating Materials 1.” (2017). 1–12.

Strankowski, M., Włodarczyk, D., Piszczyk, Ł., and Strankowska, J. (2016). “Polyurethane Nanocomposites Containing Reduced Graphene Oxide, FTIR, Raman, and XRD Studies.” *Journal of Spectroscopy*, 2016.

- Šupová, M., Martynková, G. S., and Barabaszová, K. (2011). "Effect of nanofillers dispersion in polymer matrices: A review." *Sci Adv Mater*, 3(1), 1–25.
- Suresha, B., Chandramohan, G., Rao, P. R. S., Sampathkumaran, P., Seetharamu, S., and Venkateswarlu, V. (2006). "Friction and slide wear characteristics of glass-epoxy and glass-epoxy filled with SiCp composites." *Indian Journal of Engineering and Materials Sciences*, 13(6), 535–541.
- Swetha, C., and Kumar, R. (2011). "Quasi-static uni-axial compression behaviour of hollow glass microspheres/epoxy based syntactic foams." *Mater Des*, 32(8–9), 4152–4163.
- Tagliavia, G., Porfiri, M., and Gupta, N. (2009). "Vinyl Ester Glass Hollow Particle Composites: Dynamic Mechanical Properties at High Inclusion Volume Fraction." *J Compos Mater*, 43(5), 561–582.
- Tagliavia, G., Porfiri, M., and Gupta, N. (2010). "Analysis of hollow inclusion-matrix debonding in particulate composites." *Int J Solids Struct*, 47(16), 2164–2177.
- Tagliavia, G., Porfiri, M., and Gupta, N. (2012a). "Influence of moisture absorption on flexural properties of syntactic foams." *Compos B Eng*, 43(2), 115–123.
- Tagliavia, G., Porfiri, M., and Gupta, N. (2012b). "Influence of moisture absorption on flexural properties of syntactic foams." *Compos B Eng*, 43(2), 115–123.
- Tang, Y., Deng, S., Ye, L., Yang, C., Yuan, Q., Zhang, J., and Zhao, C. (2011). "Effects of unfolded and intercalated halloysites on mechanical properties of halloysite-epoxy nanocomposites." *Compos Part A Appl Sci Manuf*, 42(4), 345–354.
- Tenney, D. R., Davis John G., Jr., Johnston, N. J., Pipes, R. B., and McGuire, J. F. (2011). *Structural Framework for Flight II: NASA's Role in Development of Advanced Composite Materials for Aircraft and Space Structures*. Nasa/Cr–2019-220267, Analytical Services & Materials, Inc.
- Thakur, S., and Chauhan, S. (2014). "Effect of micron and submicron size cenosphere particulate on mechanical and tribological characteristics of vinylester composites."

Proceedings of the Institution of Mechanical Engineers, Part J: Journal of Engineering Tribology, 228(4), 415–423.

Tham, W. L., Chow, W. S., Poh, B. T., and Mohd Ishak, Z. A. (2016a). “Poly(lactic acid)/halloysite nanotube nanocomposites with high impact strength and water barrier properties.” *J Compos Mater*, 50(28), 3925–3934.

Tham, W. L., Poh, B. T., Arifin, Z., Ishak, M., and Chow, W. S. (2016b). “Characterisation of Water Absorption of Biodegradable Poly(lactic Acid)/Halloysite Nanotube Nanocomposites at Different Temperatures.” *Journal of Engineering Science*.

Ullah, H., Harland, A. R., and Silberschmidt, V. v. (2015). “Dynamic bending behaviour of woven composites for sports products: Experiments and damage analysis.” *Mater Des*, 88, 149–156.

Ullas, A. v., Qayyum, B., Kumar, D., and Roy, P. K. (2016). “Electrospun Polyamide Nanofiber-Reinforced Hybrid Syntactic Foams.” *Polymer - Plastics Technology and Engineering*, 55(17), 1797–1806.

Vidil, T., Tournilhac, F., Musso, S., Robisson, A., and Leibler, L. (2016). “Control of reactions and network structures of epoxy thermosets.” *Prog Polym Sci*, Elsevier Ltd.

Waddar, S., Jeyaraj, P., and Doddamani, M. (2018). “Influence of axial compressive loads on buckling and free vibration response of surface-modified fly ash cenosphere/epoxy syntactic foams.” *J Compos Mater*, 52(19), 2621–2630.

Wang, C., Liu, J., Du, H., and Guo, A. (2012). “Effect of fly ash cenospheres on the microstructure and properties of silica-based composites.” *Ceram Int*, 38(5), 4395–4400.

Wang, C., Roy, A., Chen, Z., and Silberschmidt, V. v. (2017a). “Braided textile composites for sports protection: Energy absorption and delamination in impact modelling.” *Mater Des*, 136, 258–269.

Wang, C., Zhao, M., Li, J., Yu, J., Sun, S., Ge, S., Guo, X., Xie, F., Jiang, B., Wujcik, E. K., Huang, Y., Wang, N., and Guo, Z. (2017b). “Silver nanoparticles/graphene oxide

decorated carbon fiber synergistic reinforcement in epoxy-based composites.” *Polymer (Guildf)*, 131, 263–271.

Wang, M., Wang, J., and Hu, W. (2020). “Preparation and corrosion behavior of Cu-8-HQ@HNTs/epoxy coating.” *Prog Org Coat*, 139.

Wang, X., and Gillham, J. K. (1993). “TG–Temperature property (TgTP) diagram for thermosetting systems: Anomalous behavior of physical properties vs. extent of cure.” *J Appl Polym Sci*, 47(3), 425–446.

Wang, X., Jiang, M., Zhou, Z., Gou, J., and Hui, D. (2017c). “3D printing of polymer matrix composites: A review and prospective.” *Compos B Eng*, Elsevier Ltd.

Woldesenbet, E. (2008). “Low velocity impact properties of nanoparticulate syntactic foams.” *Materials Science and Engineering A*, 496(1–2), 217–222.

Wouterson, E. M., Boey, F. Y. C., Hu, X., and Wong, S. C. (2007a). “Effect of fiber reinforcement on the tensile, fracture and thermal properties of syntactic foam.” *Polymer (Guildf)*, 48(11), 3183–3191.

Wouterson, E. M., Boey, F. Y. C., Wong, S. C., Chen, L., and Hu, X. (2007b). “Nanotoughening versus micro-toughening of polymer syntactic foams.” *Compos Sci Technol*, 67(14), 2924–2933.

Wright, W. W. (1991). “International encyclopedia of composites: Volumes 1 & 2 Edited by Stuart M. Lee, VCH Publishers, New York, 1990. Price DM 450 per Volume. Vol. 1 pp. xvi+ 563. ISBN 0-89573-731-0 Vol. 2 pp. xii+ 524. ISBN 0-89573-732-9.” Wiley Online Library.

Xiang, Q., and Xiao, F. (2020). “Applications of epoxy materials in pavement engineering.” *Constr Build Mater*, Elsevier Ltd.

Xu, L. R., Bhamidipati, V., Zhong, W. H., Li, J., Lukehart, C. M., Lara-Curzio, E., Liu, K. C., and Lance, M. J. (2004). “Mechanical property characterization of a polymeric nanocomposite reinforced by graphitic nanofibers with reactive linkers.” *J Compos Mater*, 38(18), 1563–1582.

- Yang, S., and Zhao, Y. F. (2015). "Additive manufacturing-enabled design theory and methodology: a critical review." *International Journal of Advanced Manufacturing Technology*, Springer London.
- Ye, Y., Chen, H., Wu, J., and Ye, L. (2007). "High impact strength epoxy nanocomposites with natural nanotubes." *Polymer (Guildf)*, 48(21), 6426–6433.
- Yeasmin, F., Mallik, A. K., Chisty, A. H., Robel, F. N., Shahruzzaman, M., Haque, P., Rahman, M. M., Hano, N., Takafuji, M., and Ihara, H. (2021). "Remarkable enhancement of thermal stability of epoxy resin through the incorporation of mesoporous silica micro-filler." *Heliyon*, 7(1).
- Yoshida, H., Nakamura, K., and Kobayashi, Y. (1982). "Differential Scanning Calorimetric Study of Enthalpy Relaxation in Polystyrene, Poly(4-hydroxystyrene), and Their Copolymers." *Polym J*.
- Yu, Q., Zhao, Y., Dong, A., and Li, Y. (2019). "Comparison of two different methods for producing hollow microspheres with carbon fiber reinforced composite skin used in syntactic foams." *Polym Compos*, 40(S2), E1075–E1083.
- Yuan, J., An, Z., and Zhang, J. (2020). "Effects of hollow microsphere surface property on the mechanical performance of high strength syntactic foams." *Compos Sci Technol*, 199.
- Zamani, P., A. M. H., da S. L. F., & G. D. (2022). "On the static and fatigue life of nano-reinforced Al-GFRP bonded joints under different dispersion treatments." *Fatigue Fract Eng Mater Struct*, 45(4), 1088–1110.
- Zamani, P., Jaamialahmadi, A., and Silva, L. F. M. da. (2021). "The influence of GNP and nano-silica additives on fatigue life and crack initiation phase of Al-GFRP bonded lap joints subjected to four-point bending." *Compos B Eng*, 207.
- Zeltmann, S. E., Poveda, R. L., and Gupta, N. (2015). "Accelerated environmental degradation and residual flexural analysis of carbon nanofiber reinforced composites." *Polym Degrad Stab*, 121, 348–358.

Zhang, J., Jia, Z., Jia, D., Zhang, D., and Zhang, A. (2014a). “Chemical functionalization for improving dispersion and interfacial bonding of halloysite nanotubes in epoxy nanocomposites.” *High Perform Polym*, 26(7), 734–743.

Zhang, L., and Ma, J. (2010). “Effect of coupling agent on mechanical properties of hollow carbon microsphere/phenolic resin syntactic foam.” *Compos Sci Technol*, 70(8), 1265–1271.

Zhang, L., and Ma, J. (2013). “Effect of carbon nanofiber reinforcement on mechanical properties of syntactic foam.” *Materials Science and Engineering A*, 574, 191–196.

Zhang, W. W., Biskach, M. P., Bly, V. T., Carter, J. M., Chan, K. W., Gaskin, J. A., Hong, M., Hohl, B. R., Jones, W. D., Kolodziejczak, J. J., Kolos, L. D., Mazzarella, J. R., McClelland, R. S., McKeon, K. P., Miller, T. M., O’Dell, S. L., Riveros, R. E., Saha, T. T., Schofield, M. J., Sharpe, M. v., and Smith, H. C. (2014b). “Affordable and lightweight high-resolution x-ray optics for astronomical missions.” *Space Telescopes and Instrumentation 2014: Ultraviolet to Gamma Ray*, SPIE, 914415.

Zhang, X., Ya, B., Huang, B., Zhou, B., Pei, L., and Jia, F. (2017). “Study on preparation and properties of carbon nanotubes/hollow glass microspheres/epoxy syntactic foam.” *Journal of Polymer Engineering*, 37(1), 93–98.

CURRICULUM VITAE

1. Name: **MOHAMMED SOHAIL BAKSHI**
2. Date of Birth: 05/10/1993
3. Permanent Address: Plot No. 32, Nalband Garden, Near Badi Kaman, J. M Road, Vijayapur 586101
4. Mobile Number: 9916335771
5. Email ID: bakshi.cnet@gmail.com
6. Education Qualification: B.E. M.Tech., Ph.D.

2015 **Bachelor of Engineering**

Institution: BLDEA's V. P. Dr P G Halakatti College of Engg. And Technology, Vijayapur 586101, Karnataka, India.

Specialization: Mechanical Engineering

2017 **Master of Engineering**

Institution: Basaveshwar Engineering College (Autonomous), Bagalkot, Karnataka, India.

Specialization: Machine Design

2023 **Doctor of Philosophy**

Institution: National Institute of Technology Karnataka, Surathkal, Karnataka, India.

Registration Date: 13/07/2017

Thesis Submission Date: 31/03/2023

Viva-Voice Date: 18/08/2023

LIST OF PUBLICATIONS BASED ON THESIS

International Journals

1. Bakshi, Mohammed Sohail and Kattimani, Subhaschandra. (2021). “Study of mechanical and dynamic mechanical behavior of halloysite nanotube-reinforced multiscale syntactic foam.” *Journal of Applied Polymer Science*; 138; 7; 49855; 0021-8995.
2. Bakshi, Mohammed Sohail and Kattimani, Subhaschandra. (2022). “Probing the effect of post-curing and halloysite nanotube reinforcement on thermo-mechanical properties of lightweight epoxy syntactic foam composites.” *Proceedings of the Institution of Mechanical Engineers, Part L: Journal of Materials: Design and Applications*; 237; 03; 697 - 713.
3. Bakshi, Mohammed Sohail and Kattimani, Subhaschandra. (2023). “Influence of moisture absorption on the compressive behavior of halloysite nanotube reinforced buoyant nanocomposite foams for maritime applications.” *Polymer Composites* (Accepted, DOI: <http://doi.org/10.1002/pc.27665>).

International Conferences

1. Bakshi, Mohammed Sohail and Kattimani, Subhaschandra. (2020). “Flexural behaviour of nanoclay filled glass fiber/epoxy polymer nanocomposites.” *AIP Conference Proceedings*; 2247; 1; 020012; 0735420068; 2020; AIP Publishing LLC.